

Master Thesis

Dimensional Phase Transition
in an
Ultracold Bose Gas

Bernhard Irsigler

September 1, 2016

Supervised by Priv.-Doz. Dr. Axel Pelster

Abstract

In this thesis we investigate the dependence of Bose-Einstein condensation on the dimension of the system. The Mermin-Wagner-Hohenberg theorem predicts no phase transition at finite temperature in one- and two-dimensional, homogeneous systems. Therefore we would expect an increment of the critical temperature when changing continuously the dimensionality of the system to $D = 3$. Inspired by the ideas of Ref. [1] we model continuous transitions between $D = 1, 2, 3$ for bosonic atoms, which are loaded into an optical lattice with tunable hopping. Our calculations of a non-interacting homogeneous Bose gas yield for the critical temperature a power-law with an exponent of $\frac{1}{2}$ in the $1D-3D$ transition and a logarithmic-like behavior in the $2D-3D$ transition. In the trapped case all critical exponents appear to be one. Furthermore we calculate respective thermodynamic quantities, such as the heat capacity, as function of the temperature and the dimensionality for both cases. In order to take into account weak interactions we use a Hartree-Fock-Bogoliubov-Popov theory and observe an increment in the critical temperature for the homogeneous system in all dimensions due to interactions. Furthermore we find that the exponent of the $1D-3D$ transition does not change with finite interaction strength. Finally we analyze a hybrid model which consists of two lattice dimensions and one continuous dimension. Our theory, including hopping energies and interactions strengths computed by means of numerically exact Wannier functions, is in much better agreement with the experimental data of Ref. [1] than a pure Hartree-Fock treatment.

Acknowledgment

During the work on this thesis I had a lot of overwhelming conversations with different people from all over the world. Therefore I would like to thank my office colleagues Javed Akram and Václav Zatloukal who were always prepared for physical discussions. I thank David Schneider especially for a final hint making the numerics work. I am thankful for the careful proofreading by Sandro Gödtel. Furthermore I am grateful for advices by Rudolf Grimm, Randall Hulet, Päivi Törmä, and Eugene Zaremba. Moreover I would like to thank my second referee Piet Brouwer who gave me the opportunity to present my topic at the Dahlem Center for Complex Quantum Systems. Special thanks go to Antun Balaž for hosting me in Belgrade, Serbia and Francisco Ednilson Alves dos Santos for hosting me in São Carlos, Brazil, their respective groups, and the DAAD for financial support. Furthermore I would like to thank Jürgen Bosse who spent a lot of time to discuss with me about very fascinating problems in physics. I am grateful for highly interesting and enlightening discussions in Kaiserslautern with Sebastian Eggert and Herwig Ott. Finally I would like to give my greatest thanks to Axel Pelster who supervised me with unsurpassed care. Although he has his position several hundreds of kilometers far away in Kaiserslautern he always spent time on personal discussions with me in Berlin. He made all of the scientific travels and stays possible from which I learned tremendously. Without him there would not be this thesis as it is.

Contents

1	Introduction	1
1.1	Bose gases in optical traps	1
1.2	Bose gases in optical lattices	1
1.3	Ultracold regime	2
1.4	Dimensional phase transitions	4
1.5	Structure of this thesis	5
2	Theoretical background	7
2.1	Low dimensions	7
2.2	Mermin-Wagner-Hohenberg theorem	8
2.2.1	Bogoliubov inequality	8
2.2.2	Derivation of Mermin-Wagner-Hohenberg theorem	9
2.3	Optical lattices and Bloch dispersion	10
2.4	Dimensional phase transition	14
2.4.1	Potential dimensional transition	14
2.4.2	Kinetic dimensional transition	14
2.4.3	Dimensional transition path	14
3	Non-interacting Bose gas in optical lattice with tunable hopping	17
3.1	Free energy	17
3.2	Thermodynamics	18
3.2.1	Number of particles	18
3.2.2	Low- and high-temperature phase	18
3.2.3	Critical temperature	19
3.2.4	Critical temperature in low dimensions	19
3.2.5	Internal energy	20
3.2.6	Heat capacity	20
3.2.7	Continuum limit	21
4	Results for homogeneous case	23
4.1	Critical temperature as function of dimensionality	23
4.2	Thermodynamic quantities as function of dimensionality	25
5	Isotropic harmonic trap	27
5.1	Free energy and critical temperature	27
5.2	Thermodynamics	29
6	Weakly interacting bosons	31
6.1	Hartree-Fock-Bogoliubov-Popov theory	31
6.1.1	Pure Hartree-Fock limit	36
6.1.2	Generalized Gross-Pitaevskii equation and chemical potential	37
6.2	Numerics of weakly interacting case	38
6.2.1	Ellipsoid method	39

Contents

6.2.2	Numerical integration sampling	40
6.2.3	Dimensionless units	42
6.2.4	Phase transition and critical temperature	42
6.3	Shift of critical temperature in three dimensions	44
6.4	Results for weakly interacting, homogeneous Bose gas	46
6.4.1	Dimensional phase transition with finite interaction strength	46
6.4.2	1D-3D-transition with finite interaction strength	47
7	Hybrid model and comparison with experiment	51
7.1	Hartree-Fock theory of hybrid model	51
7.1.1	Critical density	52
7.1.2	Hopping energy	53
7.1.2.1	Analytic approximation for deep optical lattices	53
7.1.2.2	Bloch eigenvalue problem	53
7.1.2.3	Effective mass approximation	56
7.1.3	Effective interaction strength	57
7.1.3.1	Tight-binding approximation	58
7.1.3.2	Wannier functions	59
7.1.4	Critical chemical potential within Hartree-Fock theory	60
7.2	Hartree-Fock-Bogoliubov-Popov theory of hybrid model	61
8	Conclusion	63
9	Outlook	65
	Bibliography	67

1 Introduction

The field of ultracold quantum gases deals with the investigation of highly exciting quantum states of matter which occur at very low temperatures. At room temperature $T \sim 300$ K an atomic gas of usual density $n \sim 10^{19} \text{ cm}^{-3}$ is well described by classical thermodynamics. When such a gas is cooled to really low temperatures in the range of μK - nK , the quantum character of the particles becomes important and they begin to behave as wave packets. In case the particles are bosons one observes a phase transition. At a distinct critical temperature, where the extent of the wave packets becomes comparable to the interatomic distance, the wave packets start to overlap with each another. As a result the wave packets descent to the lowest energy state and grow together as a new giant quantum wave. Thus the particle character is completely gone at this stage because they behave absolutely coherently. Since the low temperature forces the particles into low energy states, the occupation of the lowest single quantum state is now macroscopically high. This is the macroscopic quantum phenomenon of Bose-Einstein condensation (BEC). The effect of a macroscopic occupation was first proposed by Einstein [2] based on a statistical derivation of Planck's law of radiation by Bose [3]. The critical temperature of BEC can be raised by increasing the density. However in experiments the density is typically held small in order to avoid three-body recombinations and thus preventing the gas from forming a solid. Experiments usually take place at temperatures in the nano-Kelvin regime. Good candidates to form a BEC are mostly alkali and alkaline earth metals. It is crucial to use a bosonic isotope for the BEC which requires an even number of neutrons in the atomic nucleus. The setups for BEC experiments need high technical effort to reach such low temperatures. Laser cooling exploits the relativistic Doppler effect to slow down atoms which on the long run decreases the temperature of the gas sample. Evaporative cooling, which is the combination of the evaporation of the fastest atoms and a rethermalization process, is used to finally reach the ultracold regime of a few nK.

1.1 Bose gases in optical traps

In order to prevent heating of the gas sample one needs to isolate it from the environment. Due to light-matter interactions the atoms can be trapped in an optical potential using distinctly detuned laser beams. These traps are commonly harmonic. In the case of a harmonic confinement the macroscopic occupation of the lowest energy level, which can be measured in momentum space, is also observable in configuration space. Furthermore harmonic traps can also be aligned anisotropically. A crucial feature of BEC clouds is that they preserve the anisotropic shape if released from the trap. This is not the case for thermal clouds and therefore an evidence for the occurrence of BEC. The first Bose-Einstein condensates were successfully observed at the institutes of JILA-NIST [4] with rubidium and MIT [5] with sodium, both in 1995. In Fig. 1.1 we show the experimental observation of BEC taken from [4]. The sharp peak at the trap center (white) as well as its elliptical shape are evidence for a BEC.

1.2 Bose gases in optical lattices

The most important experimental breakthrough in the field of ultracold quantum gases after the first observations of a BEC in 1995 is the realization of an optical lattice in 2002 [6]. They can be realized with two counterpropagating laser beams of the same frequency. The atoms

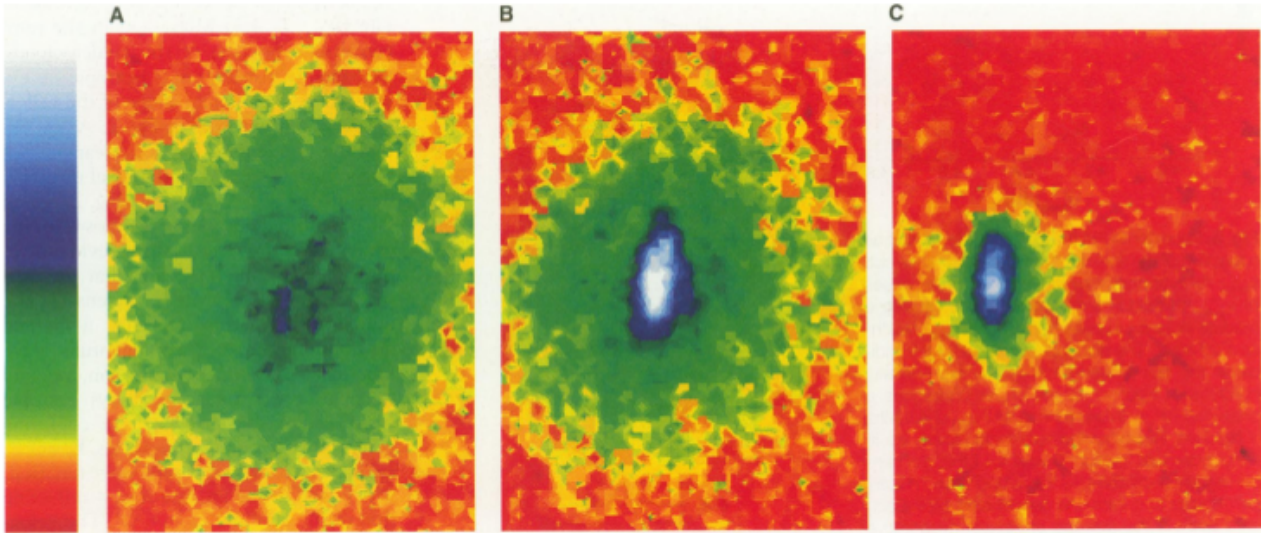


Figure 1.1: First observation of Bose-Einstein condensation taken from Ref. [4]: Velocity distribution in false colors. Red denotes a vanishing density and white represents the highest measured density. (A) Spherically shaped, thermal cloud right above the critical temperature. (B) Just below the critical temperature: Spherically shaped, thermal cloud with elliptic condensate peak on top. (C) Even lower temperature: The thermal cloud has almost vanished and only the elliptic condensate peak remains.

then distribute according to the lattice periodicity due to the same light-matter interaction as for the optical traps. Optical lattices are very flexible in the properties, such as the lattice depth, the lattice constant, and the lattice structure. All these parameters can experimentally be tuned in a comparatively simple way by adjusting the laser frequencies and intensities. Furthermore a so-called Mott-Superfluid quantum phase transition within an optical lattice is possible. The Mott phase and the superfluid phase are inherently different in their excitation spectra. The Mott phase has an energy gap, whereas the superfluid phase exhibits a Goldstone mode. By slightly tilting the optical lattice the bosons either start to flow due to their Goldstone excitations in the superfluid phase or they are locked due to the energy gap in the Mott phase. This is how the location of the quantum phase transition is measured [6–8]. The two phases are schematically depicted in Fig. 1.2 taken from Ref. [9]. In a shallow lattice the atoms are in the superfluid phase and are allowed to hop between the sites. Their number at one site is uncertain. However there is global phase coherence and their phase is determined. By increasing the lattice depth one passes the Mott-Superfluid transition. The number of atoms per site is now strictly integer valued and the same for all sites. But this completely destroys the phase coherence and no matter-wave exists any more.

1.3 Ultracold regime

The Doppler laser cooling is the first method to reach low temperatures in experiments. However, there is a certain limit when approaching lower temperatures. We explain this following Ref. [10]. The key feature of Doppler cooling is the spontaneous emission of formerly absorbed photons in random directions. Therefore the mean velocity of the ensemble vanishes which corresponds to a cooling effect. However the mean square velocity does not average out due to a remaining momentum of the atoms and a heating occurs. At equilibrium the two effects cancel and one is able to find a minimum temperature $T_D = \hbar\Gamma/2k_B$ which is

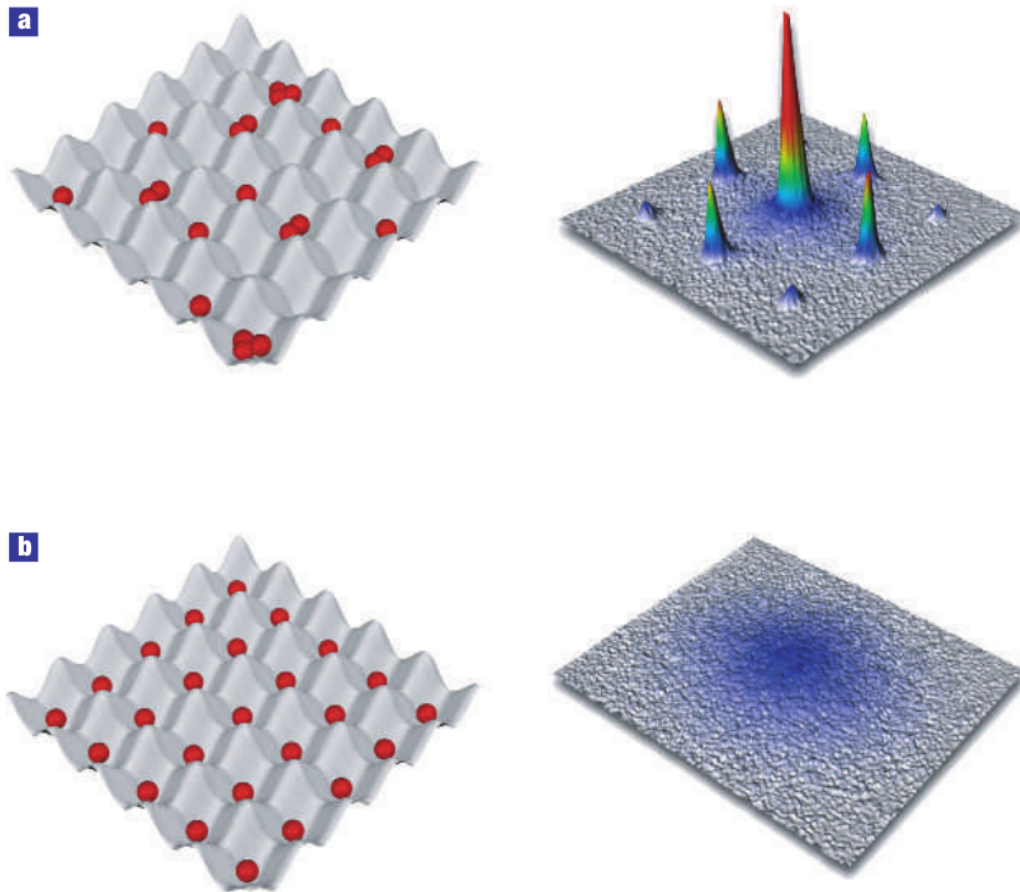


Figure 1.2: Schematic superfluid and Mott insulator within an optical lattice reproduced from Ref. [9]: **a** Superfluid phase: The number of particles per site is uncertain but the phase is coherent over the whole system. The particles are delocalized in configuration space but are localized in momentum space. **b** Mott insulating phase: The number of particles per site is determined, thus there is no phase coherence and the particles are localized in configuration space but not in momentum space.

the limit of Doppler cooling. Here Γ denotes the spectral linewidth of the laser and k_B stands for the Boltzmann constant. In order to reach temperatures beyond T_D one makes use of different techniques like evaporative cooling. Furthermore an important energy scale in the context of BEC is given by the recoil energy $E_r = \hbar^2 k_L^2 / 2M$, where \hbar denotes the reduced Planck constant, k_L represents the wavevector of a photon of the surrounding light field, and M stands for the atomic mass. The recoil energy denotes the energy which an atom gains by absorbing a photon of the light field. The terms "cold" and "ultracold" can now be distinguished by the following definition from Ref. [11]: Systems wherein the thermal energy is below the Doppler energy and above the recoil energy $k_B T_D > k_B T > E_r$ are said to be cold, whereas those with a thermal energy below the recoil energy $k_B T < E_r$ are called ultracold. In an optical lattice a typical value of the Doppler temperature ranges at about $100 \mu\text{K}$, whereas the recoil temperature $T_r = E_r / k_B$ is about thousand time less. Correspondingly we turn to a brief numerical example for ^{87}Rb atoms in an optical lattice with a wavelength of $\lambda = 780 \text{ nm}$. The natural linewidth of the rubidium $5S_{1/2} \rightarrow 5P_{3/2}$ transition is about $2\pi \times 6 \text{ MHz}$ [12]. This yields a Doppler temperature of $T_D \approx 144 \mu\text{K}$. For the recoil temperature, however, we obtain $T_r \approx 184 \text{ nK}$ using the laser frequency and the wavevector of the optical lattice $k_L = 2\pi/\lambda$. Thus, we find a ratio of the respective temperature of about $T_D/T_r \approx 782$. We try to derive this value for the temperature ratio by using the classical prediction of the linewidth

1 Introduction

of spontaneous emission. According to Ref. [13, §86. (5)] it reads $\Gamma = e^2\omega^2/6\pi\epsilon_0M_e c^3$ when transferred to the proper unit system. Here e denotes the unit charge, ω the atomic transition frequency, ϵ_0 the vacuum permittivity, M_e the electron mass, and c the speed of light. Furthermore we approximate that the necessary detuning between transition frequency and laser frequency is small and can thus be neglected. Upon using all this we find the temperature ratio to be $T_D/T_r = 2M\alpha/3M_e$, where $\alpha = e^2/4\pi\epsilon_0c\hbar$ denotes the Sommerfeld fine-structure constant, which equals approximately $\alpha \approx 1/137$. Hence we theoretically find for the temperature ratio $T_D/T_r \approx 777$ in good agreement with the above mentioned example.

In order to motivate this thesis we now turn to dimensional phase transitions in the context of ultracold atoms.

1.4 Dimensional phase transitions

Common physical experiments take place in one, two, and three dimensions. Due to a certain confinement the dimensionality of our usual three-dimensional world can be reduced as is demonstrated, for instance, by one-dimensional carbon nanotubes [14, 15], and two-dimensional graphene layers [16]. Furthermore, physics in those lower dimensions can be quite different from the 3D case. For example repulsive bosons in one dimension form for strong interactions a Tonks-Girardeau gas, which corresponds to a non-interacting Fermi gas [17], and in two dimensions they form a state of vortex-antivortex pairs at the Berezinskii-Kosterlitz-Thouless transition temperature [18]. In 2004 the one-dimensional Tonks-Girardeau gas [19] and in 2006 the two-dimensional Berezinskii-Kosterlitz-Thouless transition [20] have been observed in the context of ultracold quantum gases. The lack of certain spatial degrees of freedom causes higher importance of phase fluctuations in the physical systems. This is elaborated in the Mermin-Wagner-Hohenberg theorem [21, 22], which states that for a homogeneous system there is no phase transition of a continuous, broken symmetry at finite temperature in one and two dimensions. Especially there is no Bose-Einstein condensation (BEC) at finite temperature in one- and two-dimensional, homogeneous systems. However the existence of the homogeneous BEC in three dimensions has been theoretically studied very well. In the presence of a confinement, i.e. breaking the translational invariance, the Mermin-Wagner-Hohenberg theorem does not hold any more. Therefore low-dimensional BEC can be observed in a confining, commonly harmonic trap. By deforming the BEC cloud with an anisotropic trapping potential it is possible to reduce the dimensionality. Experimental examples for low dimensional BECs are Ref. [23] in two dimensions and Ref. [24] in one and two dimensions.

Dimensional phase transitions which are realized by such a potential deformation we call potential dimensional phase transition. In this thesis we want to follow another approach which we call kinetic dimensional phase transition. To this end we exploit the possibilities of an optical lattice which is loaded with bosons. By varying the hopping energies between the neighboring lattice sites we effectively vary the kinetic energy of the bosons. As a result one and two dimensions can be modeled without using an anisotropic confining trap. This has already been done experimentally in Ref. [1].

This work basically connects the theory of BEC on a lattice - governed by the Bose-Hubbard model - and the physics of low dimensions in order to investigate the kinetic dimensional phase transitions of bosons in optical lattices.

1.5 Structure of this thesis

We will initiate this work with a theoretical background in Chapter 2 including a derivation of the Mermin-Wagner-Hohenberg theorem. To give a basic understanding of dimensional phase transitions of the Bose gas we will first of all focus on non-interacting systems. Therein we will start with the investigation of the homogeneous case for which the Mermin-Wagner-Hohenberg theorem is applicable in Chapter 3 and show results in Chapter 4. Hereafter we will turn to the case of harmonically trapped bosons in Chapter 5. Afterwards we discuss the many-body problem of a weakly interacting Bose gas in the scope of dimensional phase transitions in Chapter 6. To this end we will make use of the Hartree-Fock-Bogoliubov-Popov theory (HFBP). Eventually in Chapter 7 we compare our theory with experimental data of Ref. [1]. For this purpose we will introduce a hybrid model which consists of two lattice dimensions and one continuous dimension. We will use the HFBP theory as an improvement to a pure Hartree-Fock theory (HF) to compute the critical chemical potential during the $1D$ - $3D$ -phase transition. Furthermore, in order to use hopping energies and interaction strengths over the whole dimensional range, we calculate them using numerically exact Wannier functions. Finally, Chapters 8 and 9 summarize our results and provide an outlook for possible, related studies.

2 Theoretical background

In this chapter we review the theoretical background for our approach. We start with the peculiar role of low dimensions and a derivation of the seminal Mermin-Wagner-Hohenberg theorem. Then we introduce optical lattices, and eventually present our method of continuously changing the dimensionality of the system.

2.1 Low dimensions

The Bose-Einstein condensation of a homogeneous Bose gas in three dimensions is well studied. It occurs in the non-interacting case below a critical temperature T_c such that $n\lambda_T^3 \gtrsim 2.6$ [25,26], where n denotes the particle density in the system and $\lambda_T = h/\sqrt{2\pi M k_B T}$ stands for the thermal de Broglie wavelength. Here h denotes the Planck constant and T stands for the temperature. Remarkably homogeneous BEC does not occur in low dimensions, i.e. in one or two dimensions, at finite temperature as it does in three dimensions. In the following paragraph we briefly justify this statement following Refs. [26,27]. The macroscopic number of non-interacting bosonic particles N in the system can be represented by

$$N = \int_0^\infty d\epsilon g(\epsilon) f_{\text{BE}}(\epsilon). \quad (2.1)$$

Here $g(\epsilon)$ is the density of states, $f_{\text{BE}}(\epsilon) = \{\exp[\beta(\epsilon - \mu)] - 1\}^{-1}$ represents the statistical Bose-Einstein distribution, and ϵ denotes the energy of the system. The density of states $g(\epsilon)$ as a function of energy differs very much in different dimensions. In fact it can be computed to satisfy a power law

$$g(\epsilon) = C_\alpha \epsilon^{\alpha-1} \quad (2.2)$$

where in the homogeneous case $\alpha = D/2$ with D being the dimension of the system and C_α is some prefactor. We notice that $g(0)$ vanishes only in three dimensions. This is the reason why a macroscopic amount of particles can occupy the lowest lying state. In low dimensions $g(\epsilon) > 0$ for all ϵ such that a macroscopic, i.e. diverging, occupation is not possible, while demanding a finite number of particles. We note that in two dimensions the density of states is even independent of the energy. This is the marginal situation and it turns out to possess no true BEC at finite temperatures. Therefore there is no homogeneous BEC in low dimensions. However for a harmonically trapped Bose gas it turns out within the semi-classical approximation that $\alpha = D$ and BEC is also possible in the low-dimensional case at finite temperature. Here the marginal situation is in one dimension since the density of states is then constant as it was in the two-dimensional homogeneous system. The important difference between these marginal cases is, however, that in the harmonically confined Bose gas the energy levels are discrete such that a macroscopic occupation is energetically enhanced and thus BEC can occur [26].

The reason for the peculiar role of low dimensions is the enhanced importance of phase fluctuations, which destroy coherence among the quantum particles and therefore BEC itself. Referring to Ref. [27] the phase fluctuations can be approximated by

$$\langle \phi^2 \rangle \simeq \frac{M k_B T}{N \hbar^2} \frac{V_D}{(2\pi)^D} \int d^D k \frac{1}{k^2} \quad (2.3)$$

2 Theoretical background

where $\hbar = h/2\pi$ denotes the reduced Planck constant and V_D represents the D -dimensional volume of the system. The remarkable point here is that the last integral is infrared divergent in one and two dimensions, but it is not in three dimensions.

2.2 Mermin-Wagner-Hohenberg theorem

The Mermin-Wagner-Hohenberg theorem, separately formulated by Mermin and Wagner [21] and Hohenberg [22], states for homogeneous systems that there is no phase transition at finite temperature in one and two dimensions. Since it is crucial for our investigation of dimensional phase transition we now provide a derivation of the theorem according to Ref. [26] for bosons at finite temperature. It is based on the Bogoliubov inequality which we proof at first and use afterwards to derive the actual theorem.

2.2.1 Bogoliubov inequality

The Bogoliubov inequality reads

$$\langle \{\hat{A}, \hat{A}^\dagger\} \rangle \langle [\hat{B}^\dagger, [\hat{H}, \hat{B}]] \rangle \geq 2k_B T |\langle [\hat{A}, \hat{B}] \rangle|^2, \quad (2.4)$$

where \hat{A} and \hat{B} represent arbitrary operators, \hat{H} denotes the Hamiltonian of the system, and the anticommutator and commutator are defined as

$$\{\hat{A}, \hat{B}\} = \hat{A}\hat{B} + \hat{B}\hat{A}, \quad [\hat{A}, \hat{B}] = \hat{A}\hat{B} - \hat{B}\hat{A}. \quad (2.5)$$

The thermal average in bra-ket notation is given by

$$\langle \hat{O} \rangle = \sum_m p_m \langle m | \hat{O} | m \rangle, \quad p_m = \frac{e^{-\beta E_m}}{\text{Tr} e^{-\beta \hat{H}}}. \quad (2.6)$$

Here $\beta = 1/k_B T$ denotes the inverse temperature, $\text{Tr} \hat{A}$ stands for the trace of the operator \hat{A} , and $|m\rangle$ and E_m represent the eigenstates and eigenvalues of \hat{H} , respectively. The eigenstates satisfy the completeness relation

$$\sum_m |m\rangle \langle m| = \hat{1}. \quad (2.7)$$

We will first proof Bogoliubov's inequality (2.4). For this we define an inner product [21]:

$$(\hat{A}, \hat{B}) := \sum_{m,n} \langle m | \hat{A} | n \rangle^* \langle m | \hat{B} | n \rangle \frac{p_m - p_n}{E_n - E_m}, \quad (2.8)$$

which satisfies the Schwarz-Cauchy inequality

$$(\hat{A}, \hat{A})(\hat{C}, \hat{C}) \geq |(\hat{A}, \hat{C})|^2, \quad (2.9)$$

where \hat{C} is another arbitrary operator and the asterisk $*$ denotes complex conjugation. In order to proof (2.4) we subsequently calculate all three inner products of (2.9). We start with (\hat{A}, \hat{A}) :

$$(\hat{A}, \hat{A}) = \sum_{m,n} |\langle m | \hat{A} | n \rangle|^2 \frac{p_m - p_n}{E_n - E_m}, \quad (2.10)$$

for which we find an upper boundary as follows. To this end we use $\tanh(x)/x \leq 1$ and set $x = \beta(E_m - E_n)/2$:

$$\begin{aligned} \frac{\tanh \left[\frac{\beta}{2}(E_m - E_n) \right]}{\frac{\beta}{2}(E_m - E_n)} &= \frac{2}{\beta(E_m - E_n)} \frac{e^{\beta(E_m - E_n)/2} - e^{-\beta(E_m - E_n)/2}}{e^{\beta(E_m - E_n)/2} + e^{-\beta(E_m - E_n)/2}} \\ &= \frac{2}{\beta(E_m - E_n)} \frac{p_n - p_m}{p_n + p_m} \leq 1. \end{aligned} \quad (2.11)$$

Thus we find

$$\frac{p_m - p_n}{E_n - E_m} \leq \frac{\beta}{2}(p_m + p_n). \quad (2.12)$$

Upon inserting (2.12) into (2.10) and using (2.7) we obtain

$$\begin{aligned} (\hat{A}, \hat{A}) &\leq \frac{\beta}{2} \sum_{m,n} |\langle m|\hat{A}|n\rangle|^2 (p_m + p_n) = \frac{\beta}{2} \left[\sum_m p_m \langle m|\hat{A}\hat{A}^\dagger|m\rangle + \sum_n p_n \langle n|\hat{A}^\dagger\hat{A}|n\rangle \right] \\ &= \frac{\beta}{2} \langle \{\hat{A}, \hat{A}^\dagger\} \rangle. \end{aligned} \quad (2.13)$$

Now we set $\hat{C} = [\hat{B}^\dagger, \hat{H}]$ and calculate (\hat{C}, \hat{C}) :

$$\begin{aligned} (\hat{C}, \hat{C}) &= \sum_{m,n} \langle m|\hat{C}|n\rangle^* \langle m|[\hat{B}^\dagger, \hat{H}]|n\rangle \frac{p_m - p_n}{E_n - E_m} \\ &= \sum_{m,n} \langle m|\hat{C}|n\rangle^* \left(\langle m|\hat{B}^\dagger\hat{H}|n\rangle - \langle m|\hat{H}\hat{B}^\dagger|n\rangle \right) \frac{p_m - p_n}{E_n - E_m} \\ &= \sum_{m,n} \langle n|\hat{C}^\dagger|m\rangle \langle m|\hat{B}^\dagger|n\rangle (p_m - p_n) \\ &= - \langle [\hat{C}^\dagger, \hat{B}^\dagger] \rangle = \langle [\hat{B}^\dagger, [\hat{H}, \hat{B}]] \rangle, \end{aligned} \quad (2.14)$$

where we used that $|n\rangle$ and $\langle m|$ are eigenvectors of \hat{H} in the third line and (2.7) in the last line. The third inner product is computed as

$$\begin{aligned} (\hat{A}, \hat{C}) &= \sum_{m,n} \langle m|\hat{A}|n\rangle^* \langle m|[\hat{B}^\dagger, \hat{H}]|n\rangle \frac{p_m - p_n}{E_n - E_m} \\ &= \sum_{m,n} \langle n|\hat{A}^\dagger|m\rangle \langle m|\hat{B}^\dagger|n\rangle (p_m - p_n) \\ &= - \langle [\hat{A}^\dagger, \hat{B}^\dagger] \rangle = \langle [\hat{A}, \hat{B}] \rangle^*. \end{aligned} \quad (2.15)$$

Inserting (2.13) – (2.15) into (2.9) leads to (2.4), which is thus proofed.

2.2.2 Derivation of the Mermin-Wagner-Hohenberg theorem

In order to derive the Mermin-Wagner-Hohenberg theorem we set the operators in (2.4)

$$\hat{A} = \hat{b}_p^\dagger, \quad \hat{B} = \hat{\rho}_p := \sum_k \hat{b}_k^\dagger \hat{b}_{k+p}, \quad (2.16)$$

where \hat{b}_p^\dagger (\hat{b}_p) creates (annihilates) a boson with wavenumber p . The corresponding commutation relations are

$$[\hat{b}_p, \hat{b}_k^\dagger] = \delta_{p,k}, \quad [\hat{b}_p, \hat{b}_k] = [\hat{b}_p^\dagger, \hat{b}_k^\dagger] = 0, \quad (2.17)$$

in which $\delta_{p,k}$ denotes the Kronecker delta. The averaged anticommutator $\langle \{\hat{A}, \hat{A}^\dagger\} \rangle$ using (2.17) then reads

$$\langle \{\hat{A}, \hat{A}^\dagger\} \rangle = 2n_p + 1. \quad (2.18)$$

Here $n_p = \langle \hat{b}_p^\dagger \hat{b}_p \rangle$ represents the number of particles with wavenumber p in the system. In order to calculate the commutator $[\hat{B}^\dagger, [\hat{H}, \hat{B}]]$ from (2.4) we start with the Hamiltonian in

2 Theoretical background

momentum representation, which contains both the single-particle dispersion ϵ_p and the two-body interaction V_k

$$\begin{aligned}\hat{H} &= \sum_p \epsilon_p \hat{b}_p^\dagger \hat{b}_p + \frac{1}{2} \sum_{k,p,q} V_k \hat{b}_{p-k}^\dagger \hat{b}_{q+k}^\dagger \hat{b}_p \hat{b}_q \\ &= \sum_p \epsilon_p \hat{b}_p^\dagger \hat{b}_p + \frac{1}{2} \sum_k V_k \hat{\rho}_k^\dagger \hat{\rho}_k - \frac{1}{2} \hat{N} \sum_k V_k,\end{aligned}\tag{2.19}$$

where we used (2.16), (2.17), and the total number operator $\hat{N} = \sum_p \hat{b}_p^\dagger \hat{b}_p = \hat{\rho}_0$. Furthermore, we apply the commutation relations

$$[\hat{b}_p, \hat{\rho}_k] = \hat{b}_{p+k}, \quad [\hat{\rho}_k, \hat{b}_p^\dagger] = -\hat{b}_{p-k}^\dagger, \quad [\hat{\rho}_p, \hat{\rho}_k] = 0, \quad [\hat{N}, \hat{\rho}_p] = 0\tag{2.20}$$

as well as $\hat{\rho}_p^\dagger = \hat{\rho}_{-p}$ in order to find

$$\begin{aligned}[\hat{H}, \hat{\rho}_p] &= \sum_k (\epsilon_k - \epsilon_{k+p}) \hat{b}_k^\dagger \hat{b}_{k+p}, \\ [\hat{\rho}_p^\dagger, [\hat{H}, \hat{\rho}_p]] &= \sum_k (\epsilon_{k+p} - 2\epsilon_k + \epsilon_{k-p}) \hat{b}_k^\dagger \hat{b}_k.\end{aligned}\tag{2.21}$$

Upon substituting the homogeneous single-particle dispersion relation $\epsilon_k = \hbar^2 k^2 / 2M$ in (2.21) we obtain

$$[\hat{\rho}_p^\dagger, [\hat{H}, \hat{\rho}_p]] = \frac{\hbar^2 p^2}{M} \hat{N}.\tag{2.22}$$

The last commutator in (2.4) using (2.20) results in

$$[\hat{b}_p^\dagger, \hat{\rho}_p] = -\hat{b}_0^\dagger.\tag{2.23}$$

We now insert (2.18), (2.22), and (2.23) into the Bogoliubov inequality (2.4) and rearrange it. Thus we obtain

$$n_p \geq \frac{k_B T M |\langle \hat{b}_0 \rangle|^2}{N \hbar^2 p^2} - \frac{1}{2}.\tag{2.24}$$

Summing over all momenta p provides the total number of particles on the left-hand side. We observe that the right-hand side is infrared divergent in one and two dimensions given $T \neq 0$ and $\langle \hat{b}_0 \rangle \neq 0$. Since the right-hand side is a lower boundary for the number of particles this leads to a contradiction to a finite number of particles in the system. Since $\langle \hat{b}_0 \rangle$ is the order parameter for BEC we conclude that there is no BEC at finite temperatures in one and two dimensions.

The aim of this work is to show how the critical temperature of BEC grows to a finite value when we continuously change the dimensionality of the system from low dimensions to three dimensions. This we are going to realize using optical lattices of which we will tune the hopping energies in a certain manner such that we can continuously change the dimensionality of the system. Hence we now turn to the theory of optical lattices.

2.3 Optical lattices and Bloch dispersion

Optical lattices are a great technique in the field of cold atoms and quantum optics. With their experimental realization optical lattices on the one hand are a candidate for a quantum simulator [28], on the other hand they are versatile in use for quantum gases. It is the

flexibility of the lattice depth, the hopping, and the dimensionality which makes them so useful for the investigation of quantum gases. Furthermore they can be experimentally realized using lasers. Essential for optical lattices as well as for confining optical traps is the force which light exerts on atoms [9]. The force of coherent light with frequency ω , which acts on the atom within the light field in the dipole approximation, is given by [25]

$$\mathbf{F}(\mathbf{r}) = \frac{1}{2}\alpha(\omega)\nabla I(\mathbf{r}). \quad (2.25)$$

Here $I(\mathbf{r})$ is the spatially varying intensity field and $\alpha(\omega)$ is the polarizability of the two-level atom which satisfies:

$$\alpha(\omega) \propto \frac{\omega_0}{\omega_0^2 - \omega^2}, \quad (2.26)$$

where $\hbar\omega_0$ is the energy of an atomic excitation. Please consult Ref. [29] for details. We see that the force (2.25) points towards the intensity minimum for a blue detuned laser light $\omega > \omega_0$ and towards the maximum for red detuned laser light $\omega < \omega_0$. A simple, one-dimensional, static optical lattice can be built using two counter-propagating laser beams of the same frequency. More complex lattices can be realized adding more laser pairs with different frequencies and rotation angles. For instance a cubic lattice is built aligning three laser pairs of the same frequency which are orthogonal to each another. The resulting periodic potential of a general, orthogonal optical lattice is then

$$V(\mathbf{r}) = \sum_{i=1}^D V_{0,i} \sin^2 \left(\frac{r_i}{a_i} \pi \right), \quad (2.27)$$

where $V_{0,i}$ is the lattice depth and a_i is the lattice constant in r_i -direction. The lattice depths $V_{0,i}$ are proportional to the applied laser intensities $I_i(\mathbf{r})$ and the lattice constants are half of the wavelengths λ_i of the laser, i.e. $a_i = \lambda_i/2$. We note that the properties of the lattice in one direction are completely independent of those in the other directions for an orthogonal lattice.

Atoms loaded in optical lattices are well described by the Bose-Hubbard model, which we will use to briefly derive the Bloch dispersion relation for quasi-bound particles. The principle idea for this dispersion relation comes from the solid-state physics of quasi-bound electrons in the periodic potential of a metallic crystal [30]. This emphasizes again the close relation of optical lattices and solid-state physics. Typically the Bose-Hubbard model is derived for a weakly interacting Bose gas on a lattice. Here we restrict ourselves to the non-interacting case and follow Refs. [31, 32]. The Hamiltonian in second-quantized form with $\hat{\psi}^\dagger(\mathbf{r})$ ($\hat{\psi}(\mathbf{r})$) being the creation (annihilation) operators reads

$$\hat{H} = \int d\mathbf{r} \hat{\psi}^\dagger(\mathbf{r}) \left[-\frac{\hbar^2}{2M} \nabla^2 + V(\mathbf{r}) \right] \hat{\psi}(\mathbf{r}). \quad (2.28)$$

Since we treat bosons, the creation and annihilation operators obey commutation relations

$$\left[\hat{\psi}(\mathbf{r}), \hat{\psi}^\dagger(\mathbf{r}') \right] = \delta(\mathbf{r} - \mathbf{r}'), \quad \left[\hat{\psi}(\mathbf{r}), \hat{\psi}(\mathbf{r}') \right] = \left[\hat{\psi}^\dagger(\mathbf{r}), \hat{\psi}^\dagger(\mathbf{r}') \right] = 0, \quad (2.29)$$

where $\delta(\mathbf{x})$ signifies the Dirac delta-function. Particles exposed to the periodic potential of a lattice possess a band structured dispersion relation due to the Bloch theorem. It states that the wavefunction of the n -th band within a lattice periodic in \mathbf{R} fulfills the periodicity

$$\phi_{n,k}(\mathbf{r}) = \frac{1}{\sqrt{V}} e^{i\mathbf{k}\mathbf{r}} u_{n,k}(\mathbf{r}), \quad u_{n,k}(\mathbf{r}) = u_{n,k}(\mathbf{r} + \mathbf{R}), \quad (2.30)$$

2 Theoretical background

where V signifies the volume of the system and \mathbf{k} is a vector of the reciprocal lattice. The Wannier functions $w_n(\mathbf{r} - \mathbf{r}_j)$ are the Fourier transforms of the Bloch wavefunctions

$$w_n(\mathbf{r} - \mathbf{r}_j) = \frac{1}{\sqrt{N_s}} \sum_{\mathbf{k} \in \text{BZ}} \phi_{n,\mathbf{k}}(\mathbf{r}) e^{-i\mathbf{r}_j \mathbf{k}}. \quad (2.31)$$

Here BZ stands for the first Brillouin zone and N_s signifies the number of sites in the lattice. The Wannier functions are localized in configuration space around $\mathbf{r} = \mathbf{r}_j$, they fall off exponentially fast, and they form an orthonormal set of wavefunctions

$$\int d\mathbf{r} w_n^*(\mathbf{r} - \mathbf{r}_j) w_m(\mathbf{r} - \mathbf{r}_l) = \delta_{n,m} \delta_{j,l}, \quad \sum_j \sum_n w_n^*(\mathbf{r} - \mathbf{r}_j) w_n(\mathbf{r}' - \mathbf{r}_j) = \delta(\mathbf{r} - \mathbf{r}'). \quad (2.32)$$

Thus we can decompose the creation and annihilation operators according to

$$\hat{\psi}^\dagger(\mathbf{r}) = \sum_{n,j} w_n^*(\mathbf{r} - \mathbf{r}_j) \hat{a}_{n,j}^\dagger, \quad \hat{\psi}(\mathbf{r}) = \sum_{n,j} w_n(\mathbf{r} - \mathbf{r}_j) \hat{a}_{n,j}, \quad (2.33)$$

where the sum over j runs over all lattice sites. The operator $\hat{a}_{n,j}^\dagger$ ($\hat{a}_{n,j}$) creates (annihilates) a particle in the n -th band at lattice site j and obeys the bosonic commutation relations

$$[\hat{a}_{n,j}, \hat{a}_{m,l}^\dagger] = \delta_{n,m} \delta_{j,l} \quad (2.34)$$

with all other commutators being zero. We can now rewrite (2.28) using (2.33)

$$\hat{H} = \sum_{j,l,n,n'} \hat{a}_{n,j}^\dagger \hat{a}_{n',l} \int d\mathbf{r} w_n^*(\mathbf{r} - \mathbf{r}_j) \left[-\frac{\hbar^2}{2M} \nabla^2 + V(\mathbf{r}) \right] w_{n'}(\mathbf{r} - \mathbf{r}_l). \quad (2.35)$$

Now we use that the Wannier functions decay exponentially fast and assume that they overlap only with their nearest neighbors. Since we deal with very low temperatures we may simplify even further by restricting to the lowest Bloch band only. Therefore, we will drop the band indices n and n' from now on. This gives us hence

$$\begin{aligned} \hat{H} \approx & \sum_{\langle j,l \rangle} \hat{a}_j^\dagger \hat{a}_l \int d\mathbf{r} w^*(\mathbf{r} - \mathbf{r}_j) \left[-\frac{\hbar^2}{2M} \nabla^2 + V(\mathbf{r}) \right] w(\mathbf{r} - \mathbf{r}_l) \\ & + \sum_j \hat{a}_j^\dagger \hat{a}_j \int d\mathbf{r} w^*(\mathbf{r} - \mathbf{r}_j) \left[-\frac{\hbar^2}{2M} \nabla^2 + V(\mathbf{r}) \right] w(\mathbf{r} - \mathbf{r}_j), \end{aligned} \quad (2.36)$$

where $\langle i, j \rangle$ denotes the sum over all nearest neighbor lattice site pairs. Note that there are 2D nearest neighbors in a cubic lattice. The Hamiltonian (2.36) can be diagonalized in (quasi)momentum basis

$$\hat{a}_j^\dagger = \frac{1}{\sqrt{N_s}} \sum_{\mathbf{k}} \hat{b}_{\mathbf{k}}^\dagger e^{i\mathbf{k} \mathbf{r}_j}, \quad \hat{a}_j = \frac{1}{\sqrt{N_s}} \sum_{\mathbf{k}} \hat{b}_{\mathbf{k}} e^{-i\mathbf{k} \mathbf{r}_j}, \quad (2.37)$$

where $\hat{b}_{\mathbf{k}}^\dagger$ and $\hat{b}_{\mathbf{k}}$ are the creation and annihilation operators, which obey the bosonic commutation relations (2.17). For a orthogonal lattice with lattice constants a_x , a_y , and a_z we obtain

$$\hat{H} \approx \sum_{\mathbf{k}} \hat{b}_{\mathbf{k}}^\dagger \hat{b}_{\mathbf{k}} \{ -2 [J_x \cos(k_x a_x) + J_y \cos(k_y a_y) + J_z \cos(k_z a_z)] + \mu' \}. \quad (2.38)$$

The respective hopping energies J_i and the energy offset μ' [33] are defined as

$$J_i = - \int d\mathbf{r} w^*(\mathbf{r}) \left[-\frac{\hbar^2}{2M} \nabla^2 + V(\mathbf{r}) \right] w(\mathbf{r} - a_i \mathbf{e}_i), \quad (2.39)$$

$$\mu' = \int d\mathbf{r} w^*(\mathbf{r}) \left[-\frac{\hbar^2}{2M} \nabla^2 + V(\mathbf{r}) \right] w(\mathbf{r}). \quad (2.40)$$

The hopping energy is an analog of the usual kinetic energy in the lattice describing the motion of the particle from site to site due to tunneling. In the limit $V_{0,i} \gg E_{ri}$ the hopping energy can be obtained from exact results of the one-dimensional Mathieu equation [34]. It is thus related to the experimental quantity of $V_{0,i}$ which corresponds to the laser intensity in \mathbf{e}_i -direction:

$$J_i = \frac{4}{\sqrt{\pi}} E_{ri} \left(\frac{V_{0,i}}{E_{ri}} \right)^{3/4} e^{-2\sqrt{V_{0,i}/E_{ri}}}. \quad (2.41)$$

Here E_{ri} is the recoil energy which represents a useful energy unit when dealing with optical lattices. It is the energy an atom gains when absorbing a photon of the optical lattice given by

$$E_{ri} = \frac{\hbar^2 k_{Li}^2}{2M} = \frac{\hbar^2 \pi^2}{2a_i^2 M} = \frac{h^2}{8a_i^2 M}. \quad (2.42)$$

In typical experiments the recoil energy is roughly of the order $E_r \approx h \times 25 \text{ kHz} \sim 10^{-10} \text{ eV}$ [9, 35]. The Hamiltonian (2.38) is diagonal and can be written as

$$\hat{H} = \sum_{\mathbf{k}} \hat{b}_{\mathbf{k}}^\dagger \hat{b}_{\mathbf{k}} (\epsilon_{\mathbf{k}} - \mu). \quad (2.43)$$

We specialize the so far treated three-dimensional orthogonal lattice to a three-dimensional cubic lattice with $a_x = a_y = a_z = a$. Hence, the recoil energy is the same for all three directions $E_{rx} = E_{ry} = E_{rz} = E_r$. Thus the Bloch dispersion within (2.43) for the lowest band in a cubic lattice follows as

$$\epsilon_{\mathbf{k}} = 2(J_x + J_y + J_z) - 2J_x \cos(k_x a) - 2J_y \cos(k_y a) - 2J_z \cos(k_z a). \quad (2.44)$$

We artificially shifted the dispersion relation by an energy offset

$$\mu = \mu' - 2(J_x + J_y + J_z), \quad (2.45)$$

in order to avoid negative energies such that $\epsilon(\mathbf{0}) = 0$. Note that the new chemical potential (2.45) corresponds to the real chemical potential with an constant energy offset. In the limit of a vanishing lattice constant we recover the quadratic dispersion of free particles

$$\lim_{a \rightarrow 0} \epsilon_{\mathbf{k}} = J_x (k_x a)^2 + J_y (k_y a)^2 + J_z (k_z a)^2, \quad (2.46)$$

so we can make the identification

$$J_i a^2 = \frac{\hbar^2}{2M_i^*}, \quad (2.47)$$

where M_i^* denotes the direction dependent effective mass of the particle within the lattice. Thus in the limit of a vanishing lattice the hopping energies diverge quadratically with respect to the lattice constant a and they are inversely proportional to the effective mass of the atom. To give a quick example of an effective mass we calculate it for the instance of a rubidium atom in an optical lattice with lattice constant $a = 387 \text{ nm}$. The atomic mass of rubidium is approximately $M = 1.42 \cdot 10^{-25} \text{ kg}$. For a shallow lattice depth of $V_0 = 5E_r$ the mass ratio is $M^*/M \approx 1.2$ thus the effective mass approximately corresponds to the atomic mass. However for a deep lattice $V_0 = 30E_r$ the effective mass becomes really heavy $M^*/M \approx 200$.

2 Theoretical background

2.4 Dimensional phase transition

In this section we discuss how a dimensional phase transition can be performed. The main aim is to continuously reduce the dimensionality of the common three-dimensional system. Within the field of cold quantum gases there are, in principle, two possibilities.

2.4.1 Potential dimensional transition

The first one makes use of the trapping technique of cold atoms through laser-induced optical traps. Since these optical traps are very flexible by only tuning the laser parameters one can arrange anisotropic optical traps. The approach to dimensional transitions through anisotropic traps has already been theoretically [36–39] and experimentally [40–45] investigated. In the case of anisotropic harmonic traps the effective potential of the trap to which the atom is exposed is

$$V(\mathbf{r}) = \frac{1}{2}M(\omega_x^2 x^2 + \omega_y^2 y^2 + \omega_z^2 z^2), \quad (2.48)$$

where ω_i represents the trap frequency in the spatial i -direction. In order to reduce the dimensionality one can squeeze one or two spatial dimensions by increasing the corresponding trap frequency. By increasing the trap frequency one increases the energy gap between the harmonic eigenstates

$$\Delta E_i = \hbar\omega_i. \quad (2.49)$$

For sufficiently cold gases the atoms occupy only the ground state in this direction and can not be thermally excited to higher states. Thus a particular degree of freedom is frozen and the dimensionality of the whole system is lowered. Since this transition is performed by externally manipulating the potential energy we call it potential dimensional phase transition. The computational disadvantage of the procedure is that one can not apply the semi-classical approximation for harmonic trapping potential of the frozen dimension.

2.4.2 Kinetic dimensional transition

The second way of changing the dimensionality is to make use of optical lattices discussed above. By tuning the laser intensity one can tune the hopping between neighboring lattice sites. A continuous variation of the hopping energies $\mathbf{J} = (J_x, J_y, J_z)$ allows for continuously changing the dimensionality. The pure integer dimensions are given as follows

$$D = \begin{cases} 3 & \text{if } J_i = J_j = J_k \neq 0 \\ 2 & \text{if } J_i = J_j \neq 0, \quad J_k = 0 \\ 1 & \text{if } J_i \neq 0, \quad J_j = J_k = 0. \end{cases} \quad (2.50)$$

Note that (2.50) contains a certain three-fold symmetry: There are three possibilities to get $D = 1$ or $D = 2$ but only one for $D = 3$.

2.4.3 Dimensional transition path

In order to model all three continuous transitions between the respective integer dimensions we set the values of \mathbf{J} to be on a sphere of radius $E = \sqrt{J_x^2 + J_y^2 + J_z^2}$ in the three-dimensional vector space of the hopping energies. On this sphere we choose a certain path which models exactly all the three dimensional transitions as depicted in Fig. 2.1. We assign a path parameter

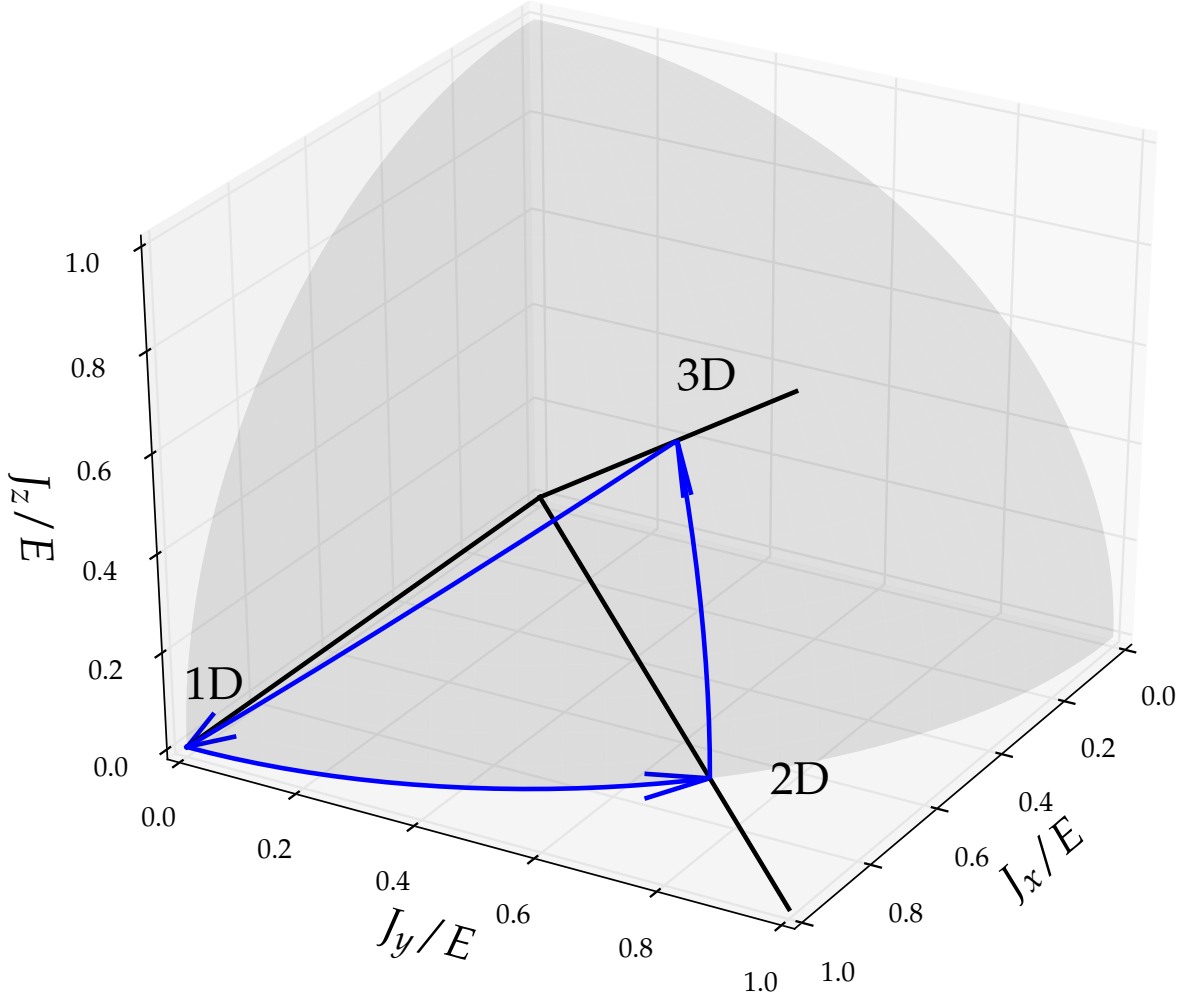


Figure 2.1: Dimensional transition path: chosen values of the path in the three-dimensional vector space are depicted in blue. The assigned path parameter λ goes from 0 to 3 and has values: $\lambda = 0, 3$ (1D), $\lambda = 1$ (2D), $\lambda = 2$ (3D).

λ to this distinct path. The relation between λ and J is

$$J(\lambda) = E \begin{cases} (\cos(\alpha_1 \lambda), \sin(\alpha_1 \lambda), 0) & ; 0 \leq \lambda \leq 1 \\ (\frac{1}{\sqrt{2}} \cos(\alpha_2(\lambda - 1)), \frac{1}{\sqrt{2}} \cos(\alpha_2(\lambda - 1)), \sin(\alpha_2(\lambda - 1))) & ; 1 \leq \lambda \leq 2 \\ (\cos(\alpha_3(3 - \lambda)), \frac{1}{\sqrt{2}} \sin(\alpha_3(3 - \lambda)), \frac{1}{\sqrt{2}} \sin(\alpha_3(3 - \lambda))) & ; 2 \leq \lambda \leq 3 \end{cases} \quad (2.51)$$

with $\alpha_1 = \frac{\pi}{4}$, $\alpha_2 = \sin^{-1} \frac{1}{\sqrt{3}}$, and $\alpha_3 = \sin^{-1} \sqrt{\frac{2}{3}}$. In this thesis we investigate the λ -dependence of various thermodynamic quantities of interest. The choice, that the transition path lies on a sphere as depicted in Fig. 2.1, is rather arbitrary. However it is motivated through the continuum limit (2.46) where we have quadratic contributions from each spatial dimension.

3 Non-interacting Bose gas in optical lattice with tunable hopping

In this chapter we focus on non-interacting bosons loaded into a cubic, optical lattice with tunable hopping energies. There will be no confining trap so we have the homogeneous case. The inhomogeneous case is treated later on in Chapter 5.

3.1 Free energy

In the following we derive the grand-canonical free energy of bosons in a cubic optical lattice with lattice constant a in order to determine the respective thermodynamic quantities of interest. Our starting point is the expression for the grand-canonical free energy for non-interacting bosons given in [46, (4.198)]

$$\mathcal{F} = -\mu N_0 + \frac{1}{\beta} \sum_{\mathbf{k}} \ln \left(1 - e^{-\beta(\epsilon_{\mathbf{k}} - \mu)} \right). \quad (3.1)$$

Here μ represents the chemical potential and N_0 is the number of condensed bosons. In order to evaluate (3.1) we can substitute the logarithm by its power series:

$$\ln(1 - e^{-x}) = - \sum_{m=1}^{\infty} \frac{1}{m} e^{-mx}. \quad (3.2)$$

Upon inserting (3.2) into (3.1) we obtain

$$\mathcal{F} = -\mu N_0 - \frac{1}{\beta} \sum_{\mathbf{k}} \sum_{m=1}^{\infty} \frac{1}{m} e^{-m\beta(\epsilon_{\mathbf{k}} - \mu)}. \quad (3.3)$$

We now exchange the \mathbf{k} -sum with the sum over the index m and perform the thermodynamic limit

$$\sum_{\mathbf{k}} \rightarrow \frac{V}{(2\pi)^3} \int d\mathbf{k}. \quad (3.4)$$

Hence we result in an integral over the first Brillouin zone due to the lattice

$$\mathcal{F} = -\mu N_0 - \frac{1}{\beta} \sum_{m=1}^{\infty} \frac{1}{m} \frac{V}{(2\pi)^3} \int_{\text{BZ}} d\mathbf{k} e^{-m\beta(\epsilon_{\mathbf{k}} - \mu)}. \quad (3.5)$$

Rearranging this equation gives

$$\mathcal{F} = -\mu N_0 - \frac{V}{(2\pi)^3 \beta} \sum_{m=1}^{\infty} \frac{1}{m} \int_{-\pi/a}^{\pi/a} dk_x \int_{-\pi/a}^{\pi/a} dk_y \int_{-\pi/a}^{\pi/a} dk_z e^{-m\beta(\epsilon_{\mathbf{k}} - \mu)}. \quad (3.6)$$

We make the quasi-momenta \mathbf{k} dimensionless according to the substitution $k_i a \rightarrow k_i$ with $i = x, y, z$. This leads to

$$\mathcal{F} = -\mu N_0 - \frac{V}{(2\pi a)^3 \beta} \sum_{m=1}^{\infty} \frac{1}{m} \int_{-\pi}^{\pi} dk_x \int_{-\pi}^{\pi} dk_y \int_{-\pi}^{\pi} dk_z e^{-m\beta(\epsilon_{\mathbf{k}} - \mu)}. \quad (3.7)$$

3 Non-interacting Bose gas in optical lattice with tunable hopping

We now insert the dispersion relation (2.44) and obtain

$$\mathcal{F} = -\mu N_0 - \frac{V}{(2\pi a)^3 \beta} \sum_{m=1}^{\infty} \frac{1}{m} e^{m\beta\mu} \prod_{i \in \{x,y,z\}} e^{-2m\beta J_i} \int_{-\pi}^{\pi} dk_i e^{2m\beta J_i \cos k_i}. \quad (3.8)$$

The value of the integral is given by the modified Bessel function of the first kind and order $\nu = 0$ [47, (9.6.19)]

$$I_0(x) = \frac{1}{2\pi} \int_{-\pi}^{\pi} dt e^{x \cos(t)}. \quad (3.9)$$

Upon inserting (3.9) into (3.8) we end up with an expression for the grand-canonical free energy, which consists of a product of exponentially damped modified Bessel functions for each of the three spatial dimensions:

$$\mathcal{F} = -\mu N_0 - \frac{V}{a^3 \beta} \sum_{m=1}^{\infty} \frac{1}{m} e^{m\beta\mu} \prod_{i \in \{x,y,z\}} e^{-2m\beta J_i} I_0(2m\beta J_i). \quad (3.10)$$

3.2 Thermodynamics

Having the expression for the grand-canonical free energy (3.10) we are now able to obtain all thermodynamic quantities by its derivatives. In this section we derive the average number of particles N , the internal energy U , and the isochoric heat capacity C_V . The indices i, j, k are always meant to run over x, y, z .

3.2.1 Number of particles

The average number of particles is given as [48, (2.7.16)]

$$N = - \left. \frac{\partial \mathcal{F}}{\partial \mu} \right|_{V, \beta}. \quad (3.11)$$

Applying (3.11) to (3.10) we get

$$N = N_0 + \frac{V}{a^3} \sum_{m=1}^{\infty} e^{m\beta\mu} \prod_i e^{-2m\beta J_i} I_0(2m\beta J_i). \quad (3.12)$$

Here we observe that the total number of particles is the sum of the number of condensed particles N_0 and the number of thermally excited particles. From (3.12) we later on extract the critical temperature of the BEC to normal gas transition. To do so we first need to identify the two phases.

3.2.2 Low- and high-temperature phase

In terms of a Landau theory of phase transitions Bose-Einstein condensation occurs when the order parameter becomes non-zero. We identify the order parameter in this scope as the ground state amplitude ψ_0 of the condensate. Its absolute value squared is interpreted as the number of condensate particles $N_0 = \psi_0^* \psi_0$. Within the Landau formalism the correct order parameter must extremize the free energy according to $\partial_{\psi_0^*} \mathcal{F} = 0$. Applying this criterion to (3.10) this leads to two solutions

$$\psi_0 \mu = 0 \quad \Rightarrow \quad \begin{cases} \psi_0 = 0 \Rightarrow N_0 = 0 \text{ and } \mu \neq 0 & : \text{ normal gas phase} \\ \mu = 0 \text{ and } N_0 > 0 & : \text{ BEC phase.} \end{cases} \quad (3.13)$$

Since BEC occurs at low temperatures, the BEC phase and the normal gas phase correspond to high- and low-temperature phase, respectively. The particle number equation (3.12) determines μ in the gas phase and N_0 in the BEC phase.

3.2.3 Critical temperature

The phase transition between the two phases described in Sec. 3.2.2 occurs at the critical temperature $T = T_c$. Due to the constraints on the two phases both the chemical potential μ and the number of condensed particles N_0 must vanish at $T = T_c$. Using this in (3.12) we obtain an implicit equation for the critical temperature $\beta_c = 1/k_B T_c$ as function of the hopping parameters J and the total number of particles N :

$$N = \frac{V}{a^3} \sum_{m=1}^{\infty} \prod_i e^{-2m\beta_c(J)J_i} I_0(2m\beta_c(J)J_i). \quad (3.14)$$

This equation must be solved numerically for general J , which we do in Sec. 4.1. It is convenient to define the number of particles per lattice site with n being the total particle density:

$$\bar{n} = \frac{N}{N_s} = N \frac{a^3}{V} = na^3. \quad (3.15)$$

This quantity is also known as the filling factor.

3.2.4 Critical temperature in low dimensions

Through a short analytic investigation we will show that there can not be a finite value for T_c if $D = 1, 2$. For this purpose we set

$$J(\lambda) = (J_x, J_y, 0) \text{ with } J_x > 0, J_y \geq 0, \quad (3.16)$$

such that we are in one dimension if $J_y = 0$ and in two dimensions if $J_y = J_x$. We insert (3.16) into (3.14) and use the property $I_0(0) = 1$ in order to obtain with (3.15)

$$\bar{n} = \sum_{m=1}^{\infty} e^{-2m\beta_c(J_x+J_y)} I_0(2m\beta_c J_x) I_0(2m\beta_c J_y). \quad (3.17)$$

We can decompose this sum into two contributions, where the first one contains the first m_c summands with m_c being large and the second one contains the infinitely many rest summands:

$$\bar{n} = \bar{n}^{(m_c)} + \sum_{m=m_c+1}^{\infty} e^{-2m\beta_c(J_x+J_y)} I_0(2m\beta_c J_x) I_0(2m\beta_c J_y). \quad (3.18)$$

In the second contribution the m -index is large, since m_c is chosen to be sufficiently large. Thus we can use the asymptotic form of the Bessel functions [47, (9.7.1)]

$$I_\nu(x) = \frac{e^x}{\sqrt{2\pi x}} \left[1 + \mathcal{O}\left(\frac{1}{x}\right) \right], \quad x \rightarrow \infty. \quad (3.19)$$

In the 2D case this leads to

$$\sum_{m=m_c+1}^{\infty} e^{-2m\beta_c(J_x+J_y)} I_0(2m\beta_c J_x) I_0(2m\beta_c J_y) = \frac{1}{4\pi\beta_c\sqrt{J_x J_y}} \sum_{m=m_c+1}^{\infty} \frac{1}{m}. \quad (3.20)$$

But this series does not converge for finite β_c such that the critical temperature must vanish. In the 1D case $J_y = 0$ and therefore we find

$$\sum_{m=m_c+1}^{\infty} e^{-2m\beta_c J_x} I_0(2m\beta_c J_x) = \frac{1}{\sqrt{4\pi\beta_c J_x}} \sum_{m=m_c+1}^{\infty} \frac{1}{m^{1/2}}, \quad (3.21)$$

using $I_0(0) = 1$ and the same argument as in the 2D case holds.

3 Non-interacting Bose gas in optical lattice with tunable hopping

3.2.5 Internal energy

Now we aim at computing the heat capacity of bosons in the lattice. For this we first need an expression for the internal energy U . According to Ref. [48, (2.7.14)] this is

$$U = \mathcal{F} + TS + \mu N, \quad (3.22)$$

where S , the entropy of the system is given as [48, (2.7.16)]

$$S = - \left. \frac{\partial \mathcal{F}}{\partial T} \right|_{V, \mu}. \quad (3.23)$$

For convenience we rearrange (3.23) in order to calculate the second term of the right-hand side of (3.22)

$$TS = -T \left. \frac{\partial \mathcal{F}}{\partial T} \right|_{V, \mu} = -T \frac{\partial \beta}{\partial T} \left. \frac{\partial \mathcal{F}}{\partial \beta} \right|_{V, \mu} = T \frac{1}{k_B T^2} \left. \frac{\partial \mathcal{F}}{\partial \beta} \right|_{V, \mu} = \beta \left. \frac{\partial \mathcal{F}}{\partial \beta} \right|_{V, \mu}. \quad (3.24)$$

The derivative of the Bessel function of order $\nu = 0$ is given by $I'_0(x) = I_1(x)$ according to Ref. [47, (9.6.27)]. From (3.10) we calculate the entropy term to be

$$TS = \frac{V}{a^3} \sum_{m=1}^{\infty} e^{m\beta\mu} \left\{ \left[\frac{1}{\beta m} - \mu \right] \prod_i e^{-2m\beta J_i} I_0(2m\beta J_i) + \sum_i J_i e^{-2m\beta J_i} [I_1(2m\beta J_i) - I_0(2m\beta J_i)] \prod_{j \neq i} e^{-2m\beta J_j} I_0(2m\beta J_j) \right\}. \quad (3.25)$$

Now we insert (3.10), (3.12), and (3.25) in (3.22) and obtain for the internal energy

$$U = 2 \frac{V}{a^3} \sum_{m=1}^{\infty} e^{m\beta\mu} \sum_i J_i e^{-2m\beta J_i} [I_0(2m\beta J_i) - I_1(2m\beta J_i)] \prod_{j \neq i} e^{-2m\beta J_j} I_0(2m\beta J_j). \quad (3.26)$$

3.2.6 Heat capacity

In the vicinity of the normal gas/BEC transition the heat capacity exhibits a characteristic peak as a function of the temperature. According to Ref. [48, (3.2.2a)] the isochoric heat capacity is

$$C_V = \left. \frac{\partial U}{\partial T} \right|_{V, N}. \quad (3.27)$$

Please note that the partial derivative is performed at constant number of particles N and not at constant chemical potential μ . Thus, the chemical potential itself has to be considered as a function of the temperature $\mu = \mu(\beta)$ for a fixed particle number. In order to take this explicitly into account, we rearrange (3.27):

$$C_V = \left. \frac{\partial \beta}{\partial T} \frac{\partial U}{\partial \beta} \right|_{V, N} = - \frac{1}{k_B T^2} \left. \frac{\partial U}{\partial \beta} \right|_{V, N} \Rightarrow \frac{C_V}{k_B} = -\beta^2 \left. \frac{\partial U}{\partial \beta} \right|_{V, N}. \quad (3.28)$$

Applying (3.28) to (3.26) leads to

$$\begin{aligned}
\frac{C_V}{k_B} = & -2\beta^2 \frac{V}{a^3} \sum_{m=1}^{\infty} m e^{m\beta\mu} \\
& \times \left\{ \left(e^{-\beta\mu} \partial_{\beta} e^{\beta\mu} \right)_{V,N} \sum_i J_i e^{-2m\beta J_i} [I_0(2m\beta J_i) - I_1(2m\beta J_i)] \prod_{i \neq j} e^{-2m\beta J_j} I_0(2m\beta J_j) \right. \\
& + 2 \sum_i J_i^2 e^{-2m\beta J_i} \left[-\frac{3}{2} I_0(2m\beta J_i) + 2I_1(2m\beta J_i) - \frac{1}{2} I_2(2m\beta J_i) \right] \\
& \times \prod_{i \neq j} e^{-2m\beta J_j} I_0(2m\beta J_j) + 2 \sum_i J_i e^{-2m\beta J_i} [I_0(2m\beta J_i) - I_1(2m\beta J_i)] \\
& \left. \times \prod_{i \neq j} e^{-2m\beta J_j} [I_0(2m\beta J_j) - I_1(2m\beta J_j)] \times \prod_{k \neq i,j} e^{-2m\beta J_k} I_0(2m\beta J_k) \right\}. \tag{3.29}
\end{aligned}$$

We need to determine the temperature derivative of μ , which appears in the second line of (3.29). This we can do by differentiating (3.12) with respect to T keeping V and N constant [46, (4.216)]. Thus we get

$$\begin{aligned}
\left(e^{-\beta\mu} \partial_{\beta} e^{\beta\mu} \right)_{V,N} = & \\
\frac{2 \sum_{m=1}^{\infty} m e^{m\beta\mu} \sum_i J_i e^{-2m\beta J_i} [I_0(2m\beta J_i) - I_1(2m\beta J_i)] \prod_{i \neq j} e^{-2m\beta J_j} I_0(2m\beta J_j)}{\sum_{m=1}^{\infty} m e^{m\beta\mu} \prod_i e^{-2m\beta J_i} I_0(2m\beta J_i)}, & \tag{3.30}
\end{aligned}$$

which is valid in the high-temperature phase. In the low-temperature phase it is zero since then the left-hand side of (3.30) is zero due to the vanishing chemical potential as described in Sec. 3.2.2.

3.2.7 Continuum limit

The results (3.12), (3.26), and (3.29) all apply for bosons in a lattice. We now show how to reach the familiar results of homogeneous, non-interacting low-temperature physics in the continuum limit, which is performed by shrinking the lattice constant $\lim_{a \rightarrow 0}$. At the same time the hopping energies J_i behave according to (2.47), i.e. they diverge quadratically in a , and we can set the effective mass equal to the atomic mass $M^* = M$. With this we get for the number of particles (3.12)

$$\begin{aligned}
N = N_0 + \lim_{a \rightarrow 0} \frac{V}{a^3} \sum_{m=1}^{\infty} e^{m\beta\mu} \prod_i e^{-2m\beta J_i} I_0(2m\beta J_i) \\
= N_0 + \lim_{a \rightarrow 0} \frac{V}{a^3} \sum_{m=1}^{\infty} e^{m\beta\mu} \left[e^{-\frac{m\beta\hbar^2}{Ma^2}} I_0 \left(\frac{m\beta\hbar^2}{Ma^2} \right) \right]^3. \tag{3.31}
\end{aligned}$$

Using (3.19) we find

$$N = N_0 + \frac{V}{(2\pi\beta\hbar^2/M)^{3/2}} \sum_{m=1}^{\infty} e^{m\beta\mu} = N_0 + \frac{V}{\lambda_T^3} \zeta_{\frac{3}{2}} \left(e^{m\beta\mu} \right). \tag{3.32}$$

Here $\zeta_{\nu}(x) = \sum_{m=1}^{\infty} x^m / m^{\nu}$ denotes the polylogarithm and λ_T is the thermal de Broglie wavelength defined in Sec. 3.2.4. The result (3.32) corresponds to the known result in the homogeneous continuum [46, (4.205)]. The limits of (3.26) and (3.29) are found analogously.

4 Results for homogeneous case

In this chapter we present the results of the thermodynamic quantities derived above for non-interacting bosons in an optical lattice.

4.1 Critical temperature as function of dimensionality

In Fig. 4.1 we show the resulting critical temperature T_c as a function of the path parameter λ . The blue curve is the numerical result of evaluating (3.12). Since the numerics diverges logarithmically slowly in the interval $\lambda \in [0, 1]$, we set T_c artificially to zero due to the arguments in Sec. 2.1. For the number of particles per lattice site we used the experimental value $\bar{n} = 0.77$ extracted from Ref. [1]. Therein a critical line density of $n_c^{1D} \approx 2 \text{ nm}^{-1}$ is measured. With a lattice constant of $a = 387 \text{ nm}$ this gives the just mentioned value of the filling factor of (3.15). The red curve in Fig. 4.1 is an analytic approximation of the critical temperature for $\lambda \gtrsim 2$, i.e. the $2D \rightarrow 3D$ transition close to two dimensions, which we derive as follows. Approximating the trigonometric functions to first order in (2.51) gives

$$J(\lambda) \approx E \left(\frac{1}{\sqrt{2}}, \frac{1}{\sqrt{2}}, \alpha_2(\lambda - 1) \right) \text{ at } \lambda \gtrsim 1. \quad (4.1)$$

Substituting this in (3.14) yields

$$\bar{n} = \sum_{m=1}^{\infty} e^{-2\sqrt{2}m\beta_c E} I_0^2(\sqrt{2}m\beta_c E) e^{-2m\beta_c E \alpha_2(\lambda-1)} I_0(2m\beta_c E \alpha_2(\lambda-1)). \quad (4.2)$$

The expansion of the Bessel function for small arguments is [47, (9.6.12)]

$$I_0(x) = 1 + \mathcal{O}(x^2). \quad (4.3)$$

Using the fact of Fig. 4.1 that T_c goes to zero, i.e. β_c goes to infinity, we insert (3.19) and (4.3) in (4.2), which leads to

$$\bar{n} = \sum_{m=1}^{\infty} \frac{1}{4\pi\sqrt{2}m\beta_c E} e^{-2m\beta_c E \alpha_2(\lambda-1)} = \frac{1}{4\pi\sqrt{2}\beta_c E} \zeta_1 \left(e^{-2\beta_c E \alpha_2(\lambda-1)} \right). \quad (4.4)$$

The limit of the composition of functions

$$\lim_{\beta\mu \nearrow 0} \zeta_\nu \left(e^{\beta\mu} \right) \quad (4.5)$$

is described by the Robinson formula [46, (4.267)]:

$$\zeta_\nu \left(e^{\beta\mu} \right) = \Gamma(1 - \nu) (-\beta\mu)^{\nu-1} + \sum_{k=0}^{\infty} \frac{(\beta\mu)^k}{k!} \zeta(\nu - k), \quad (4.6)$$

where $\zeta(\nu) = \sum_{m=1}^{\infty} m^{-\nu}$ represents the Riemann ζ -function and $\Gamma(x)$ denotes the Gamma function. The special case for $\nu = 1$ is given by Ref. [46, (4.294)]:

$$\zeta_1(e^{\beta\mu}) = -\ln(-\beta\mu) + \sum_{k=1}^{\infty} \frac{(\beta\mu)^k}{k!} \zeta(1 - k). \quad (4.7)$$

4 Results for homogeneous case

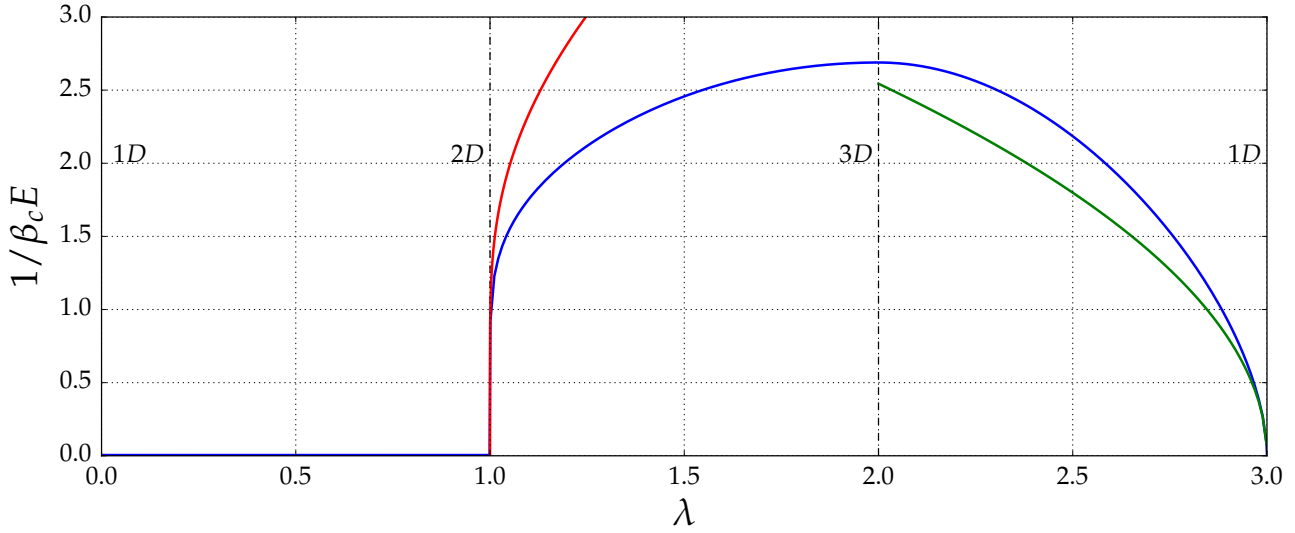


Figure 4.1: Critical temperature of homogeneous case as function of path parameter at $\bar{n} = 0.77$: the blue curve corresponds to numerical results, the red and green curve are analytic approximations (4.9) and (4.14) close to $D = 2$ and $D = 1$, respectively.

To lowest order we get for (4.5) with (4.7)

$$\lim_{\beta\mu \nearrow 0} \zeta_1 \left(e^{\beta\mu} \right) \approx -\ln(-\beta\mu). \quad (4.8)$$

Inserting this into (4.4) gives an implicit equation for T_c :

$$\bar{n} = -\frac{1}{4\pi\sqrt{2}\beta_c E} \ln[-2\beta_c E \alpha_2(\lambda - 1)], \quad \lambda \gtrsim 1. \quad (4.9)$$

Thus we obtain a logarithmic-like behavior in the $2D \rightarrow 3D$ transition. For the $3D \rightarrow 1D$ approximation, which is the green curve in Fig. 4.1, we expand again (2.51)

$$J(\lambda) \approx E \left(1, \frac{\alpha_3}{\sqrt{2}}(3 - \lambda), \frac{\alpha_3}{\sqrt{2}}(3 - \lambda) \right), \quad \lambda \lesssim 3. \quad (4.10)$$

Inserting this into (3.14) we get

$$\bar{n} = \sum_{m=1}^{\infty} e^{-2m\beta_c E} I_0(2m\beta_c E) e^{-4m\beta_c E \frac{\alpha_3}{\sqrt{2}}(3-\lambda)} I_0^2 \left(2m\beta_c E \frac{\alpha_3}{\sqrt{2}}(3 - \lambda) \right). \quad (4.11)$$

Now we use again (3.19), (4.3), and $\beta_c \rightarrow \infty$ leading to

$$\bar{n} = \sum_{m=1}^{\infty} \frac{1}{\sqrt{4\pi m\beta_c E}} e^{-4m\beta_c E \frac{\alpha_3}{\sqrt{2}}(3-\lambda)} = \frac{1}{\sqrt{4\pi\beta_c E}} \zeta_{\frac{1}{2}} \left(e^{-4\beta_c E \frac{\alpha_3}{\sqrt{2}}(3-\lambda)} \right). \quad (4.12)$$

We apply the Robinson formula (4.6) and keep only the leading term. Thus we get to lowest order

$$\bar{n} = \frac{\Gamma(\frac{1}{2})}{\sqrt{4\pi\beta_c E}} \left[4\beta_c E \frac{\alpha_3}{\sqrt{2}}(3 - \lambda) \right]^{-\frac{1}{2}}. \quad (4.13)$$

Using $\Gamma(\frac{1}{2}) = \sqrt{\pi}$ we rearrange the equation and obtain

$$T_c = \frac{4\bar{n}E}{k_B} \sqrt{\frac{\alpha_3}{\sqrt{2}}(3 - \lambda)}^{\frac{1}{2}}. \quad (4.14)$$

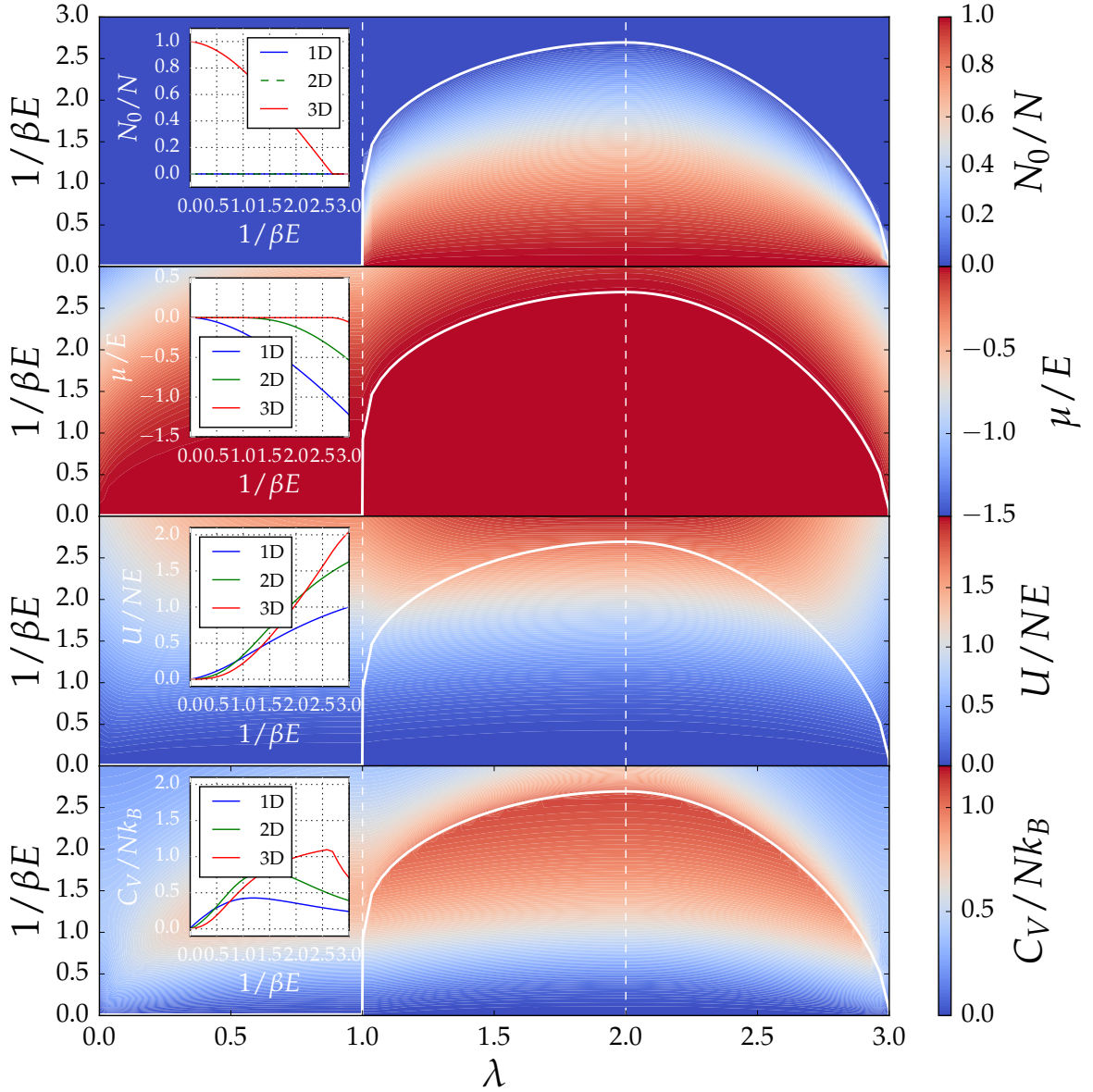


Figure 4.2: Thermodynamic quantities of homogeneous case as function of path parameter λ and temperature T at $\bar{n} = 0.77$: the white curve corresponds to the critical temperature T_c .

Therefore we can assign a power-law exponent $\frac{1}{2}$ for the increment of T_c when going from $D = 1$ to $D = 3$.

4.2 Thermodynamic quantities as function of dimensionality

In this section we discuss the numerical results leading to the condensate fraction, the chemical potential, the internal energy, and the heat capacity as functions of the dimensionality and the temperature.

To this end we show in Fig. 4.2 the respective thermodynamic quantities as function of λ and T . The result of the condensate fraction agrees with the Mermin-Wagner-Hohenberg theorem since we do not observe a BEC in low dimensions, i.e. $0 \leq \lambda \leq 1$. The chemical potential landscape is evaluated by solving implicitly (3.12) with the boundary conditions in (3.13). We use the result of the chemical potential to further compute the internal energy and the heat capacity. The internal energy is evaluated from (3.26). The heat capacity is the derivative of

4 Results for homogeneous case

the internal energy with respect to temperature. The analytical expression is given by (3.29) together with (3.30) and the resulting landscape in the T, λ -space is also presented in Fig. 4.2. Please note that the heat capacity converges to zero in the limit of high temperatures. This is a direct contradiction to the Dulong-Petit law which states that the heat capacity will saturate at the value of $fNk_B/2$ where f is the number of degrees of freedom. Thus the Dulong-Petit law is violated here. The reason for this is the lattice dispersion relation (2.44) of our approach. The Dulong-Petit law relies on the equipartition theorem that every quadratic degree of freedom has a average contribution of $k_B T/2$ to the internal energy at high temperatures. Since our dispersion is not quadratic, this does not hold here. Furthermore (2.44) has even an upper bound due to our restriction to the lowest Bloch band such that the internal energy will saturate and thus the heat capacity as its derivative has to vanish in the limit $T \rightarrow \infty$. Eventually we see that the heat capacity fulfills the third law of thermodynamics since it vanishes at $T = 0$.

5 Isotropic harmonic trap

In this chapter we repeat the considerations made above for the homogeneous case but now with an additional confining trapping potential. We restrict ourselves on investigating isotropic traps because we are only interested in the kinetic dimensional phase transitions as explained in Sec. 2.4.2. However anisotropic traps represent an elegant method to detect the existence of BEC, since after switching off the trapping potential, a BEC cloud expands keeping its anisotropic shape while a thermal clouds would expand isotropically [49].

5.1 Free energy and critical temperature

For the sake of brevity we skip the calculations and mention only the differences to the homogeneous case in Chapter 3. We assume a shallow trapping potential, thus we can make use of the semi-classical approximation. The dispersion (2.44) is now modified by adding an isotropic, harmonic potential as

$$\epsilon_k \rightarrow \epsilon_k + \frac{1}{2}M\omega^2(x^2 + y^2 + z^2). \quad (5.1)$$

Here ω denotes the trapping frequency. Since the potential is shallow, all eigenvalues of the harmonic trap lie very closely together. Therefore we may consider the spatial degrees of freedom in (5.1) as continuous quantum numbers and we substitute the volume V in (3.4) by an integration over the whole configuration space. Hence the free energy results in

$$\mathcal{F} = (E_0 - \mu)N_0 - \frac{1}{\beta(\beta E_a)^{3/2}} \sum_{m=1}^{\infty} \frac{1}{m^{5/2}} e^{m\beta(\mu - E_0)} \prod_i e^{-2m\beta J_i} I_0(2m\beta J_i). \quad (5.2)$$

Here $E_0 = 3\hbar\omega/2$ is the ground state energy and $E_a = M\omega^2 a^2/2\pi$ is an energy which depends on the lattice constant a . The number of particles follows as

$$N = N_0 + \frac{1}{(\beta E_a)^{3/2}} \sum_{m=1}^{\infty} \frac{1}{m^{3/2}} e^{m\beta(\mu - E_0)} \prod_i e^{-2m\beta J_i} I_0(2m\beta J_i). \quad (5.3)$$

The resulting critical temperature is shown in Fig. 5.1. The most important result is that T_c is non-zero also in 2D and 1D which still agrees with the Mermin-Wagner-Hohenberg theorem since it applies only for homogeneous systems. The green dots in Fig. 5.1 denote analytical results of Ref. [50] with adjusted particle numbers for T_c in a trap but without an optical lattice. In one dimension the critical temperature is implicitly given as

$$N_{1D} = \frac{k_B T_c}{\hbar\omega} \ln \left(\frac{2k_B T_c}{\hbar\omega} \right), \quad (5.4)$$

in two dimensions it reads

$$T_c = \frac{\hbar\omega}{k_B} \sqrt{\frac{N_{2D}}{\zeta(2)}}, \quad (5.5)$$

and in three dimensions it is

$$T_c = \frac{\hbar\omega}{k_B} \left(\frac{N}{\zeta(3)} \right)^{1/3}. \quad (5.6)$$

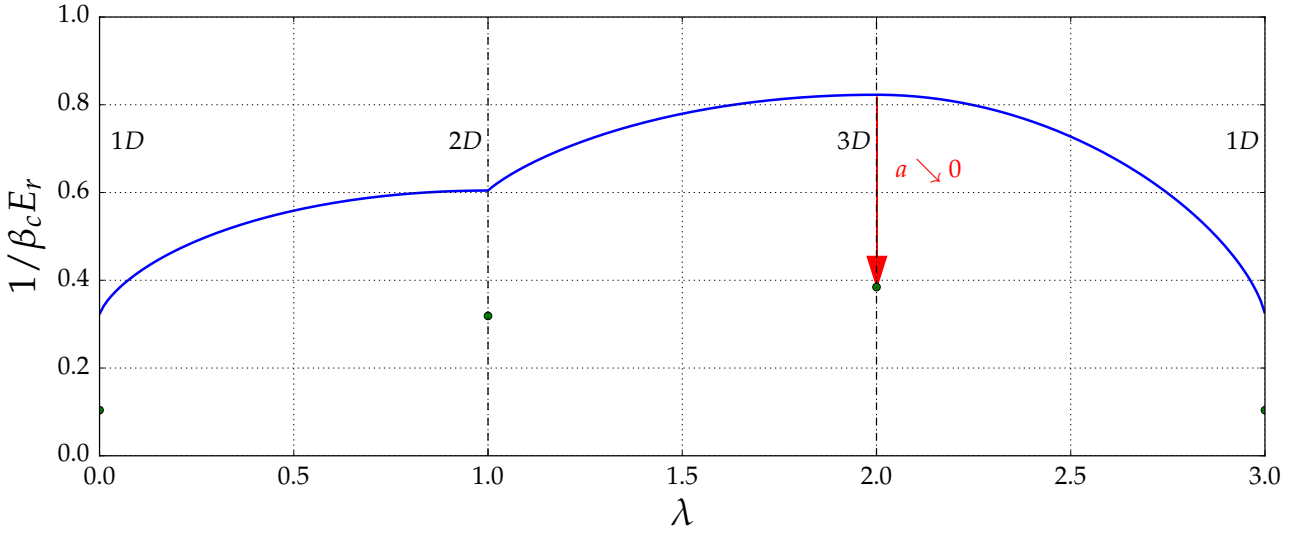


Figure 5.1: Critical temperature for harmonically trapped case as function of path parameter λ and temperature T for ^{87}Rb atoms with $N = 10^6$ and $\omega = 100$ Hz: the blue curve is the numerical result, the green dots are analytical results of Ref. [50] for T_c in a trap but without an optical lattice provided in (5.4) – (5.6) using (5.7) and (5.8). The red arrow indicates the limit of a vanishing lattice for the three-dimensional case.

Here N_{1D} , N_{2D} , and N are the numbers of particles in one, two, and three dimensions as explained below. Remember that these formulae apply for bosons in an isotropic harmonic trap without an optical lattice. It is crucial to note that throughout the kinetic dimensional phase transition the number of particles turns out to be not conserved. Imagine our optical lattice as a cube with length L . Setting the hopping energies to zero corresponds to a slicing of this cube, e.g. if we set $J_z = 0$ the cube would become a stack of independent, two-dimensional "pancakes", if we set $J_x = J_y = 0$ the cube would become an array of independent, one-dimensional "cigars". The following estimate holds for the number of particles in one pancake or one cigar. An atom inside our optical lattice spatially occupies the volume n^{-1} on average. The number of atoms in a pancake with a thickness of $n^{-1/3}$ then follows as

$$N_{2D} = n \cdot L^2 n^{-1/3} = N^{2/3} \quad (5.7)$$

and correspondingly for a "cigar"

$$N_{1D} = n \cdot L n^{-2/3} = N^{1/3}. \quad (5.8)$$

Therefore the values for the green dots in Fig 5.1 are given by (5.4) – (5.6) with (5.7) and (5.8). Performing the continuum limit of (5.3) as introduced in Sec. 3.2.7 our result in the case of three dimensions is found to be

$$N = \frac{1}{(\beta_c E_a)^{3/2}} \sum_{m=1}^{\infty} \left(\frac{M a^2}{2\pi m^2 \beta_c \hbar^2} \right)^{3/2} = \frac{1}{(\beta_c \hbar \omega)^3} \zeta(3), \quad (5.9)$$

where we used the definition of E_a given below (5.2) after the second equality sign. Upon rearranging (5.9) we recover (5.6). The continuum results for the 1D and 2D cases cannot be achieved as the respective limit of (5.3) since our system is a three-dimensional system which can only be effectively transformed to lower dimensions. Because of the three-dimensional,

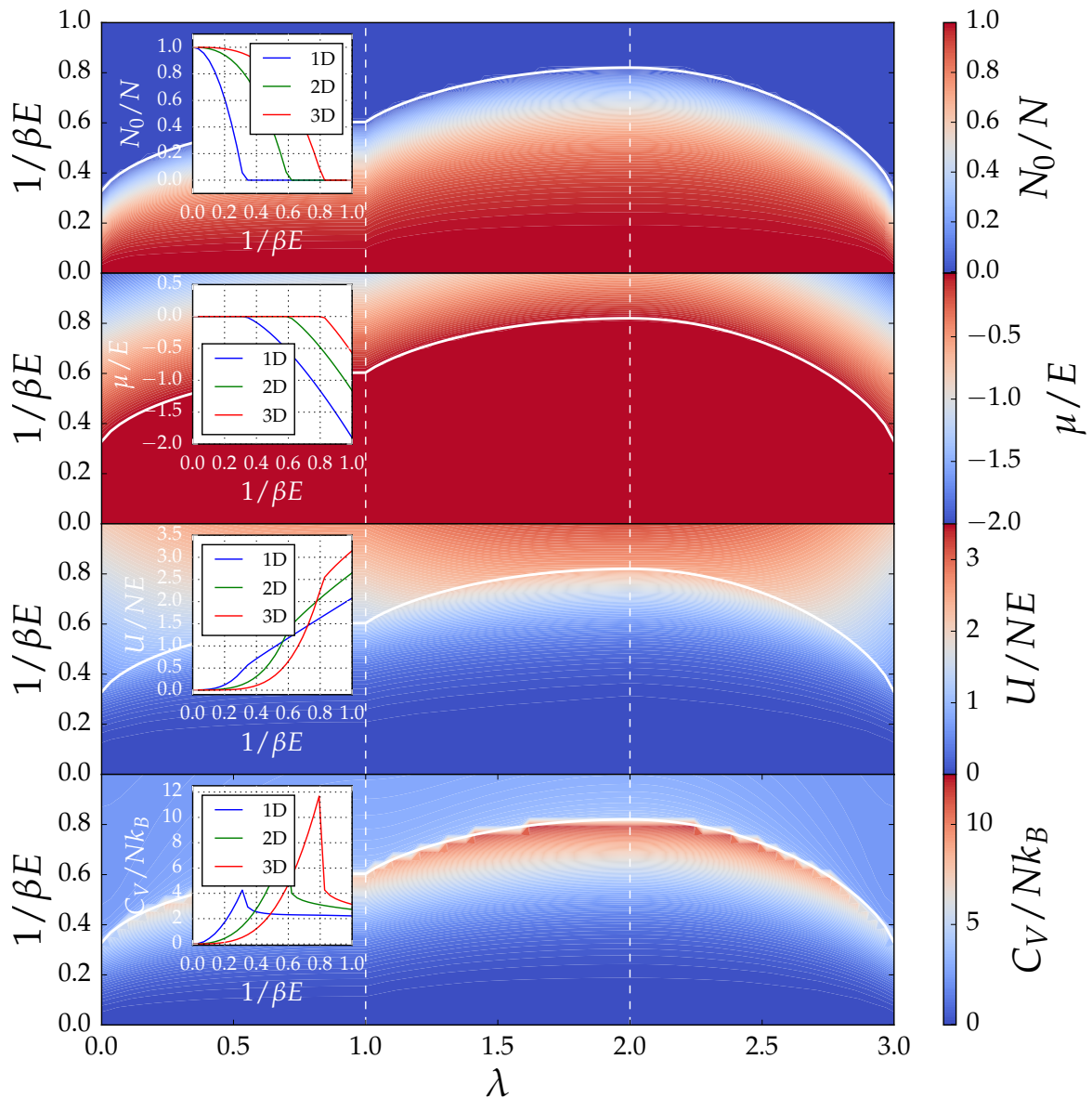


Figure 5.2: Thermodynamic quantities for harmonically trapped case as function of path parameter λ and temperature T for ^{87}Rb atoms with $N = 10^6$ and $\omega = 100$ Hz: the white curve corresponds to the critical temperature.

isotropic trap we use, additional degrees of freedom of the harmonic oscillator remain. Since there is no proper limit going from a trapped system to a free system we would achieve the wrong exponent of the m -denominator in (5.3). This would lead to the wrong order of the ζ -function.

Furthermore we observe in Fig. 5.1 that the increment of the critical temperature as a function of the dimensionality behaves differently from the homogeneous case as it no longer vanishes in 1D or 2D. Now T_c grows linearly in the vicinity of the pure integer dimension, which corresponds to a trivial critical exponent 1. Remember in Sec. 4.1 we found an exponent $\frac{1}{2}$ for the 1D \rightarrow 3D transition and a logarithmic-like behavior for the 2D \rightarrow 3D transition.

5.2 Thermodynamics

Following exactly the same procedure as for the homogeneous case we show the analytic results for all the respective thermodynamic quantities. The internal energy is

$$\begin{aligned}
 U = E_0 N + & \frac{3}{2} \frac{1}{\beta(\beta E_a)^{3/2}} \sum_{m=1}^{\infty} \frac{1}{m^{5/2}} e^{m\beta(\mu-E_0)} \prod_i e^{-2m\beta J_i} I_0(2m\beta J_i) \\
 & + \frac{2}{(\beta E_a)^{3/2}} \sum_{m=1}^{\infty} \frac{1}{m^{3/2}} e^{m\beta(\mu-E_0)} \sum_i J_i e^{-2m\beta J_i} [I_0(2m\beta J_i) - I_1(2m\beta J_i)] \prod_{j \neq i} e^{-2m\beta J_j} I_0(2m\beta J_j).
 \end{aligned} \tag{5.10}$$

Furthermore the heat capacity is found to be

$$\begin{aligned}
 \frac{C_V}{k_B} = & \frac{1}{(\beta E_a)^{3/2}} \sum_{m=1}^{\infty} e^{m\beta(\mu-E_0)} \left\{ \frac{15}{4} \frac{1}{m^{5/2}} \prod_i e^{-2m\beta J_i} I_0(2m\beta J_i) \right. \\
 & + 6 \frac{\beta}{m^{3/2}} \sum_i J_i e^{-2m\beta J_i} [I_0(2m\beta J_i) - I_1(2m\beta J_i)] \prod_{j \neq i} e^{-2m\beta J_j} I_0(2m\beta J_j) \\
 & - 2 \frac{\beta^2}{m^{1/2}} \sum_i J_i e^{-2m\beta J_i} [I_0(2m\beta J_i) - I_1(2m\beta J_i)] \prod_{j \neq i} e^{-2m\beta J_j} I_0(2m\beta J_j) \left(e^{-\beta\mu} \partial_{\beta} e^{\beta\mu} \right)_{V,N} \\
 & + 4 \frac{\beta^2}{m^{1/2}} \sum_i J_i^2 e^{-2m\beta J_i} \left[\frac{3}{2} I_0(2m\beta J_i) - 2I_1(2m\beta J_i) + \frac{1}{2} I_2(2m\beta J_i) \right] \prod_{j \neq i} e^{-2m\beta J_j} I_0(2m\beta J_j) \\
 & + 4 \frac{\beta^2}{m^{1/2}} \sum_i J_i e^{-2m\beta J_i} [I_0(2m\beta J_i) - I_1(2m\beta J_i)] \sum_{j \neq i} J_j e^{-2m\beta J_j} [I_0(2m\beta J_j) - I_1(2m\beta J_j)] \\
 & \left. \times \prod_{k \neq i,j} e^{-2m\beta J_k} I_0(2m\beta J_k) - \frac{3}{2} \frac{\beta}{m^{3/2}} \prod_i e^{-2m\beta J_i} I_0(2m\beta J_i) \left(e^{-\beta\mu} \partial_{\beta} e^{\beta\mu} \right)_{V,N} \right\} \tag{5.11}
 \end{aligned}$$

with the partial derivative of the chemical potential obtained in the same way as in (3.30)

$$\begin{aligned}
 \left(e^{-\beta\mu} \partial_{\beta} e^{\beta\mu} \right)_{V,N} = & \frac{3 \sum_{m=1}^{\infty} \frac{1}{m^{3/2}} e^{m\beta(\mu-E_0)} \prod_i e^{-2m\beta J_i} I_0(2m\beta J_i)}{2\beta \sum_{m=1}^{\infty} \frac{1}{m^{1/2}} e^{m\beta(\mu-E_0)} \prod_i e^{-2m\beta J_i} I_0(2m\beta J_i)} \\
 & - 2 \frac{\sum_{m=1}^{\infty} \frac{1}{m^{1/2}} e^{m\beta(\mu-E_0)} \sum_i J_i e^{-2m\beta J_i} [I_1(2m\beta J_i) - I_0(2m\beta J_i)] \prod_{j \neq i} e^{-2m\beta J_j} I_0(2m\beta J_j)}{\sum_{m=1}^{\infty} \frac{1}{m^{1/2}} e^{m\beta(\mu-E_0)} \prod_i e^{-2m\beta J_i} I_0(2m\beta J_i)}.
 \end{aligned} \tag{5.12}$$

In the BEC phase (5.12) is set to zero. The corresponding results for the condensate fraction, the chemical potential, the internal energy and the heat capacity for the harmonically trapped system are depicted in Fig. 5.2. Note that the heat capacity now converges to $3k_B N/2$ in the high temperature limit. This is due to the three additional quadratic degrees of freedom of the harmonic trap. This can not be directly observed in Fig. 5.2, since the influence of the kinetic energy is still high at $1/\beta E_r = 1$. However the evaluation at higher temperatures $1/\beta E_r = 10$ yields the expected result of $C_v \approx 3k_B N/2$.

We observe that the critical temperature seems to have a maximum at three dimensions in both the homogeneous Fig. 4.1 and the trapped case Fig. 5.1. In order to proof this we parametrize the hopping energies J in (3.12) with spherical coordinates (θ, ϕ) and extremize (3.12). Evaluating the system of equations $\partial_{\theta} N = 0$ and $\partial_{\phi} N = 0$ with $\partial_{\theta} \beta = \partial_{\phi} \beta = 0$ gives numerically $J = (E/\sqrt{3}, E/\sqrt{3}, E/\sqrt{3})$. Since all hopping energies are the same, this corresponds to three dimensions.

6 Weakly interacting bosons

Although non-interacting calculations often provide good approximative descriptions, especially in the dilute limit, no real non-interacting systems appear in nature. Therefore it is now our aim to study the dimensional phase transitions of interacting bosons. In this work we restrict ourselves to the regime of particles interacting through a weak two-body contact potential. Thus we expect certain corrections to the non-interacting case due to a finite interaction strength. One possibility to take into account interactions is the Hartree-Fock mean field theory. However it only shifts the chemical potential by a constant and is thus for a homogeneous system as good as the non-interacting theory in our purpose of investigating the phase transition. Furthermore it does not take into account quantum fluctuations due to interactions and therefore does not exhibit any depletion effects. A first improvement to a pure HF theory is the Hartree-Fock-Bogoliubov theory. It contains contributions due to quantum fluctuations, however it is only applicable at very small temperatures since a main assumption is that the condensate fraction is much larger than the fraction of excited bosons. The next improvement is the Hartree-Fock-Bogoliubov-Popov theory (HFBP) which is also reasonable at finite temperatures. We assume it to be sufficient for our purposes.

6.1 Hartree-Fock-Bogoliubov-Popov theory

We will now provide a derivation of the HFBP theory by following Refs. [51, 52]. We restrict ourselves to the homogeneous case. To this end we start with the general grand-canonical Hamiltonian incorporating two-body interactions in second-quantized form

$$\hat{H} = \int d\mathbf{r} \hat{\psi}^\dagger(\mathbf{r}) \left\{ -\frac{\hbar^2}{2M} \nabla^2 - \mu + \frac{1}{2} \left[\int d\mathbf{r}' \hat{\psi}^\dagger(\mathbf{r}') \hat{v}(\mathbf{r}, \mathbf{r}') \hat{\psi}(\mathbf{r}') \right] \right\} \hat{\psi}(\mathbf{r}). \quad (6.1)$$

The commutation relations for the field operators are given by (2.29). Furthermore $v(\mathbf{r}, \mathbf{r}')$ represents the two-particle interaction. Since we treat ultracold, dilute Bose gases we may approximate the general two-body interacting by a contact interaction $g\delta(\mathbf{r} - \mathbf{r}')$ where g denotes the interaction strength proportional the s-wave scattering length a_s :

$$g = \frac{4\pi\hbar^2 a_s}{M}. \quad (6.2)$$

Using (6.2) the Hamiltonian (6.1) simplifies to

$$\hat{H} = \int d\mathbf{r} \hat{\psi}^\dagger(\mathbf{r}) \left\{ -\frac{\hbar^2}{2M} \nabla^2 - \mu + \frac{g}{2} \hat{\psi}^\dagger(\mathbf{r}) \hat{\psi}(\mathbf{r}) \right\} \hat{\psi}(\mathbf{r}). \quad (6.3)$$

We proceed with a Bogoliubov decomposition, where the bosonic field operators are rewritten as follows:

$$\hat{\psi}(\mathbf{r}) = \psi_0 + \delta\hat{\psi}(\mathbf{r}), \quad \hat{\psi}^\dagger(\mathbf{r}) = \psi_0^* + \delta\hat{\psi}^\dagger(\mathbf{r}). \quad (6.4)$$

Here ψ_0 and ψ_0^* stand for the amplitudes of the condensate which are defined as the mean field according to

$$\psi_0 = \langle \hat{\psi}(\mathbf{r}) \rangle, \quad \psi_0^* = \langle \hat{\psi}^\dagger(\mathbf{r}) \rangle. \quad (6.5)$$

Thus, they are only complex numbers and satisfy

$$\psi_0^* \psi_0 = n_0 \quad (6.6)$$

denoting the condensate density. Here the expectation value $\langle \dots \rangle$ is understood to be the thermal average

$$\langle \dots \rangle = \frac{1}{\mathcal{Z}} \text{Tr} \left\{ \dots e^{-\beta \hat{H}} \right\}, \quad (6.7)$$

where the grand-canonical partition function reads $\mathcal{Z} = \text{Tr} \left\{ e^{-\beta \hat{H}} \right\}$. Furthermore, $\delta \hat{\psi}(\mathbf{r})$ and $\delta \hat{\psi}^\dagger(\mathbf{r})$ in (6.4) represent fluctuation operators, which describe both quantum and thermal fluctuations. Performing the Bogoliubov decomposition (6.4) we obtain a quartic Hamiltonian

$$\begin{aligned} \hat{H} = \int d\mathbf{r} \left\{ -\mu \psi_0^* \psi_0 + \delta \hat{\psi}^\dagger(\mathbf{r}) \left[-\frac{\hbar^2}{2M} \nabla^2 - \mu \right] \delta \hat{\psi}(\mathbf{r}) + \frac{g}{2} \left[(\psi_0^* \psi_0)^2 + (\psi_0^*)^2 \delta \hat{\psi}^2(\mathbf{r}) \right. \right. \\ \left. \left. + 4\psi_0^* \psi_0 \delta \hat{\psi}^\dagger(\mathbf{r}) \delta \hat{\psi}(\mathbf{r}) + \psi_0^2 \left(\delta \hat{\psi}^\dagger(\mathbf{r}) \right)^2 + \left(\delta \hat{\psi}^\dagger(\mathbf{r}) \right)^2 \delta \hat{\psi}^2(\mathbf{r}) \right] \right\}. \end{aligned} \quad (6.8)$$

Note that we omitted all terms which are odd in the number of field operators. Eventually our theory will be Gaussian thus all odd expectation values will vanish. For instance, we read off from (6.4) and (6.5) that

$$\langle \hat{\psi}^\dagger(\mathbf{r}) \rangle = \langle \hat{\psi}(\mathbf{r}) \rangle = 0. \quad (6.9)$$

We now need to get rid of the quartic term in (6.8). To this end we perform a mean field approximation of the quartic term, where the HFBP theory neglects the anomalous densities, which contain two creation or two annihilation operators, e.g. $\langle \hat{\psi}(\mathbf{r}) \hat{\psi}(\mathbf{r}) \rangle$ [51, 52]:

$$\left(\delta \hat{\psi}^\dagger(\mathbf{r}) \right)^2 \delta \hat{\psi}^2(\mathbf{r}) \approx 4 \langle \delta \hat{\psi}^\dagger(\mathbf{r}) \delta \hat{\psi}(\mathbf{r}) \rangle \delta \hat{\psi}^\dagger(\mathbf{r}) \delta \hat{\psi}(\mathbf{r}) - 2 \langle \delta \hat{\psi}^\dagger(\mathbf{r}) \delta \hat{\psi}(\mathbf{r}) \rangle^2. \quad (6.10)$$

Here we identify the expectation value of a pair of hermitian conjugate fluctuation operators with the density of excited bosons \tilde{n} :

$$\langle \delta \hat{\psi}^\dagger(\mathbf{r}) \delta \hat{\psi}(\mathbf{r}) \rangle = \tilde{n}. \quad (6.11)$$

Thus, we conclude from (6.4), (6.5), (6.9), and (6.11) that the particle density $n = \langle \hat{\psi}(\mathbf{r}) \hat{\psi}(\mathbf{r})^\dagger \rangle$ decomposes into the sum of the condensate density and the density of excited bosons:

$$n = n_0 + \tilde{n}. \quad (6.12)$$

Upon inserting (6.6), (6.10), and (6.11) into (6.8) we obtain the quadratic Hamiltonian

$$\begin{aligned} \hat{H} = \int d\mathbf{r} \left\{ -\mu n_0 + \frac{g}{2} n_0^2 - g \tilde{n}^2 + \delta \hat{\psi}^\dagger(\mathbf{r}) \left[-\frac{\hbar^2}{2M} \nabla^2 - \mu + 2g n_0 + 2g \tilde{n} \right] \delta \hat{\psi}(\mathbf{r}) \right. \\ \left. + \frac{g}{2} \left[(\psi_0^*)^2 \delta \hat{\psi}^2(\mathbf{r}) + \psi_0^2 \left(\delta \hat{\psi}^\dagger(\mathbf{r}) \right)^2 \right] \right\}. \end{aligned} \quad (6.13)$$

In order to solve the Hamiltonian we change the basis of the field operators to momentum space such that the new wavefunctions are eigenfunctions of the single-particle Hamiltonian

$$-\frac{\hbar^2}{2M} \nabla^2 e^{i\mathbf{k}\mathbf{r}} = \epsilon_{\mathbf{k}} e^{i\mathbf{k}\mathbf{r}}, \quad (6.14)$$

where the wavefunctions obey

$$\int d\mathbf{r} e^{-i\mathbf{k}\mathbf{r}} e^{i\mathbf{k}'\mathbf{r}} = V\delta_{\mathbf{k},\mathbf{k}'}. \quad (6.15)$$

The dispersion relation of free particles is given by:

$$\epsilon_k = \frac{\hbar^2 \mathbf{k}^2}{2M}. \quad (6.16)$$

The eigenfunctions are plane waves, so we may Fourier transform the fluctuation operators

$$\delta\hat{\psi}(\mathbf{r}) = \frac{1}{\sqrt{V}} \sum_{\mathbf{k}} e^{i\mathbf{k}\mathbf{r}} \hat{b}_{\mathbf{k}} \quad \delta\hat{\psi}^\dagger(\mathbf{r}) = \frac{1}{\sqrt{V}} \sum_{\mathbf{k}} e^{-i\mathbf{k}\mathbf{r}} \hat{b}_{\mathbf{k}}^\dagger. \quad (6.17)$$

Since the operators in (6.17) describe fluctuations, the $\mathbf{k} = 0$ term in the sums is always excluded. Substituting (6.17) and performing the \mathbf{r} -integral in (6.13) we find

$$\begin{aligned} \hat{H} = V[-\mu n_0 + \frac{g}{2} n_0^2 - g\tilde{n}^2] + \sum_{\mathbf{k}} \left\{ \hat{b}_{\mathbf{k}}^\dagger \hat{b}_{\mathbf{k}} [\epsilon_k - \mu + 2gn_0 + 2g\tilde{n}] \right. \\ \left. + \frac{g}{2} [(\psi_0^*)^2 \hat{b}_{\mathbf{k}} \hat{b}_{-\mathbf{k}} + \psi_0^2 \hat{b}_{\mathbf{k}}^\dagger \hat{b}_{-\mathbf{k}}^\dagger] \right\}. \end{aligned} \quad (6.18)$$

This Hamiltonian (6.18) can be rewritten as

$$\hat{H} = H_{\text{MF}} + \sum_{\mathbf{k}} \left[\epsilon_k^{\text{HF}} \hat{b}_{\mathbf{k}}^\dagger \hat{b}_{\mathbf{k}} + \frac{g}{2} (\psi_0^*)^2 \hat{b}_{\mathbf{k}} \hat{b}_{-\mathbf{k}} + \frac{g}{2} \psi_0^2 \hat{b}_{\mathbf{k}}^\dagger \hat{b}_{-\mathbf{k}}^\dagger \right]. \quad (6.19)$$

Here we identify the first term as the mean field contribution to the energy

$$H_{\text{MF}} = V \left(-\mu n_0 + \frac{g}{2} n_0^2 - g\tilde{n}^2 \right), \quad (6.20)$$

the second one as the kinetic part of the excited bosons with the Hartree-Fock energy

$$\epsilon_k^{\text{HF}} = \epsilon_k - \mu + 2gn_0 + 2g\tilde{n}, \quad (6.21)$$

which represents is the sum of the non-interacting energy and the mean field interaction energy contribution of $2gn$ due to (6.12). The last terms in (6.19) describe decay and fusion, respectively, of two excited bosons of opposite momentum into two condensed particles.

Now we diagonalize the Hamiltonian (6.19) by means of a Bogoliubov transformation

$$\hat{b}_{\mathbf{k}} = u_{\mathbf{k}} \hat{A}_{\mathbf{k}} - v_{\mathbf{k}} \hat{A}_{-\mathbf{k}}^\dagger, \quad \hat{b}_{\mathbf{k}}^\dagger = u_{\mathbf{k}}^* \hat{A}_{\mathbf{k}}^\dagger - v_{\mathbf{k}}^* \hat{A}_{-\mathbf{k}}. \quad (6.22)$$

Due to the weak inter-particle interaction the gas behaves as a gas of free composite quasiparticles. The creation (annihilation) operators of the quasiparticles $\hat{A}_{\mathbf{k}}^\dagger$ ($\hat{A}_{\mathbf{k}}$) themselves are bosons and thus obey the bosonic commutation relations

$$[\hat{A}_{\mathbf{k}'}, \hat{A}_{\mathbf{p}}^\dagger] = \delta_{\mathbf{k},\mathbf{p}} \quad [\hat{A}_{\mathbf{k}'}, \hat{A}_{\mathbf{p}}] = [\hat{A}_{\mathbf{k}}^\dagger, \hat{A}_{\mathbf{p}}^\dagger] = 0. \quad (6.23)$$

From (6.23) we conclude that the respective amplitudes $u_{\mathbf{k}}$ and $v_{\mathbf{k}}$ in (6.22) are symmetric in \mathbf{k} and obey the following relation which can both be shown using (2.17), (6.22), and (6.23):

$$|u_{\mathbf{k}}|^2 - |v_{\mathbf{k}}|^2 = 1. \quad (6.24)$$

Performing the Bogoliubov transformation (6.22) within (6.19) we obtain

$$\begin{aligned}
 \hat{H} = H_{\text{MF}} + \sum_k \left\{ \hat{A}_k^\dagger \hat{A}_k \left[\varepsilon_k^{\text{HF}} \left(|u_k|^2 + |v_k|^2 \right) - g \psi_0^2 u_k^* v_k^* - g (\psi_0^*)^2 u_k v_k \right] \right. \\
 + \hat{A}_k^\dagger \hat{A}_{-k}^\dagger \left[-\varepsilon_k^{\text{HF}} u_k^* v_k + \frac{g}{2} \psi_0^2 (u_k^*)^2 + \frac{g}{2} (\psi_0^*)^2 v_k^2 \right] \\
 + \hat{A}_k \hat{A}_{-k} \left[-\varepsilon_k^{\text{HF}} u_k v_k^* + \frac{g}{2} (\psi_0^*)^2 u_k^2 + \frac{g}{2} \psi_0^2 (v_k^*)^2 \right] \\
 \left. + \varepsilon_k^{\text{HF}} |v_k|^2 - \frac{g}{2} \psi_0^2 u_k^* v_k^* - \frac{g}{2} (\psi_0^*)^2 u_k v_k \right\}.
 \end{aligned} \tag{6.25}$$

Bogoliubov theory describes non-interacting quasiparticles, thus the two off-diagonal terms in (6.25) must vanish. Note that they are Hermitian conjugate of each another. Therefore we get another constraint on the amplitudes according to

$$\varepsilon_k^{\text{HF}} u_k^* v_k = \frac{g}{2} \psi_0^2 (u_k^*)^2 + \frac{g}{2} (\psi_0^*)^2 v_k^2. \tag{6.26}$$

The two relations between the amplitudes (6.24) and (6.26) form an algebraic system which we solve now as follows. Starting with (6.24) we note that the amplitudes can be written in terms of hyperbolic functions

$$\cosh^2(x) - \sinh^2(x) = 1, \tag{6.27}$$

such that

$$u_k = e^{i\phi_k} \cosh(\theta_k) \quad v_k = e^{i\varphi_k} \sinh(\theta_k). \tag{6.28}$$

Here ϕ_k and φ_k denote the respective phases of the complex amplitudes. Substituting the amplitudes (6.28) in (6.26) and assigning a phase also to the condensate amplitude as $\psi_0 = \sqrt{n_0} e^{i\phi_0}$ we find

$$\varepsilon_k^{\text{HF}} e^{-i\phi_k} \cosh(\theta_k) e^{i\varphi_k} \sinh(\theta_k) = \frac{g n_0}{2} e^{2i\phi_0} e^{-2i\phi_k} \cosh^2(\theta_k) + \frac{g n_0}{2} e^{-2i\phi_0} e^{2i\varphi_k} \sinh^2(\theta_k). \tag{6.29}$$

Multiplying by the phase factors of the right-hand side the equation becomes real and we find for the phases up to multiples of 2π the relation

$$2\phi_0 = \phi_k + \varphi_k. \tag{6.30}$$

With this condition we observe that the remaining Hamiltonian (6.25) becomes real as well. We continue solving the system for the amplitudes by using properties of the hyperbolic functions. The equation (6.29) with (6.30) simplifies at first to

$$\frac{2\varepsilon_k^{\text{HF}}}{g n_0} \cosh(\theta_k) \sinh(\theta_k) = \cosh^2(\theta_k) + \sinh^2(\theta_k). \tag{6.31}$$

Then we use two addition theorems of the hyperbolic functions

$$2 \cosh(x) \sinh(x) = \sinh(2x), \quad \cosh^2(x) + \sinh^2(x) = \cosh(2x), \tag{6.32}$$

and find with (6.31)

$$\tanh(2\theta_k) = \frac{g n_0}{\varepsilon_k^{\text{HF}}}. \tag{6.33}$$

Now we express the hyperbolic sine and cosine functions in terms of the hyperbolic tangent of twice the argument. We start by using (6.27) to obtain

$$\cosh(x) = \frac{1}{\sqrt{1 - \tanh(x)}}. \quad (6.34)$$

Next we find for the sine and cosine functions using again (6.27) and the cosine addition theorem in (6.32)

$$\cosh(x) = \sqrt{\frac{1}{2} [\cosh(2x) + 1]}, \quad \sinh(x) = \sqrt{\frac{1}{2} [\cosh(2x) - 1]}. \quad (6.35)$$

Inserting (6.34) gives

$$\cosh(x) = \sqrt{\frac{1}{2} \left[\frac{1}{\sqrt{1 - \tanh(2x)}} + 1 \right]}, \quad \sinh(x) = \sqrt{\frac{1}{2} \left[\frac{1}{\sqrt{1 - \tanh(2x)}} - 1 \right]}. \quad (6.36)$$

Thus we obtain for the amplitudes using (6.28), (6.33), and (6.36)

$$u_k = e^{i\phi_k} \sqrt{\frac{1}{2} \left(\frac{1}{\sqrt{1 - gn_0/\varepsilon_k^{\text{HF}}}} + 1 \right)}, \quad v_k = e^{i\phi_k} \sqrt{\frac{1}{2} \left(\frac{1}{\sqrt{1 - gn_0/\varepsilon_k^{\text{HF}}}} - 1 \right)}. \quad (6.37)$$

We define two new energy scales. The first one reads

$$\varepsilon_k = \epsilon_k - \mu + gn_0 + 2g\tilde{n}, \quad (6.38)$$

which is the difference of the Hartree-Fock energy $\varepsilon_k^{\text{HF}}$ defined in (6.21) and the Bogoliubov contribution gn_0 . The second one is defined as

$$E_k = \sqrt{\varepsilon_k^2 + 2gn_0\varepsilon_k}, \quad (6.39)$$

and corresponds to the Bogoliubov energy, i.e. the dispersion relation of the quasiparticles as will become apparent further below. It results from

$$E_k^2 = \left(\varepsilon_k^{\text{HF}} \right)^2 - (gn_0)^2 = (\varepsilon_k + gn_0)^2 - (gn_0)^2 = \varepsilon_k^2 + 2gn_0\varepsilon_k. \quad (6.40)$$

Remembering the abbreviation $\varepsilon_k^{\text{HF}}$ defined in (6.21), the amplitudes (6.37) simplify to

$$u_k = e^{i\phi_k} \sqrt{\frac{1}{2} \left(\frac{\varepsilon_k + gn_0}{E_k} + 1 \right)}, \quad v_k = e^{i\phi_k} \sqrt{\frac{1}{2} \left(\frac{\varepsilon_k + gn_0}{E_k} - 1 \right)}. \quad (6.41)$$

Hence we are able to calculate all terms which appear in the Hamiltonian:

$$|u_k|^2 + |v_k|^2 = \frac{\varepsilon_k + gn_0}{E_k}, \quad (6.42)$$

$$\psi_0^2 u_k^* v_k^* = (\psi_0^*)^2 u_k v_k = \frac{1}{2} \frac{gn_0^2}{E_k}. \quad (6.43)$$

Eventually the Hamiltonian (6.25) reduces to

$$\hat{H} = V \left(-\mu n_0 + \frac{g}{2} n_0^2 - g\tilde{n}^2 \right) + \sum_k \left[E_k \hat{A}_k^\dagger \hat{A}_k + \frac{1}{2} (E_k - \varepsilon_k - gn_0) \right]. \quad (6.44)$$

The Hamiltonian (6.44) consists of three parts. The first one proportional to V is the mean field contribution. The second one proportional to the number operator $\hat{A}_k^\dagger \hat{A}_k$ corresponds to the kinetic term of the quasiparticles. Now we see that the Bogoliubov energy represents indeed the dispersion of the quasiparticles. Finally the last term provides the energy contribution due to quantum fluctuations. This term is non zero even at absolute zero and is therefore responsible for quantum depletion effects.

Having a quadratic Hamiltonian we are now able to compute expectation values of macroscopic observables. For this we rewrite the trace as a sum over all occupation number states of quasiparticles

$$\text{Tr} \{ \dots \} = \left(\prod_k \sum_{N_k} \right) \left(\prod_k \langle N_k | \right) \dots \left(\prod_k | N_k \rangle \right), \quad (6.45)$$

where N_k denotes the number of quasiparticles in state k with $\hat{A}_k^\dagger \hat{A}_k | N_k \rangle = N_k | N_k \rangle$. The grand-canonical partition function of the system with the Hamiltonian (6.44) follows as

$$\mathcal{Z} = e^{-\beta V (-\mu n_0 + \frac{g}{2} n_0^2 - g \tilde{n}^2)} \prod_k \frac{e^{-\frac{\beta}{2} (E_k - \epsilon_k - g n_0)}}{1 - e^{-\beta E_k}}. \quad (6.46)$$

The grand-canonical free energy is the logarithm of the grand-canonical partition function and is therefore given by

$$\mathcal{F} = -\frac{1}{\beta} \log(\mathcal{Z}). \quad (6.47)$$

Applying this on (6.46) we find for the grand-canonical free energy

$$\mathcal{F} = V \left(-\mu n_0 + \frac{g}{2} n_0^2 - g \tilde{n}^2 \right) + \frac{1}{2} \sum_k (E_k - \epsilon_k - g n_0) + \frac{1}{\beta} \sum_k \log \left(1 - e^{-\beta E_k} \right). \quad (6.48)$$

Furthermore the average number of particles N is computed by the derivative of the free energy with respect to the chemical potential

$$N = - \left. \frac{\partial \mathcal{F}}{\partial \mu} \right|_{V, \beta} = V n_0 + \sum_k \left[\frac{\epsilon_k + g n_0}{E_k} \left(\frac{1}{e^{\beta E_k} - 1} + \frac{1}{2} \right) - \frac{1}{2} \right]. \quad (6.49)$$

This result is the same as the one in Ref. [53, (15.2)]. We observe that the particle number equation recovers the non-interacting case. If g vanished the Bogoliubov energy (6.39) would become $\epsilon_k - \mu$ such that we get $(\epsilon_k + g n_0)/E_k = 1$. Therefore the two constant terms would annul and only the Bose-Einstein distribution would remain

$$N = V n_0 + \sum_k \frac{1}{e^{\beta(\epsilon_k - \mu)} - 1}, \quad (6.50)$$

which corresponds indeed to the non-interacting case.

6.1.1 Pure Hartree-Fock limit

Also the HF theory can be recovered from (6.49). To this end we neglect the off-diagonal self-energy contribution $g n_0$ in (6.40) which comes from the Bogoliubov channel and is therefore not present in a pure HF theory. We observe that the quasi-particle energy reduces then

to the Hartree-Fock energy $E_k = \varepsilon_k^{\text{HF}}$. Hence we conclude from (6.21) and (6.38) that $(\varepsilon_k + gn_0)/E_k = 1$, so we obtain the HF theory for weakly interacting bosons

$$N = Vn_0 + \sum_k \frac{1}{e^{\beta(\varepsilon_k^{\text{HF}} - \mu)} - 1}. \quad (6.51)$$

From (6.21) and (6.51) we see that, when the chemical potential reaches $2gn$ the phase transition to the BEC phase occurs. Therefore the critical chemical potential reads $\mu_c = 2gn$ for the pure HF theory with contact interaction. Thus at the critical point the HF theory (6.51) does not differ from the non-interacting one (6.50) apart from a physically irrelevant shift of the chemical potential $\mu \rightarrow 2gn$.

6.1.2 Generalized Gross-Pitaevskii equation and chemical potential

Going back to the HFBP theory we now need to focus on the behavior of the chemical potential since the equation (6.49) is not yet fully determined. In the gas phase the chemical potential is determined by the equation for the number of particles from the condition to reproduce the correct number of particles. In the condensate phase, however, the chemical potential is fixed but cannot be determined due to the finite condensate fraction. Therefore we need a further equation which describes the behavior of the condensate, i.e. the Gross-Pitaevskii equation. It is derived by computing the Heisenberg equation of motion

$$\frac{\partial}{\partial t} \hat{A}(t) = \frac{i}{\hbar} [\hat{H}, \hat{A}(t)]. \quad (6.52)$$

Here $\hat{A}(t)$ is an arbitrary operator in the Heisenberg picture. We apply (6.52) to the bosonic field operator $\hat{\psi}(\mathbf{r}, t)$ and the canonical Hamiltonian of free interacting particles featuring contact interaction in the Heisenberg picture:

$$\hat{H}_{\text{GP}} = \int d\mathbf{r} \hat{\psi}^\dagger(\mathbf{r}, t) \left\{ -\frac{\hbar^2}{2M} \nabla^2 + \frac{g}{2} \hat{\psi}^\dagger(\mathbf{r}, t) \hat{\psi}(\mathbf{r}, t) \right\} \hat{\psi}(\mathbf{r}, t). \quad (6.53)$$

Thus we obtain the equation of motion

$$i\hbar \frac{\partial}{\partial t} \hat{\psi}(\mathbf{r}, t) = \left\{ -\frac{\hbar^2}{2M} \nabla^2 + g \hat{\psi}^\dagger(\mathbf{r}, t) \hat{\psi}(\mathbf{r}, t) \right\} \hat{\psi}(\mathbf{r}, t). \quad (6.54)$$

With the ansatz $\hat{\psi}(\mathbf{r}, t) = e^{-i\mu t/\hbar} \hat{\psi}(\mathbf{r})$ we obtain the time-independent version of (6.54)

$$\mu \hat{\psi}(\mathbf{r}) = \left\{ -\frac{\hbar^2}{2M} \nabla^2 + g \hat{\psi}^\dagger(\mathbf{r}) \hat{\psi}(\mathbf{r}) \right\} \hat{\psi}(\mathbf{r}). \quad (6.55)$$

Applying the Bogoliubov decomposition (6.4) and performing the ensemble average leads to the generalized Gross-Pitaevskii equation

$$\mu \psi_0 = \left\{ -\frac{\hbar^2}{2M} \nabla^2 + g |\psi_0|^2 + 2g \langle \delta \hat{\psi}^\dagger(\mathbf{r}) \delta \hat{\psi}(\mathbf{r}) \rangle \right\} \psi_0, \quad (6.56)$$

where we omitted all terms which are odd in the fluctuation operators $\delta \hat{\psi}(\mathbf{r})$ and $\delta \hat{\psi}^\dagger(\mathbf{r})$ since those average out. Identifying the two densities (6.6) and (6.11) we obtain

$$\mu \psi_0 = \left\{ -\frac{\hbar^2}{2M} \nabla^2 + gn_0 + 2g\tilde{n} \right\} \psi_0. \quad (6.57)$$

Due to the homogeneity the condensate amplitude ψ_0 is constant, so (6.57) reduces to

$$0 = \{-\mu + gn_0 + 2g\tilde{n}\} \psi_0. \quad (6.58)$$

Since the order parameter must not be zero in the condensate phase we find the value for the fixed chemical potential being

$$\mu = gn_0 + 2g\tilde{n}. \quad (6.59)$$

This is confirmed by the Hugenholtz-Pines theorem [54] which states that a theory of repelling bosons must be gapless. The chemical potential therein equals the difference of the diagonal and the off-diagonal self-energy. In the case of the HFBP theory the diagonal self-energy coincides with the Hartree-Fock contribution $2gn$ and the off-diagonal one comes from the Bogoliubov channel and is given by gn_0 . Therefore we have in total

$$\mu = 2gn - gn_0 = 2g\tilde{n} + gn_0. \quad (6.60)$$

We observe that with (6.58) the chemical potential in ε_k in (6.39) cancels exactly and we get $\varepsilon_k = \epsilon_k$. The calculations for any thermodynamic variable are thus independent of the chemical potential in the condensate phase.

Another approach to find an equation for the chemical potential is the extremization of the free energy (6.48) with respect to the condensate density. But this leads to another expression for the chemical potential

$$\mu = gn_0 + 2 \sum_k \left[\frac{\varepsilon_k + \frac{1}{2}gn_0}{E_k} \left(\frac{1}{e^{\beta E_k} - 1} + \frac{1}{2} \right) - \frac{1}{2} \right], \quad (6.61)$$

which coincides with the result in Ref. [53, (15.3)]. We observe that the second term of (6.61) does not exactly recover the value of $2g\tilde{n}$ using (6.49) due to the factor of $\frac{1}{2}$ in front of the gn_0 term below the sum. Therefore (6.59) is not recovered and the theory would not be gapless in contrast to the Hugenholtz-Pines theorem [54]. In Ref. [52] it is shown that this can be fixed within the Beliaev theory which elaborates second order corrections in g . However, to actually proof this is beyond the scope of this thesis.

Since in our lattice structure ϵ_k is given by (2.44) and thus a complicated Bogoliubov energy emerges, an analytical calculation of (6.49) is not possible, so we need to evaluate it numerically.

6.2 Numerics of weakly interacting case

Our investigation of the weakly interacting Bose system demands the evaluation of the particle number equation (6.49). Due to the complicated form an analytical treatment seems hopeless. In this section we describe in detail how the numerical computation of (6.49) is performed. First of all the thermodynamic limit (3.4) exchanges the sum with an integral:

$$n = n_0 + \frac{1}{(2\pi)^3} \int dk \left[\frac{\varepsilon_k + gn_0}{E_k} \left(\frac{1}{e^{\beta E_k} - 1} + \frac{1}{2} \right) - \frac{1}{2} \right]. \quad (6.62)$$

Since the bosons are arranged in a lattice, the integration is performed over the first Brillouin zone. We first check the integrand for potential ultraviolet or infrared divergences. The former is easily seen to not occur since we integrate over a finite k -space volume. The infrared divergence, however, is more complicated to investigate. For this we start with a Taylor expansion of the integrand of (6.62) up to second order in k . The respective terms contained in (6.62) become

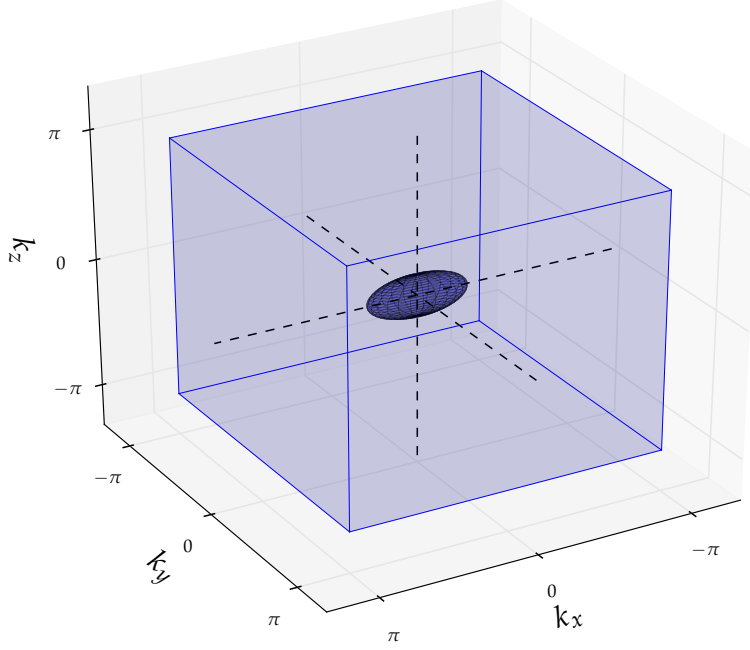


Figure 6.1: Decomposition of integration volume of first Brillouin zone in order to calculate the integral (6.62). The light-blue volume is the first Brillouin zone and the dark-blue depicts a small ellipsoid around the origin in which the integral (6.62) is analytically tractable.

$$\varepsilon_{\mathbf{k}} \simeq J_x k_x^2 a^2 + J_y k_y^2 a^2 + J_z k_z^2 a^2, \quad (6.63)$$

$$E_{\mathbf{k}} \simeq \sqrt{2gn_0 a^2 (J_x k_x^2 + J_y k_y^2 + J_z k_z^2)}, \quad (6.64)$$

$$\frac{1}{e^{\beta E_{\mathbf{k}}} - 1} \simeq \frac{1}{\beta E_{\mathbf{k}}} - \frac{1}{2} + \frac{\beta E_{\mathbf{k}}}{12}. \quad (6.65)$$

Inserting this into (6.62) we observe a quadratic divergence of the integrand for a single cartesian integral at the point where the other two values of \mathbf{k} are zero. This would make a numerical integration impossible. However, the integrand is well defined when written in ellipsoidal coordinates since the \mathbf{k} -radius appears quadratically in the interaction measure.

6.2.1 Ellipsoid method

Due to this numerical infrared divergence in cartesian coordinates we decompose the integral in (6.62) into two parts as it is visualized in Fig. 6.1. The light-blue volume marks the first Brillouin zone as the complete integration volume. The dark-blue volume is a small ellipsoid wherein the integral can be calculated analytically as it will be shown below. The advantage is now that we can use the approximation (6.63) – (6.65) since this ellipsoid is taken to be small. Then the integrand can be rewritten in ellipsoidal coordinates due to the elliptic symmetry of (6.63) and the integral for the ellipsoid is computed analytically. Everything else what is left to integrate over is calculated numerically since there we do not have any divergence problems. This means illustratively that the value of the complete integral (6.62) is the sum of the analytically determined value of the dark-blue volume in Fig. 6.1 and the numerically determined value of the light-blue without the dark-blue volume.

In order to compute the integral of the small ellipsoid we apply the substitution to ellipsoidal coordinates

$$R = \sqrt{J_x k_x^2 a^2 + J_y k_y^2 a^2 + J_z k_z^2 a^2}, \quad dk = \frac{4\pi}{a^3 \sqrt{J_x J_y J_z}} R^2 dR \quad (6.66)$$

in (6.63) and (6.65), and obtain

$$\varepsilon_k = R^2, \quad E_k = \sqrt{2gn_0}R. \quad (6.67)$$

Upon substituting this in (6.62) we find

$$n = n_0 + \frac{1}{2\pi^2 a^3 \sqrt{J_x J_y J_z}} \int_0^{R_0} dR R^2 \left[\frac{R^2 + gn_0}{\sqrt{2gn_0}R} \left(\frac{1}{\beta \sqrt{2gn_0}R} + \frac{\beta \sqrt{2gn_0}R}{12} \right) - \frac{1}{2} \right], \quad (6.68)$$

which reduces for small R_0 to

$$n = n_0 + \frac{1}{2\pi^2 a^3 \sqrt{J_x J_y J_z}} \left[\frac{R_0}{2\beta} + \left(\frac{1}{\beta gn_0} + \frac{\beta gn_0}{6} - 1 \right) \frac{R_0^3}{6} + \mathcal{O}(R_0^4) \right]. \quad (6.69)$$

Here R_0 denotes the radius of the ellipsoid in ellipsoidal coordinates and has the physical dimension of the square root of an energy. It must be small enough such that the approximation (6.63) – (6.65) is valid and large enough to prevent any divergence in the numerical treatment. Note that the term linear in R_0 in (6.69) is a sign for the emergence of numerically divergent terms in cartesian coordinates, since the integration measure in three dimensions is already quadratic in R .

6.2.2 Numerical integration sampling

The numerical integration is performed with the Simpson integration rule. It is crucial to spend some time on the sample points for the integration. In fact the choice of equidistant sample points is bad for the integration of the Bose-Einstein distribution. Since the distribution function diverges quadratically as $k \rightarrow 0$, an intuitive guess would be to choose quadratically aligned sample points such that the density of sample points is highest close to $k = 0$. As an example we calculate the value of the one-dimensional integral

$$\int_{0.01}^{\pi} dk \frac{1}{\exp[1 - \cos(k)] - 1} \quad (6.70)$$

as a function of the number of sample points. The result is shown in Fig. 6.2. There the blue and green dots represent the value of the integral (6.70) as a function of the number of steps for equidistant and quadratically aligned sample points, respectively. We clearly see much better convergence for the quadratically aligned points. Therefore we use from now on only the quadratic alignment.

In order to check the numerical results we perform the described procedure for the non-interacting case and cross-check with the known results for the non-interacting gas. To this end we numerically integrate

$$N = N_0 + \frac{1}{(2\pi)^3} \int d\mathbf{k} \frac{1}{e^{\beta(\varepsilon_k - \mu)} - 1}, \quad (6.71)$$

where the dispersion relation is given by (2.44). The formula (6.71) corresponds to the derivative of (3.1) with respect to μ in the thermodynamic limit (3.4). As an observable for

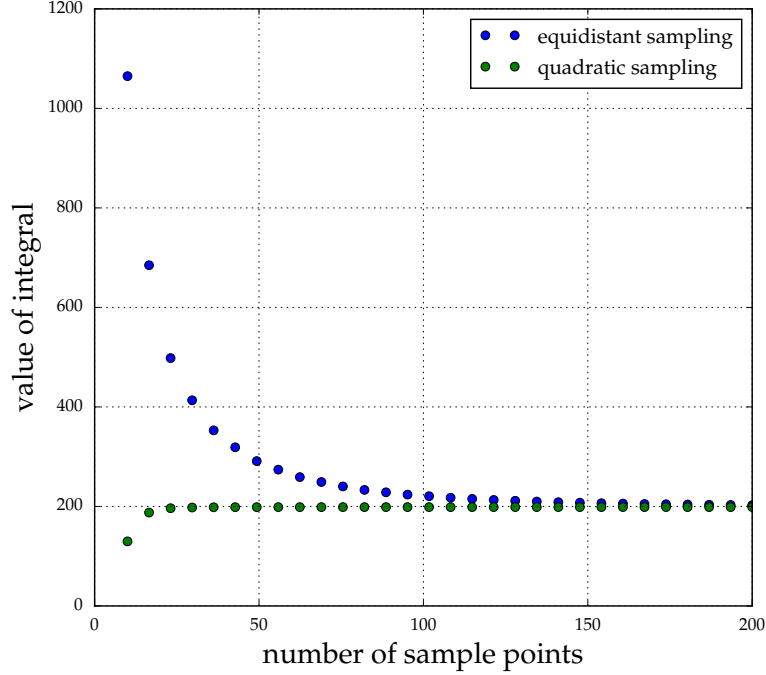


Figure 6.2: Value of the integral (6.70) as function of the number of sample points. The blue dots denote results for equidistant points, whereas the green dots represent the results of quadratically aligned sample points.

the cross-check we use the critical temperature in three dimensions for which we set $\mu = 0$. The reference value is given by the method we used to compute the critical temperature in Sec. 4.1. However it has a certain error since the infinite series in (3.12) is calculated with a cut-off. Since the summand is really slowly converging even a very large cut-off still yields a detectable discrepancy to the full infinite series. In order to find a value of T_c in three dimensions without a finite cut-off we compute T_c as a function of the inverse cut-off. This is presented in Fig. 6.3, where the blue dots denote the critical temperature calculated solving the implicit equation (3.12) with a finite cut-off N_{\max} for the infinite series. The results are then extrapolated using a square-root fitting function represented by the green line in order to find the value of T_c for $N_{\max} = \infty$. We find for this value $T_c(N_{\max} = \infty) \approx 2.663 E/k_B$. Remember that E was an energy scale which we defined in Sec. 2.4.3.

The actual cross-check is shown in Fig. 6.4. There the blue line visualizes the result achieved through the extrapolation in Fig. 6.3. The green dots are the result of the numerical integration of (6.71) with $\mu = 0$. We see an expected convergence to the reference value with increasing number of sample points. This convergence is not monotonic. The fluctuations around the reference value presumably come from the fact that we exclude all sampling points which are inside the small ellipsoid introduced above. With varying number of sample points also the number of points, which are actually used, varies due to the exclusion of the ellipsoid. Since 100^3 sample points give a value of reasonably good convergence according to Fig. 6.4, we use that number for all further computations.

Due to the fine sampling close to the origin in k -space the value of the integral is almost independent of the cut-off radius R_0 . We use the value $R_0 = 0.01\sqrt{E}$ for further calculations.

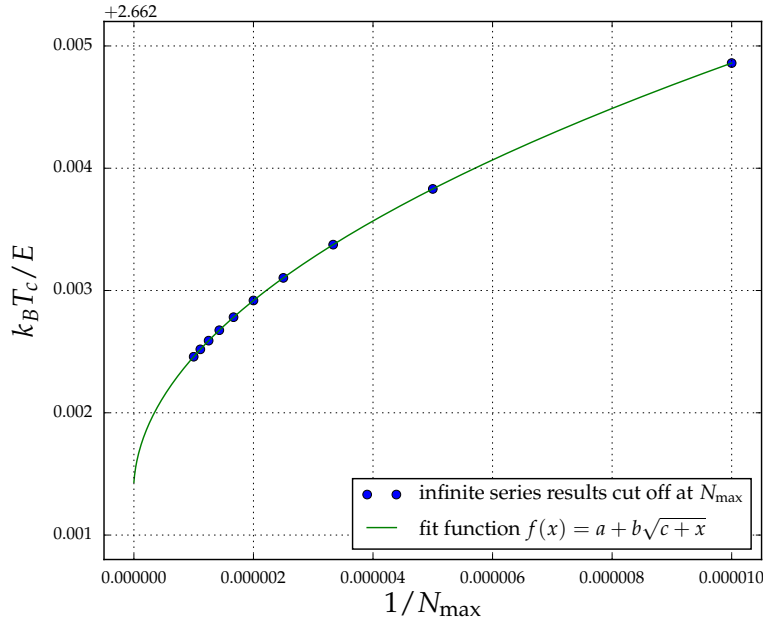


Figure 6.3: Results for the critical temperature in three dimensions (blue dots) calculated solving the implicit equation (3.12) with a finite cut-off N_{\max} for the infinite series. These results are extrapolated using a square-root fitting function (green line). The filling factor (3.15) is $\bar{n} = 0.77$ which is justified in Sec. 4.1.

6.2.3 Dimensionless units

Instead of dealing with particular values for the s-wave scattering length or the interaction strength (6.2), we make use of a dimensionless gas parameter [49] which is defined as

$$\gamma = n a_s^3. \quad (6.72)$$

In the case of the weakly interacting ^{87}Rb -atoms, the s-wave scattering length is about $100 a_0$ [27], where a_0 is the Bohr radius. For a density of 0.77 particles per $(387 \text{ nm})^3$ the gas parameter equals approximately $2 \cdot 10^{-6}$. An estimate for the gas parameter of the strongly interacting Helium is $\gamma \simeq 0.24$ [55].

6.2.4 Phase transition and critical temperature

At first we present the condensate fraction as function of the temperature for the interacting theory in Fig. 6.5. We observe a first-order phase transition of the Bose-Einstein condensation, which corresponds to expectations from HFBP theory [51]. The first-order phase transition occurs at a critical temperature T_c and a finite critical condensate density n_{0c} , where the derivative of the condensate density with respect to the temperature diverges to minus infinity:

$$\left. \frac{dn_0}{dT} \right|_{T_c} = -\infty \quad \rightarrow \quad \left. \frac{dn_0}{d\beta} \right|_{\beta_c} = \infty. \quad (6.73)$$

In order to find the critical point we need to fulfill the condition (6.73). To this end we perform

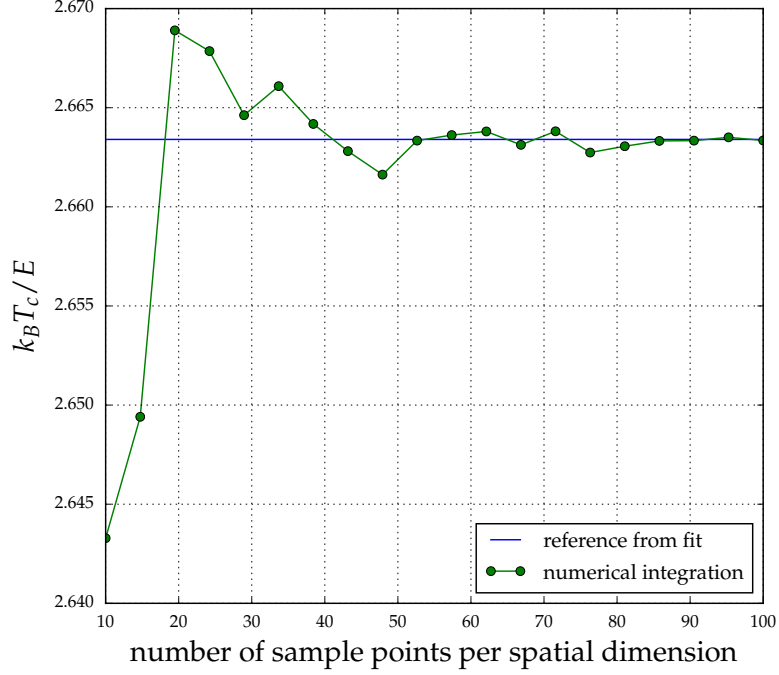


Figure 6.4: Cross-check of the critical temperature of the non-interacting, three-dimensional system. The blue reference line is the value found through the extrapolation in Fig. 6.3. The green dots correspond to the critical temperature found through bare numerical integration of (6.71) as function of the number of sample points per spatial dimension.

the derivative of (6.49) with respect to the temperature. This yields

$$0 = V \frac{dn_0}{d\beta} + \sum_k \left[\frac{g E_k^2 \frac{dn_0}{d\beta} - (\varepsilon_k + g n_0) g \varepsilon_k \frac{dn_0}{d\beta}}{E_k^3} \left(\frac{1}{e^{\beta E_k} - 1} + \frac{1}{2} \right) - \frac{\varepsilon_k + g n_0}{E_k} \left(E_k + \frac{\beta g \varepsilon_k}{E_k} \frac{dn_0}{d\beta} \right) \frac{e^{\beta E_k}}{(e^{\beta E_k} - 1)^2} \right]. \quad (6.74)$$

Evaluating this at $T = T_c$ while considering (6.73), we can neglect all terms which are not proportional to $\frac{dn_0}{d\beta}$ and find

$$-\frac{V}{g} = \sum_k \left[\frac{g n_0 \varepsilon_k}{E_k^3} \left(\frac{1}{e^{\beta E_k} - 1} + \frac{1}{2} \right) - \frac{(\varepsilon_k + g n_0) \beta \varepsilon_k}{E_k^2} \frac{e^{\beta E_k}}{(e^{\beta E_k} - 1)^2} \right]. \quad (6.75)$$

The critical temperature and the critical condensate density are then found by simultaneously solving (6.49) and (6.75). Since the expression (6.75) also seems to be quadratically infrared divergent in k in cartesian coordinates we follow the same procedure with the ellipsoid method introduced in Sec. 6.2.1. The analytical approximation for the integral in the small ellipsoid reads

$$-\frac{1}{g} = \frac{1}{2\pi^2 a^3 \sqrt{J_x J_y J_z}} \left[\left(\frac{\beta}{3} - \frac{1}{\beta g^2 n_0^2} \right) \frac{R_0^3}{12} + \mathcal{O}(R_0^4) \right]. \quad (6.76)$$

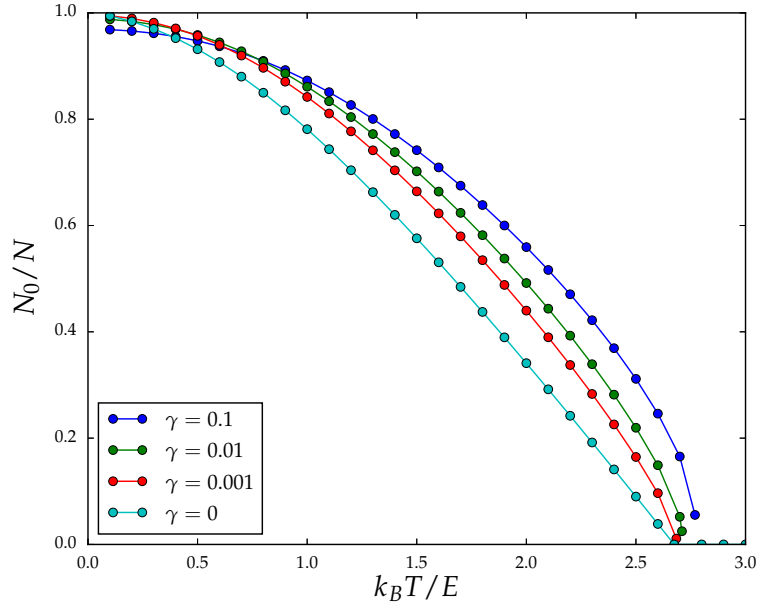


Figure 6.5: Condensate fraction as function of the temperature in three dimensions for different gas parameters γ within the HFBP theory. The non-interacting curve possesses a second-order phase transition, whereas the interacting ones exhibit a first-order transition.

Since the leading order is cubic in the ellipsoid radius R_0 , the integral is not numerically infrared divergent in cartesian coordinates. This occurs due to a delicate cancellation of the respective divergent terms. A power smaller than cubic would be a sign of divergent terms in the integrand. However there were terms proportional to R^{-2} before the expansion, thus they must have been canceled. Note, furthermore that Eq. (6.76) can be derived from (6.69) by differentiation with respect to β while taking into account higher orders. Furthermore the term linear in R_0 in (6.69) does not appear in (6.76), since it is not proportional to $\frac{dn_0}{d\beta}$ and therefore vanishes in the limit $\frac{dn_0}{d\beta} \rightarrow \infty$.

6.3 Shift of critical temperature in three dimensions

From the theoretical literature it is known that weak, repulsive interactions in a three-dimensional, homogeneous Bose gas cause a positive shift of the critical temperature which is linear in the s-wave scattering length:

$$\frac{\Delta T_c}{T_0} = c\gamma^{1/3}. \quad (6.77)$$

Here T_0 denotes the critical temperature of the non-interacting Bose gas, ΔT_c represents the difference between the critical temperature of the interacting gas and T_0 , and c stands for some dimensionless proportionality constant. For the three-dimensional, homogeneous Bose gas c was determined to be approximately equal to 1.3 by performing high-precision quantum Monte Carlo simulations [56] and by applying variational perturbation theory to this infrared problem [57, 58]. We use this value in order to compare with the HFBP theory. To this end we show the critical temperature shift as a function of the s-wave scattering length for bosons in a three-dimensional optical lattice in Fig. 6.6. It is approximately linear as expected from (6.77). However the slope of $c \approx 0.09$ is one order of magnitude off. But we have to remember

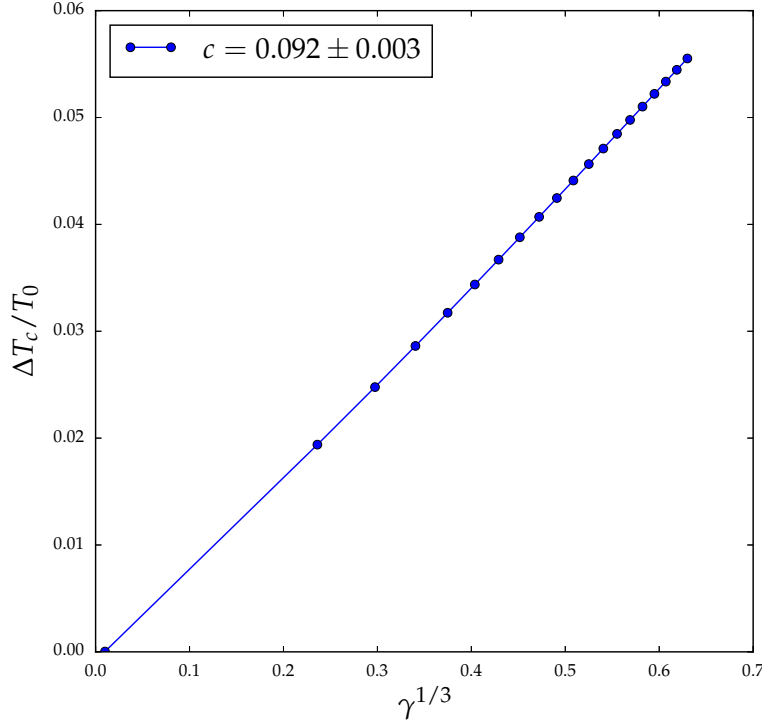


Figure 6.6: Shift of the critical temperature with increasing interaction strength for bosons in an optical lattice.

that we performed the calculations for an optical lattice, whereas the reference value of 1.3 is valid for a continuous, homogeneous Bose gas. For the sake of clarity we define the following terms for our purpose: A homogeneous system denotes a system without confinement, e.g. a harmonic trap, however it may exhibit a lattice structure, e.g. a cubic optical lattice. In contrast a continuous system signifies a system without a lattice structure, but it may possess a confinement. In order to compute the T_c -shift in the continuum we perform the continuum limit, introduced in Sec. 3.2.7, and determine a value of c which is then comparable to the value 1.3. During the limit $a \rightarrow 0$ the density must be preserved such that $\bar{n}/a^3 \rightarrow n$. Thus the filling factor vanishes with a^3 due to (3.15).

First we show the critical temperature as function of the lattice constant in Fig. 6.7. Here the connected bullets represent T_c -curves for different gas parameters γ . The dashed line denotes the value of $T_c^{(\text{cont})}$ for the non-interacting gas in the continuous system following from (6.71):

$$T_c^{(\text{cont})} = \frac{2\pi\hbar^2}{k_B M} \left(\frac{n}{\zeta(3/2)} \right)^{2/3}. \quad (6.78)$$

At first we observe in Fig. 6.7 that the non-interacting curve converges to $T_c^{(\text{cont})}$ as a vanishes. Therefore we conclude that the continuous result is recovered from the theory of the optical lattice. Please note that the numerics are not reliable at very small a and start to fluctuate. Secondly we observe that the critical temperature is always higher with higher a gas parameter γ . Very interestingly all curves exhibit a minimum of the critical temperature at about $a \approx 350$ nm. This stems from the competition between two different contributions to quantum coherence. We remember that the hopping energy diverges as a^{-2} and thus increases coherence due to a higher coupling to neighboring lattice sites. However the number of

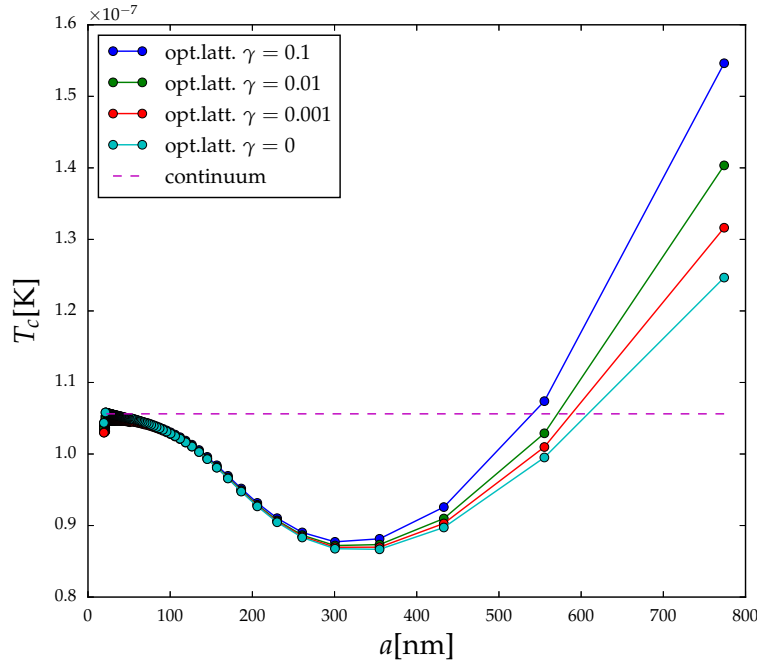


Figure 6.7: Critical temperature as function of the lattice constant a for different gas parameters in three dimensions (bullets). The value of the critical temperature of the continuous, homogeneous gas is added (dashed line).

atoms per site vanishes as a^3 and therefore causes a loss of coherence in the limit $a \rightarrow 0$. The other limit $a \rightarrow \infty$ will be an ensemble of many independent trapped Bose systems. A more detailed investigation of this T_c minimum might be a topic for future work.

From the data in Fig. 6.7 we extract the proportionality constant c of the T_c -shift as function of the lattice constant, which is shown in Fig. 6.8. Here the connected bullets represent the numerical findings. However the value for c at $a = 0$ cannot be calculated due to numerical reasons mentioned above. In order to provide an estimate, we apply an exponential fit function to the numerical data points, which are closest to $a = 0$. The choice of an exponential is arbitrary, however with this we only obtain a rough estimate for the extrapolated value at $a = 0$. We find $c(a = 0) \approx 0.4$. This is still too small compared to the value of 1.3, but it is at least of the same order of magnitude. Furthermore we would not expect a very good agreement of a rather simple HFBP theory with advanced methods of Monte-Carlo simulations [56] and five- or seven-loop diagrammatic calculations within the realm of variational perturbation theory [57,58].

6.4 Results for weakly interacting, homogeneous Bose gas

After having discussed the numerical method, which is necessary for the calculation of the weakly interacting Bose gas, we now present the results for the optical lattice with tunable hopping.

6.4.1 Dimensional phase transition with finite interaction strength

The weakly interacting analog of the non-interacting result Fig. 4.1 is shown in Fig. 6.9. We see that the qualitative shape of the curves is preserved even with a finite gas parameter. Furthermore, the critical temperature increases monotonically with the gas parameter in

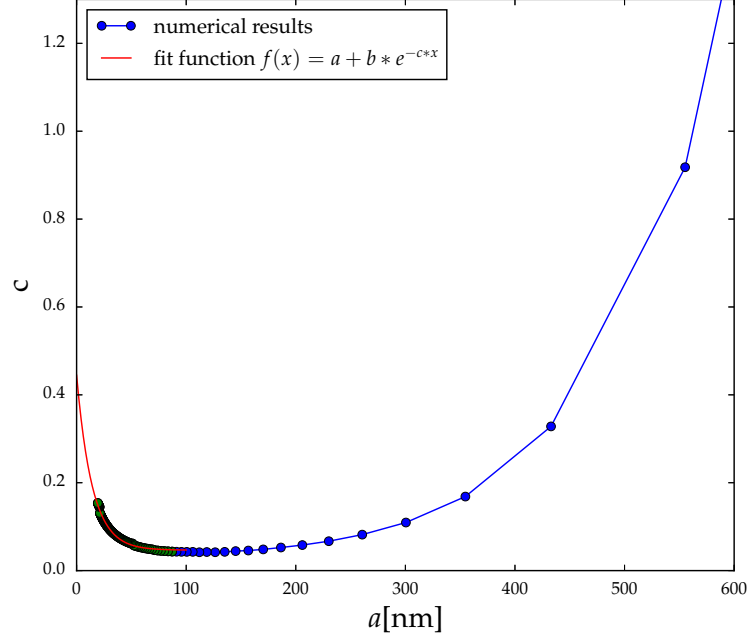


Figure 6.8: Proportionality constant c of the T_c -shift in the continuum limit. The connected bullets represent the numerical findings and the red fit curve is an exponential for extrapolating the value at $a = 0$.

all dimensions. We now focus on the $1D$ - $3D$ -transition close to $1D$ and analyze the role of interactions. This corresponds to the right-hand side in Fig. 6.9, where we have $\lambda \lesssim 3$.

6.4.2 $1D$ - $3D$ -transition with finite interaction strength

In Sec. 4.1 we found a power-law behavior with exponent $\frac{1}{2}$ for the non-interacting $1D$ - $3D$ -transition. We now investigate how this power-law changes with finite interaction. To this end we assume that the form of a power-law at $\lambda \lesssim 3$ is preserved and can be written like

$$T_c = K(3 - \lambda)^\alpha, \quad (6.79)$$

where K denotes the prefactor and α represents the exponent. Having samples of T_c and λ the prefactor and exponent can be found from the axis-intersection and the slope of

$$\ln(T_c) = \ln(K) + \alpha \ln(3 - \lambda). \quad (6.80)$$

In Fig. 6.10(a) we show the critical temperature as function of $3 - \lambda$ in the $1D$ - $3D$ -transition close to $1D$ for small values of $3 - \lambda$. This plot corresponds to a flipped zoom into the right-hand side of Fig. 6.9. The dashed line corresponds to the square root (4.14) which is exact for the non-interacting case at $\lambda = 3$. The non-interacting data curves are obtained, on the one hand, by evaluating the series (3.12) with a finite cut-off, on the other hand by numerical integration of (6.50). They are in perfect agreement. Figure 6.10(b) shows the logarithmized data of the points in Fig. 6.10(a) with the smallest values for $3 - \lambda$. This selection of only few points is done in order to improve the precision of the fit parameters. We apply linear fits and extract the fit parameters for the exponent as well as for the prefactor, shown in Fig. 6.11(a) and 6.11(b), respectively. The grey ribbon illustrates the systematic error which occurs due to the fitting in Fig. 6.10(b) of data points with finite values of $3 - \lambda$. We estimate this error as the largest deviation of the exponent and the prefactor between the non-interacting results

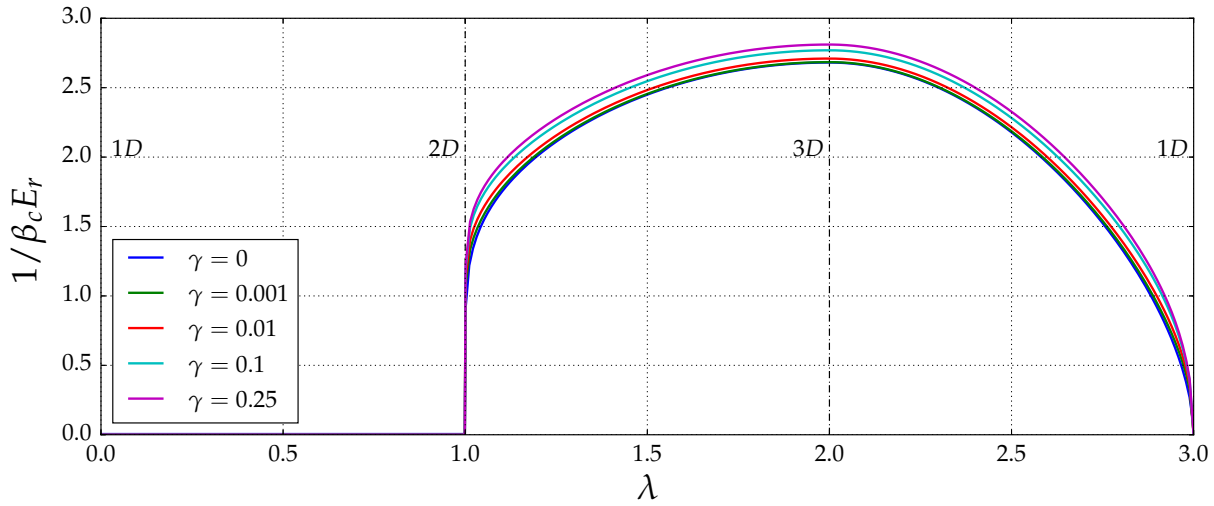


Figure 6.9: Critical temperature in the homogeneous case as function of the path parameter λ for different interaction strengths.

and the square root (4.14). The corresponding values for the square root are depicted as dashed lines

in Fig. 6.11. In Fig. 6.11(a) this error is kept constant and in Fig. 6.11(b) it varies slightly due to exponentiation. Hence we find for the 1D-3D-transition within our range of precision that the exponent remains a constant of $\frac{1}{2}$ but the prefactor increases with increasing interaction strength.

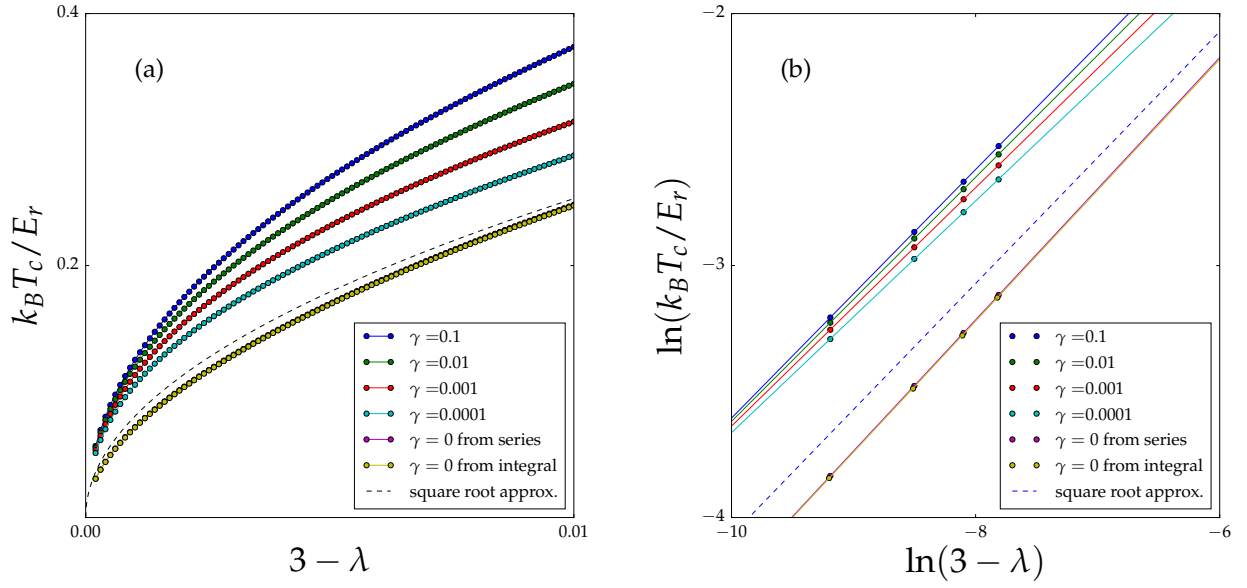


Figure 6.10: 1D-3D-transition close to 1D for critical temperature: Data in (b) is the log-log representation of (a), where we use only the points with very small $3 - \lambda$. The dashed lines correspond to the power-law (4.14). The non-interacting curves are calculated either from the series representation (3.12) or by numerical integration of (6.50).

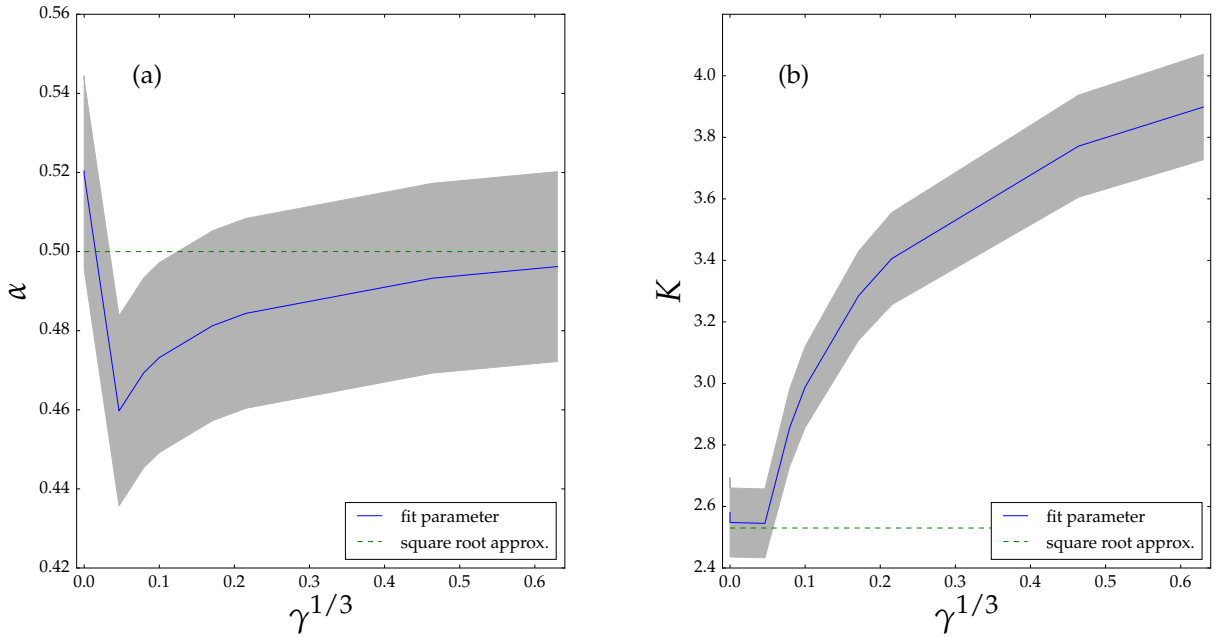


Figure 6.11: Power-law (a) exponent α and (b) prefactor K of (6.79) obtained from linear fits in Fig. 6.10(b) as function of $\gamma^{1/3}$, which is proportional to s-wave scattering length. The grey ribbon represents the systematic error.

7 Hybrid model and comparison with experiment

In this chapter we concentrate on the comparison of our theory with experimental data of Ref. [1]. To this end we specialize our theory to the particular configuration of the experiment. The dimensional phase transition therein is performed through a three-dimensional harmonically trapped Bose gas which consists of a two-dimensional lattice, whose depth is tuned in order to induce the dimensional phase transition, and one continuous degree of freedom, as depicted in Fig. 7.1. Therein we introduced the dimensionless lattice depth s as

$$s = \frac{V_0}{E_r}. \quad (7.1)$$

At very deep lattices, for instance $s \approx 30$, the system consists of an array of decoupled one-dimensional tubes. Decreasing the lattice depth increases the coupling of neighboring tubes and a correspondingly increasing hopping of atoms from tube to tube occurs. In the limit of a vanishing lattice, i.e. $s \rightarrow 0$, the system is purely three-dimensional. Hence the $1D$ - $3D$ -transition can be investigated by only adjusting the lattice depth s . We call this system a hybrid model since it has two degrees of freedom with a lattice structure and a third continuous one. Furthermore the optical lattice is quadratic with lattice constant a and has the same depth in both directions. In order to transform our theory into the hybrid model, we need to perform the continuum limit in one direction. The experimentally measured observable of interest is the critical chemical potential μ_c . We want to investigate the quantity $g_{\text{eff}}n_c$, since it has been analyzed as well in Ref. [1]. It actually corresponds to one half of the critical chemical potential as shown in Sec. 6.1.1. The critical chemical potential μ_c is related to an effective interaction strength g_{eff} , which will be discussed later on, as well as to the critical density n_c . The main issue now is thus to find the critical density.

In Ref. [1] the density profiles along the axial direction is measured which is reproduced in Fig. 7.2. The first assumption is that at very deep lattices there is only a thermal distribution. Every deviation from this thermal curve at shallower lattices is interpreted as condensation. Thus, there is a critical density n_c at which condensation takes place. By means of the local density approximation the axial position in Fig. 7.2 is equivalent to an effective chemical potential. Therefore the inhomogeneous density distribution actually corresponds to slices of homogeneous systems with different chemical potential. Finally there is one distinct slice which exactly describes the critical density as if it would be homogeneous. Hence the determination of the critical density simplifies to a homogeneous problem. This justifies to determine in the following the critical density as a function of the lattice depth in a purely homogeneous treatment.

7.1 Hartree-Fock theory of hybrid model

Besides the experimental data Ref. [1] also provides a Hartree-Fock approach to compare with. We reproduce these results by analyzing the hybrid model within a HF mean field theory. As explained in Sec. 6.1.1 the HF theory for a homogeneous Bose gas does not differ from the non-interacting one at the critical point. Therefore the calculations are the same with the only difference that it has a mean field interaction contribution of $2gn$ and the chemical potential can be tuned up to that value.

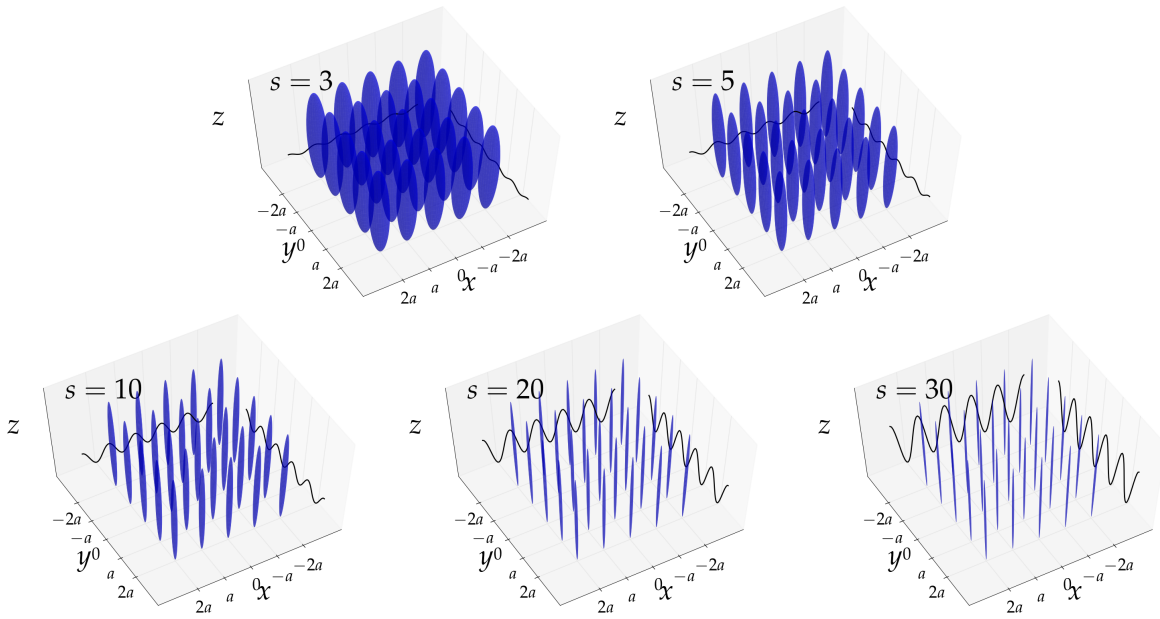


Figure 7.1: Schematic setup of the hybrid model for different dimensionless lattice depths $s = V_0/E_r$: The blue cigars denote the cloud of bosons with a certain extent and the black lines represent the optical lattice potential, which exists only in the two transverse directions.

7.1.1 Critical density

As a generalization of (3.12) the equation for the number of particles in an orthogonal optical lattice with hopping energies J_i in a HF theory reads

$$N = N_0 + \frac{V}{a_x a_y a_z} \sum_{m=1}^{\infty} e^{m\beta(\mu-2gn)} \prod_{i \in \{x,y,z\}} e^{-2m\beta J_i} I_0(2m\beta J_i). \quad (7.2)$$

In order to transform this to the hybrid model at hand we set $a_x = a_y = a$ and $J_x = J_y = J$. Furthermore, we set for the continuum limit of the z -direction $J_z = \hbar^2/2Ma_z^2$ and perform $a_z \rightarrow 0$. Thus we find

$$N = N_0 + \frac{V}{a^2} \sum_{m=1}^{\infty} e^{m\beta(\mu-2gn)} e^{-4m\beta J} I_0^2(2m\beta J) \lim_{a_z \rightarrow 0} \frac{1}{a_z} e^{-m\beta \hbar^2/Ma_z^2} I_0(m\beta \hbar^2/Ma_z^2). \quad (7.3)$$

Using (3.19) we obtain

$$\lim_{a_z \rightarrow 0} \frac{1}{a_z} e^{-m\beta \hbar^2/Ma_z^2} I_0(m\beta \hbar^2/Ma_z^2) = \frac{1}{m^{1/2} \lambda_T}, \quad (7.4)$$

where $\lambda_T = \sqrt{2\pi\beta\hbar^2/M}$ is the thermal de-Broglie length. Eventually the equation for the number of particles of the hybrid model is given by

$$N = N_0 + \frac{V}{a^2 \lambda_T} \sum_{m=1}^{\infty} \frac{1}{m^{1/2}} e^{m\beta(\mu-2gn)} e^{-4m\beta J} I_0^2(2m\beta J). \quad (7.5)$$

We divide by N and introduce the pseudo-one-dimensional density $n^{(1D)}$ as it is used in Ref. [1]:

$$\frac{V}{a^2 N} = \frac{1}{a^2 n^{(3D)}} = \frac{1}{n^{(1D)}}. \quad (7.6)$$

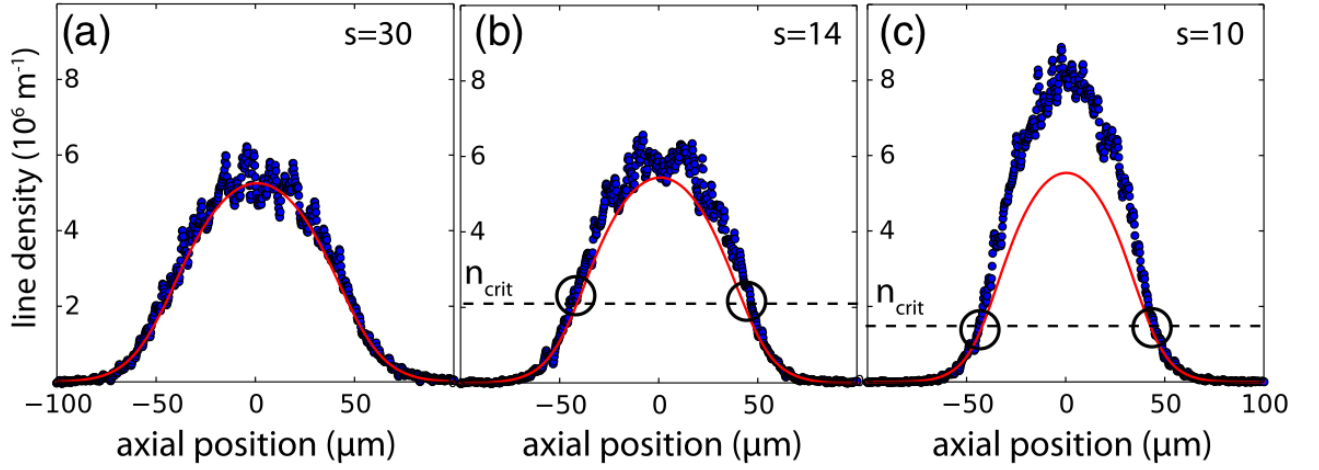


Figure 7.2: Measured density profiles of a tube $1.2 \mu\text{m}$ shifted from the trap center for different lattice depths taken from Ref. [1]: (a) is assumed to be purely thermally distributed. It is fitted by the red curve. Deviations in (b) and (c), which are larger than the standard deviation from this curve, determine the critical density.

Thus we find from (7.5) and (7.6)

$$1 = \frac{N_0}{N} + \frac{1}{\lambda_T n^{(1D)}} \sum_{m=1}^{\infty} \frac{1}{m^{1/2}} e^{m\beta(\mu-2gn)} e^{-4m\beta J} I_0^2(2m\beta J). \quad (7.7)$$

At the critical point we have $N_0 = 0$ and $n^{(1D)} = n_c^{(1D)}$. Additionally we know the value of the critical chemical potential from Sec. 6.1.1 to be $\mu_c = 2gn$. Hence it follows

$$n_c^{(1D)} = \frac{1}{\lambda_T} \sum_{m=1}^{\infty} \frac{1}{m^{1/2}} e^{-4m\beta J} I_0^2(2m\beta J). \quad (7.8)$$

We observe that (7.8) is independent of the interaction strength and reproduces therefore the non-interacting theory as expected. Since J is a function of the lattice depth s , i.e. $J = J(s)$, Eq. (7.8) determines the critical density as a function of the lattice depth.

7.1.2 Hopping energy

Since the computation of the critical density depends sensitively on the relation between the hopping energy J and the lattice depth s , we now discuss three different methods of how to calculate the hopping energy for a given lattice depth.

7.1.2.1 Analytic approximation for deep optical lattices

The most simple possibility is given by the Zwerger formula, which was already introduced in (2.41). However this expression is only valid for deep optical lattices, i.e. $s \gtrsim 10$. At shallow lattices it becomes even unphysical reproducing a vanishing hopping energy for a vanishing lattice depth.

7.1.2.2 Bloch eigenvalue problem

The most promising method to calculate $J(s)$ is by evaluating the actual dispersion relation of the lattice problem. In order to show this we follow the derivation of Ref. [33]. We start

with the Hamiltonian (2.28) including the lattice potential (2.27) for a three-dimensional cubic lattice. The corresponding single-particle Schrödinger equation reads

$$\left[-\frac{\hbar^2}{2M} \nabla^2 + V_0 \sum_{i=1}^3 \sin^2 \left(\frac{r_i}{a} \pi \right) \right] \phi_{n,k}(\mathbf{r}) = E_{n,k} \phi_{n,k}(\mathbf{r}), \quad (7.9)$$

where the Bloch functions $\phi_{n,k}(\mathbf{r})$ are defined in (2.30). Since this is a cubic lattice the wavefunctions factorize $\phi_{n,k}(\mathbf{r}) = \phi_{n,k_x}(x) \phi_{n,k_y}(y) \phi_{n,k_z}(z)$. With this it is sufficient to solve (7.9) for one direction only, where we omit the x -label of the k component,

$$\left[-\frac{\hbar^2}{2M} \frac{\partial^2}{\partial x^2} + V_0 \sin^2 \left(\frac{x}{a} \pi \right) \right] \phi_{n,k}(x) = E_{n,k} \phi_{n,k}(x). \quad (7.10)$$

We rewrite (7.10) by introducing dimensionless quantities

$$x' = \frac{\pi x}{a} \quad \frac{\partial}{\partial x} = \frac{\pi}{a} \frac{\partial}{\partial x'}, \quad (7.11)$$

and by using

$$\sin^2(y) = \frac{1}{2} [1 - \cos(2y)]. \quad (7.12)$$

Upon dividing by the recoil energy (2.42) and using (7.1) we obtain from (7.10)

$$\left\{ -\frac{\partial^2}{\partial x'^2} + \frac{s}{2} [1 - \cos(2x')] \right\} \phi_{n,k}(x') = \tilde{E}_{n,k} \phi_{n,k}(x'). \quad (7.13)$$

Here the dimensionless energy is $\tilde{E}_{n,k} = E_{n,k}/E_r$. We now insert the decomposition of the Bloch states (2.30), which follows from the Bloch theorem, and restrict ourselves to the lowest band, i.e. we set $n = 0$ and omit the label. Hence, we find

$$\left\{ k^2 - 2ik \frac{\partial}{\partial x'} - \frac{\partial^2}{\partial x'^2} + \frac{s}{2} [1 - \cos(2x')] \right\} u_k(x') = \tilde{E}_k u_k(x'). \quad (7.14)$$

Since $u_k(x')$ is a periodic function the Fourier transform exists and we can expand it in a series as:

$$u_k(x') = \sum_{l=-\infty}^{\infty} A_l e^{2ilx'}. \quad (7.15)$$

Thus, we have to solve our problem by determining the Fourier coefficients A_l . Furthermore, we rewrite the cosine via the Euler formula

$$\cos(y) = \frac{1}{2} (e^{iy} + e^{-iy}). \quad (7.16)$$

Using (7.14) – (7.16) we obtain

$$\sum_{l=-\infty}^{\infty} e^{2ilx'} \left\{ \left[(k + 2l)^2 + \frac{s}{2} \right] A_l - \frac{s}{4} A_{l+1} - \frac{s}{4} A_{l-1} \right\} = \sum_{l=-\infty}^{\infty} \tilde{E}_k A_l e^{2ilx'}. \quad (7.17)$$

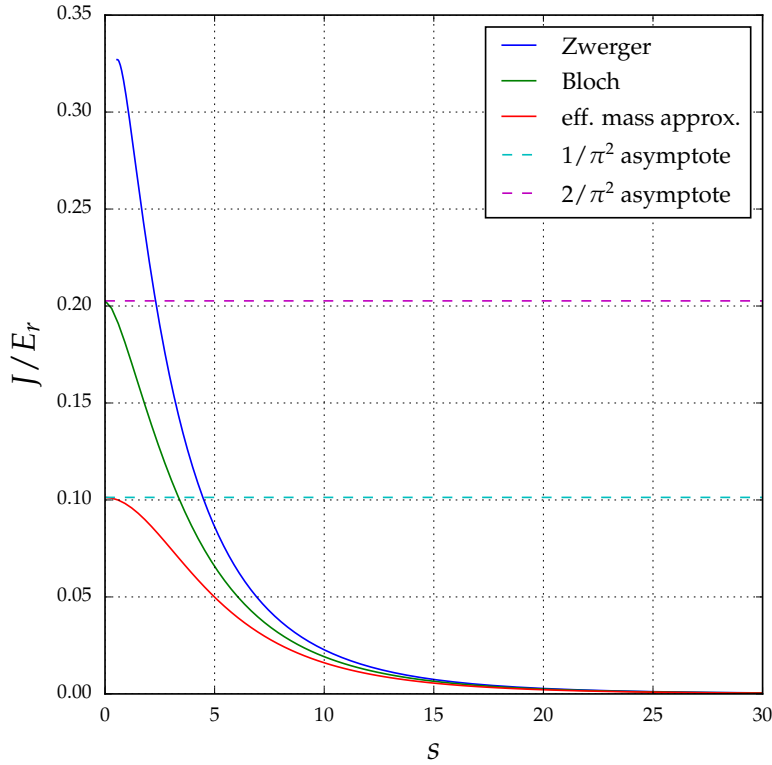


Figure 7.3: Hopping energy J as function of lattice depth s for the three different methods discussed in Sec. 7.1.2: The Zwenger curve is plotted only up its maximum value, since it drops to zero for vanishing s .

Since the Bloch functions are eigenfunctions of the Hamiltonian in the brackets, it simplifies to the lattice dispersion. Due to the orthonormality of the Bloch functions we thus end up with

$$J_x = -\frac{1}{N_s^x} \sum_{k \in \text{BZ}} E_k e^{-ika}, \quad (7.24)$$

thus the hopping energy is the Fourier transform of the band energy.

7.1.2.3 Effective mass approximation

The third method uses the approximation for small k where the band energy can be described through a free particle with an effective mass M^* . It also determines first the dispersion E_k solving the eigenvalue problem (7.18). This dispersion is then fitted by a parabola around the minimum. In this regime the dispersion is approximated by

$$E_k \approx \frac{\hbar^2 k^2}{2M^*}. \quad (7.25)$$

Hence the fit parameter yields the effective mass, which is then used to compute the hopping energy according to (2.47).

In Fig. 7.3 we show the resulting hopping energy J as a function of the lattice depth s . All the curves exhibit the same qualitative behavior. The Bloch method is known to be the most exact one. The Zwenger formula is good only for deep lattices and overestimates the hopping energy, whereas it is systematically underestimated by the effective mass method.

Interestingly the value of $J(s = 0)$ for the Bloch method and for the effective mass method seem to differ by a factor of exactly 2 as it is highlighted by the two asymptotic values in Fig. 7.3.

In order to understand this huge discrepancy we first discuss the value $J(s = 0)$ in the context of the Bloch eigenvalue problem, as it has been done in Ref. [61]. In the continuum the Bloch functions become plane waves:

$$\phi_k(x) = \frac{1}{\sqrt{L}} e^{ikx}, \quad (7.26)$$

where $L = N_s^x a$ denotes the length of the system in x -direction. Furthermore we look at the one-dimensional Wannier function (7.22) in the thermodynamic limit:

$$w(x - x_i) = \frac{1}{\sqrt{N_s^x}} \frac{L}{2\pi} \int_{-\pi/a}^{\pi/a} dk \phi_k(x) e^{-ikx_i}. \quad (7.27)$$

Upon inserting (7.26) into (7.27) we obtain for the one-dimensional Wannier function in the continuum limit $s = 0$ [62]:

$$w(x - x_i) = \frac{1}{\sqrt{a}} \frac{\sin[\pi(x - x_i)/a]}{\pi(x - x_i)/a}. \quad (7.28)$$

According to Ref. [61] we use this in (7.21) and find the value of the hopping energy in the continuum computed by Wannier functions to be

$$\frac{J(s = 0)}{E_r} = \frac{2}{\pi^2}. \quad (7.29)$$

We now turn to the computation of the same value $J(s = 0)$ but now in the context of the effective mass approximation. In the continuum the effective mass becomes the atomic mass $M^* = M$. Using (2.47) we hence get

$$\frac{J(s = 0)}{E_r} = \frac{1}{\pi^2}. \quad (7.30)$$

Here the difference of factor 2 is most clearly highlighted. The reason for this stems from the formula (2.47) which is derived from (2.44). Since this dispersion originates from the quasi-bound approximation it is not applicable in the continuum limit. Equation (2.44) remains a cosine even if we had no lattice at all, but without a lattice we would have a parabolic dispersion. Hence this is the source of the wrong result in (7.30).

For further investigation we also show the hopping energy as a function of the lattice constant a in Fig. 7.4. Therein the two asymptotic values of the respective methods also differ by a factor 2. The reason for this come from the dimensionless lattice depth s . It is inversely proportional to the recoil energy E_r , which is itself inversely to the square of the lattice constant a . Hence, by decreasing the lattice constant, also the lattice depth decreases.

Having discussed the hopping energy in detail we now focus on the interaction strength.

7.1.3 Effective interaction strength

Instead of the usual three-dimensional interaction strength (6.2) an effective interaction strength enters the equation of state $g_{\text{eff}} n_c$ in the context of the dimensional phase transition. In a purely one-dimensional system the bosons possess a certain one-dimensional interaction strength $g^{(1D)}$. At shallow lattices the coupling with neighboring tubes becomes finite. Due to increasing coherence the interaction strength $g^{(1D)}$ is reduced. Therefore $g^{(1D)}$ is itself a function of the lattice depth.

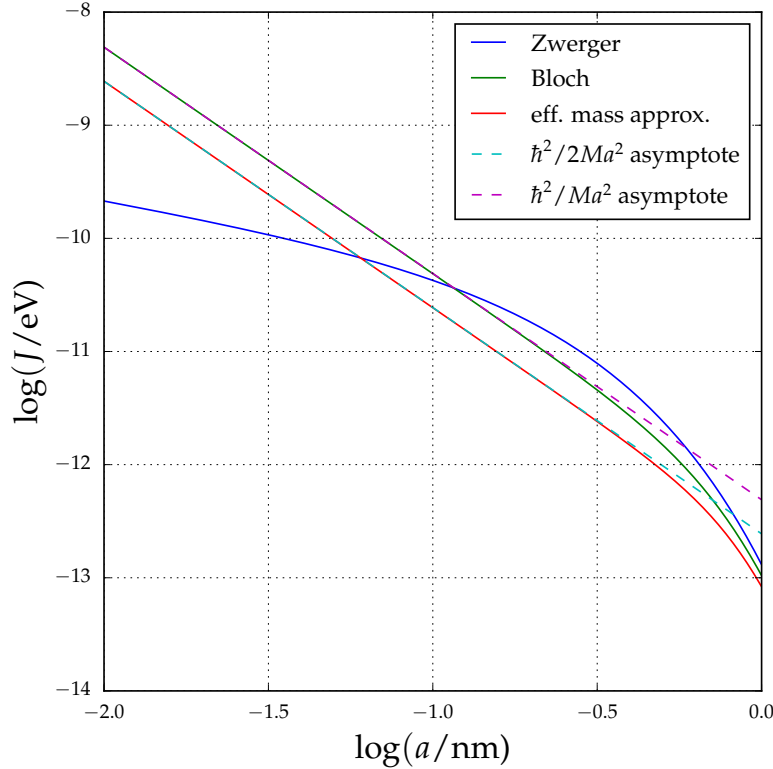


Figure 7.4: Hopping energy J as function of lattice constant a for the three different methods discussed in Sec. 7.1.2 in absolute units: The hopping energy diverges for vanishing lattice constant, thus it is plotted double logarithmically.

7.1.3.1 Tight-binding approximation

According to Ref. [63] the one-dimensional interaction strength to leading order is given as

$$g_{\text{eff}}^{(1D)}(s) \simeq 2\hbar a_s \omega_{\perp}(s). \quad (7.31)$$

Here $\omega_{\perp}(s)$ represents the transverse confining frequency of a single tube. In a tight-binding approximation it can be determined for deep optical lattices according to Ref. [6]. To this end the lattice potential $V(x, y)$ is expanded up to harmonic order. Thus we can assign a frequency as

$$V(x, y) = V_0 \left[\sin^2 \left(\frac{x}{a} \pi \right) + \sin^2 \left(\frac{y}{a} \pi \right) \right] \approx \frac{V_0 \pi^2}{a^2} (x^2 + y^2) \stackrel{!}{=} \frac{1}{2} M \omega_{\perp}^2(s) (x^2 + y^2). \quad (7.32)$$

We find for the transverse frequency with the recoil energy (2.42)

$$\omega_{\perp}^2(s) = \frac{2\pi^2 V_0}{M a^2} = \frac{4E_r^2}{\hbar^2} s. \quad (7.33)$$

Hence we obtain for (7.31)

$$g_{\text{eff}}^{(1D)} \simeq 4a_s E_r \sqrt{s}. \quad (7.34)$$

We observe that the tight-binding approximation predicts a vanishing interaction strength (7.34) for a vanishing lattice. This is not physical because we expect also finite interactions in the continuum limit. Therefore we now focus on the computation of the effective interaction strength using numerically exact Wannier functions.

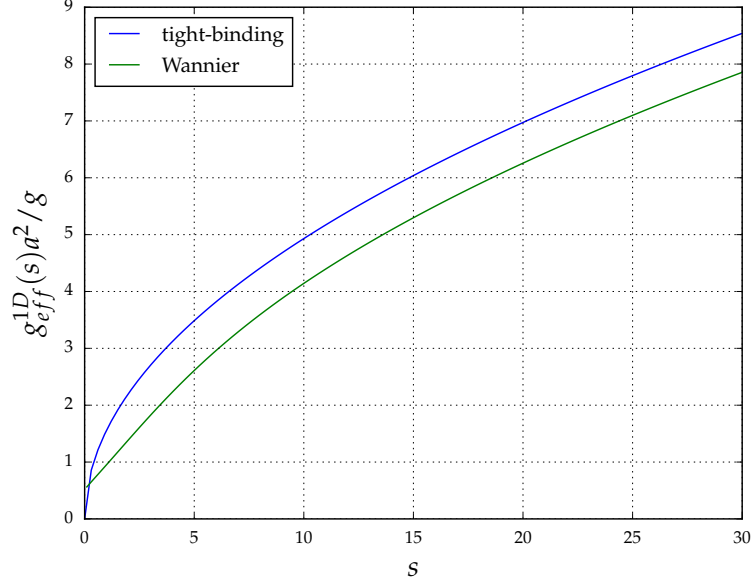


Figure 7.5: Effective interaction strength g_{eff}^{1D} as a function of the lattice depth s . The tight-binding approximation (7.34) drops down to zero at $s = 0$ which is not physical.

7.1.3.2 Wannier functions

In order to determine the Wannier functions numerically we follow the procedure of Refs. [33, 59]. This is done by solving the Bloch eigenvalue problem as introduced in Sec. 7.1.2.2. From this we obtain eigenvalues as well as the Bloch eigenstates. Hence one computes the Wannier functions (2.31) and eventually the interaction strength

$$U = g \int d\mathbf{r} |w(\mathbf{r})|^4. \quad (7.35)$$

Since the hybrid model corresponds to a two-dimensional optical lattice only two spatial dimensions contribute to the interaction strength. In a cubic lattice the Wannier functions factorize and we obtain

$$U = g \left[\int dx |w(x)|^4 \right]^3. \quad (7.36)$$

From this we extract a one-dimensional effective interaction strength where only two directions contribute

$$g_{\text{eff}}^{(1D)} = g \left[\int dx |w(x)|^4 \right]^2. \quad (7.37)$$

At deep optical lattices the Wannier functions are highly localized and $g_{\text{eff}}^{(1D)}$ is large. At shallow lattices, however, the Wannier functions broaden due to coherence with neighboring sites, which causes a reduction of the on-site amplitude. The fourth power decreases even further, thus the interaction strength is reduced in the 3D regime. We briefly show that (7.34) can be derived from (7.37) in a tight-binding approximation. To this end we insert the Gaussian approximation of the Wannier functions provided by Ref. [64]

$$w(x - x_i) = \sqrt[4]{\frac{\pi\sqrt{s}}{a^2}} \exp \left\{ -\frac{\pi^2}{2} \sqrt{s} \left(\frac{x - x_i}{a} \right)^2 \right\}, \quad (7.38)$$

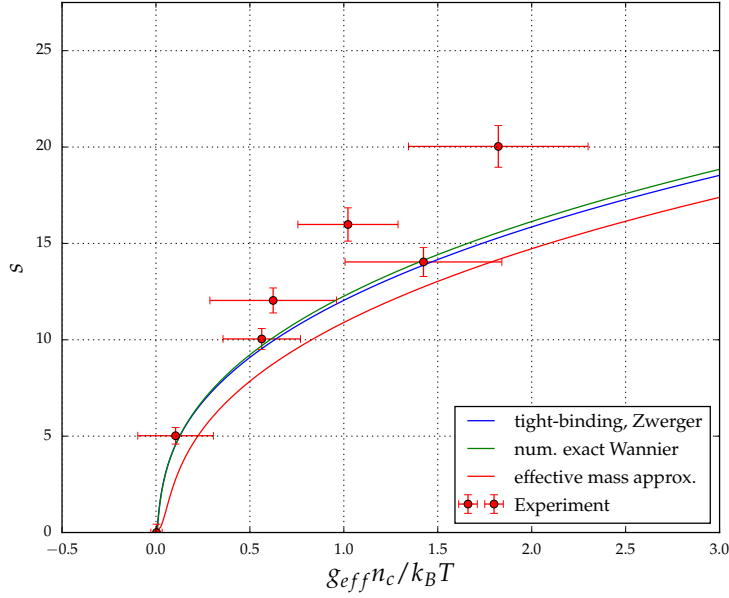


Figure 7.6: Hartree-Fock results of half the critical chemical potential $\mu_c/2 = g_{\text{eff}}n_c$ as a function of the lattice depth s : The Zwerger and the effective mass result are computed according to (7.39). Note that the red curve exactly reproduces the red curve of Fig. 7.7 which is taken from Ref. [1]. As temperature the experimental mean value of 35 nK from Ref. [1] has been used.

into (7.37), which yields (7.34) as expected. We compare the two methods for the effective interaction strength in Fig. 7.5. Both curves monotonically increase with increasing lattice depth. For deep lattices the discrepancy between them is almost constant and therefore the relative deviation decreases. At vanishing lattice depth, the tight-binding approximation vanishes as well, which is unphysical, since it should be finite in the three-dimensional regime.

7.1.4 Critical chemical potential within Hartree-Fock theory

Having the hopping energy as well as the effective interaction strength, we are now able to calculate the critical chemical potential as function of the lattice depth. In the tight-binding approximation the equation of state $g_{\text{eff}}n_c$ follows using (7.8) and (7.34) as

$$g_{\text{eff}}(s)n_c(s) = \frac{4a_s E_r \sqrt{s}}{\lambda_T} \sum_{m=1}^{\infty} \frac{1}{m^{1/2}} e^{-4m\beta J(s)} I_0^2(2m\beta J(s)). \quad (7.39)$$

Results of the critical chemical potential as function of the lattice depth for three different methods are shown in Fig. 7.6. We used a constant temperature of 35 nK which corresponds to the experimental mean value of Ref. [1]. The red curve exactly reproduces the red curve of Fig. 7.7 as expected. However compared to the experimental data the effective mass approximation is bad compared to the other two methods. Even the Zwerger formula reproduces the data more accurately also at shallow lattices. We observe that the calculation with numerical exact Wannier functions only slightly influences the tight-binding result. The achieved deviation is much less than the experimental error bars to compare with.

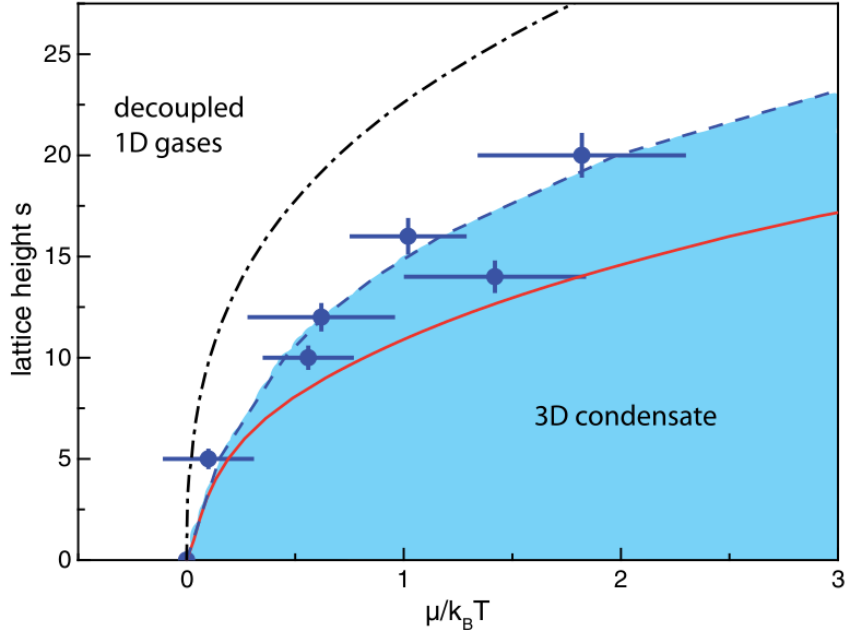


Figure 7.7: Results of Ref. [1] for the phase diagram in the μ - s -plane. Here μ is understood to be $\mu = g_{\text{eff}} n_c$ [1]. The blue dots represent the experimental data, the red curve denotes the Hartree-Fock result, and the dashed-dotted line depicts a prediction of Ref. [65] within a Luttinger liquid theory. The blue dashed line is a guide to the eye.

7.2 Hartree-Fock-Bogoliubov-Popov theory of hybrid model

In this section we present the HFPB theory for the hybrid model as an improvement of the pure HF theory discussed above. We know from Sec. 6.2.4 that the HFPB theory yields a first-order transition. Unlike in Sec. 6.2.4 we do not have a phase transition at a certain critical temperature T_c and critical condensate density n_{0c} since we look for the critical density n_c of the hybrid model. However, we can show that this is equivalent by looking at the schematic phase diagram of Fig. 7.8 in the n - T -plane. The phases are separated by a first-order transition depicted as the white line. The dashed line denotes a curve of constant density, whereas the dashed-dotted line represents a curve of constant temperature. The condensate fraction as function of the respective quantities is shown on the right-hand side of Fig. 7.8. We observe a first-order jump of the condensate fraction in either curve. Therefore the statement, that the phase transition occurs at the point, where dn_0/dT diverges, is equivalent to the statement that dn_0/dn diverges. Thus the former defines the two critical variables n_{0c} and T_c , and the latter n_{0c} and n_c .

In order to find this pair of critical variables n_{0c} and n_c we first solve (6.75) to get n_{0c} since it is independent of the total density n . Having n_{0c} we insert it in (6.49) to find n_c . To this end the numerics is performed in the same manner as explained in Sec. 6.2. Specializing our theory to the hybrid model we numerically perform the continuum limit of the z -direction as described in Sec. 3.2.7. The hopping energies of the transverse directions are set to be equal and can be tuned with the lattice depth.

Figure 7.9 shows our HFBP result for the hybrid model in comparison with the HF curve and the experimental data. We observe a much better agreement with the experiment compared to the pure HF result. We remember the importance of phase fluctuations in low dimensions explained in Sec. 2.1. Due to the fact that HFBP takes quantum fluctuations into account we have better agreement in the low-dimensional regime, where the lattice is deep. In Fig. 7.9 we observe that HF and HFBP agree at small s . This is where the system is more 3D-like.

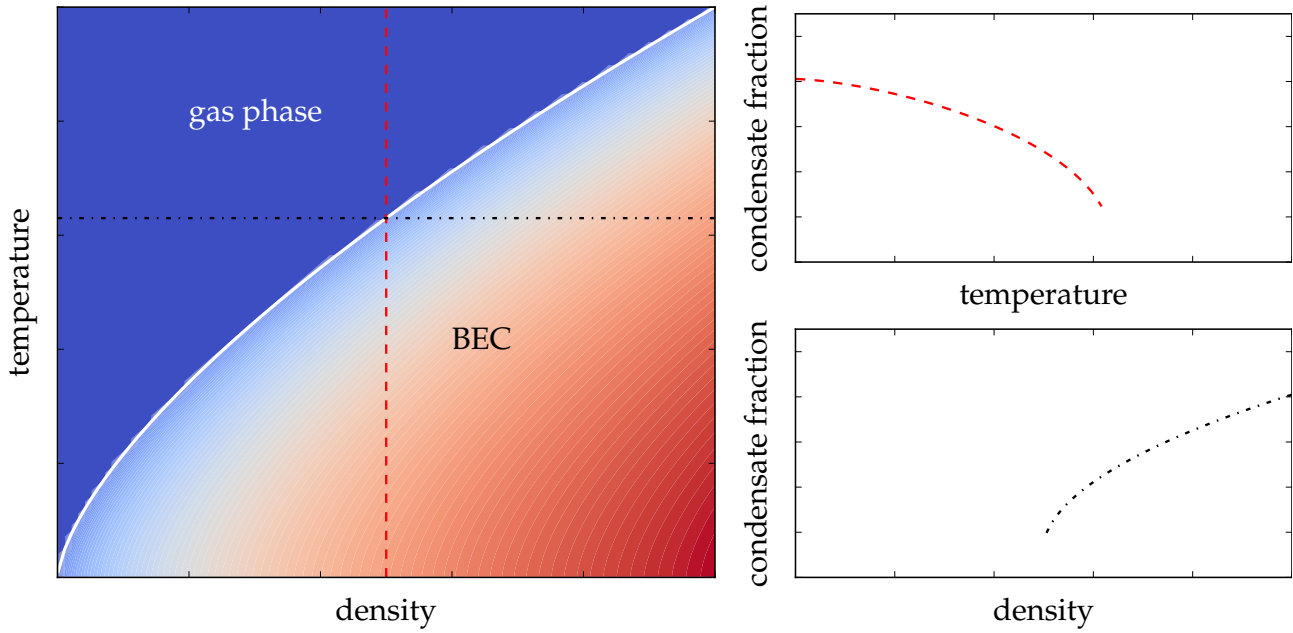


Figure 7.8: Schematic phase diagram in n - T -plane: The white line corresponds to a first-order phase transition. The dashed and dashed dotted lines denote slices at constant density and constant temperature, respectively. On the right-hand side the respective two slices are shown. A first-order jump occurs in both directions.

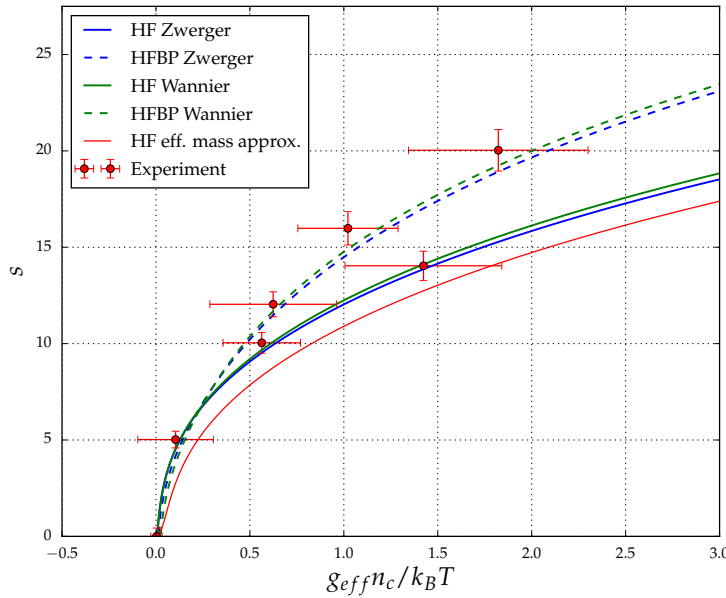


Figure 7.9: Hartree-Fock-Bogoliubov-Popov results for half the critical chemical potential $\mu_c/2 = g_{\text{eff}}n_c$ as function of the lattice depth s . HFBP theory turns out to be a huge improvement for reproducing the experimental data compared to HF theory.

However at large s HF breaks down due to the higher importance of phase fluctuations in low dimensions, which are not included in the pure HF theory.

8 Conclusion

This work consists of three main parts which investigate the dimensional phase transition of the ultracold Bose gas. We first developed a simple theory for the dimensional phase transitions of non-interacting bosons by means of a kinetic dimensional transition induced through tunable hopping energies. We were able to model all dimensional transitions from one to three dimensions choosing a certain path in parameter space. All our results were in agreement with the Mermin-Wagner-Hohenberg theorem and we found a power-law behavior for the $1D$ - $3D$ transition with an exponent of $\frac{1}{2}$, which is non-perturbative, and a logarithmic-like behavior for the $2D$ - $3D$ transition of the critical temperature in the homogeneous case. In the harmonically trapped case, however, the critical behavior is lost and all exponents become trivially 1, which corresponds to a first-order perturbative result. Furthermore, we showed that the critical temperature is highest in three dimensions according to our expectation due to the higher importance of phase fluctuations in lower dimensions.

Secondly we derived the Hartree-Fock-Bogoliubov-Popov theory for a weakly interacting homogeneous Bose gas which provides a first-order phase transition. The expected linear shift of the critical temperature due to weak interactions was smaller, but of the same order of magnitude, as predictions of more advanced theories in the continuous, three-dimensional system. We focused on the $1D$ - $3D$ transition to investigate the power-law behavior found in the non-interacting case. Our results show no significant change of the exponent when going to finite interaction strength, instead only the prefactor of the power-law changes.

Finally we introduced a hybrid model and compared our theory with the experimental data of the $1D$ - $3D$ transition from Ref. [1]. We computed the critical chemical potential during the ramping of the optical lattice in a Hartree-Fock as well as in a Hartree-Fock-Bogoliubov-Popov formalism. Figure 7.9 showed much better agreement of the HF-PB theory than the pure HF one. This improvement stems from the contribution of quantum fluctuations in the HF-PB theory.

9 Outlook

As a side effect we found in the continuum limit of the optical lattice a non-monotonic behavior of the critical temperature of the homogeneous, three-dimensional system both for weak as well as vanishing interactions, as depicted in Fig. 6.7. Therefore questions for the T_c minimum or a positive T_c -shift at larger lattice constants arise.

In the weakly interacting case we concentrated on the $1D$ - $3D$ transition and investigated the power-law behavior. One could also study the change of the $2D$ - $3D$ transition, for which we found a logarithm-like behavior in the non-interacting case, due to weak interactions. However, the two-dimensional, interacting Bose gas exhibits another possible phase. We discussed earlier that there is no BEC in two dimensions and therefore no long-range order exists. However, incorporating interactions a quasi long-range order can emerge and the Berezinsky–Kosterlitz–Thouless (BKT) phase forms, where low energetic excitations are present through the unbinding of vortex-antivortex pairs. The BKT phase has totally been neglected so far and could also be studied in the realm of dimensional phase transitions, as it has been measured as function of the interaction strength in Ref. [66].

Furthermore it would be interesting to perform the dimensional path with a finite transition time. A theory of this would include temperature as well as time and needs therefore advanced frameworks such as the Keldysh formalism. In the case of an adiabatic change possible questions would be whether the condensate picks up a finite quantum phase by performing once the complete path or whether some adiabatic cooling or heating occurs.

Our many-body problem describes the regime of weak interactions only. Hence the strong coupling limit would represent a challenging task to investigate. Furthermore such systems can be used to compare with bosonic hard-core Quantum-Monte-Carlo simulations [67], since the hard-core case corresponds to a strongly repelling contact interaction. An analytic approach to this could be the perturbative expansion of the kinetic Bose-Hubbard term as it is worked out in detail in Refs. [68,69].

Eventually also the dimensional phase transition of the Fermi gas is of great scientific interest. These fermionic systems exhibit the famous BEC-BCS crossover which can be tuned via Feshbach resonances and could be induced in a dimensional manner. Furthermore the $1D$ - $3D$ transition of fermions is a candidate for exotic quantum phases. At this stage fundamental work for the exploration of the exotic Fulde-Ferrell-Larkin-Ovchinnikov phase [70], which is a superconducting state of non-zero momentum Cooper pairs, in spin-imbalanced Fermi gases has already been done. Quantum fluctuations in the $1D$ - $3D$ -crossover using dynamical mean field theory were theoretically investigated [71]. Furthermore phase diagrams for a potential dimensional crossover have been computed. Finally the $1D$ - $3D$ - transition of a two-component spin-imbalanced Fermi gas has recently been measured [72].

Bibliography

- [1] A. VOGLER, R. LABOUVIE, G. BARONTINI, S. EGGERT, V. GUARRERA, and H. OTT, *Phys. Rev. Lett.* **113**, 215301 (2014).
- [2] A. EINSTEIN, *Sitzber. preuss. Akad.* **1924**, 261 (1924).
- [3] S. BOSE, *Z. Phys.* **26**, 178 (1924).
- [4] M. ANDERSON, J. ENSHER, M. MATTHEWS, C. WIEMAN, and E. CORNELL, *Science* **269**, 198 (1995).
- [5] K. DAVIS, M. MEWES, M. ANDREWS, N. VAN DRUTEN, D. DURFEE, D. KURN, and W. KETTERLE, *Phys. Rev. Lett.* **75**, 3969 (1995).
- [6] M. GREINER, O. MANDEL, T. ESSLINGER, T. HÄNSCH, and I. BLOCH, *Nature (London)* **415**, 39 (2002).
- [7] S. FÖLLING, A. WIDERA, T. MÜLLER, F. GERBIER, and I. BLOCH, *Phys. Rev. Lett.* **97**, 060403 (2006).
- [8] W. S. BAKR, A. PENG, M. E. TAI, R. MA, J. SIMON, J. I. GILLEN, S. FÖLLING, L. POLLET, and M. GREINER, *Science* **329**, 547 (2010).
- [9] I. BLOCH, *Nat. Phys.* **1**, 23 (2005).
- [10] P. D. LETT, W. D. PHILLIPS, S. L. ROLSTON, C. E. TANNER, R. N. WATTS, and C. I. WESTBROOK, *J. Opt. Soc. Am. B* **6**, 2084 (1989).
- [11] K.-A. SUOMINEN, *J. Phys. B* **29**, 5981 (1996).
- [12] M. XIAO, Y.-Q. LI, S.-Z. JIN, and J. GEA-BANACLOCHE, *Phys. Rev. Lett.* **74**, 666 (1995).
- [13] M. BORN, *Optik: Ein Lehrbuch der elektromagnetischen Lichttheorie*, Springer-Verlag Berlin Heidelberg, 3rd edition, 1972.
- [14] J. W. G. WILDER, L. C. VENEMA, A. G. RINZLER, R. E. SMALLEY, and C. DEKKER, *Nature* **391**, 59 (1998).
- [15] M. M. CALBI, M. W. COLE, S. M. GATICA, M. J. BOJAN, and G. STAN, *Rev. Mod. Phys.* **73**, 857 (2001).
- [16] A. H. CASTRO NETO, F. GUINEA, N. M. R. PERES, K. S. NOVOSELOV, and A. K. GEIM, *Rev. Mod. Phys.* **81**, 109 (2009).
- [17] M. GIRARDEAU, *J. Math. Phys.* **1**, 516 (1960).
- [18] J. KOSTERLITZ and D. THOULESS, *J. Phys. C* **6**, 1181 (1973).
- [19] B. PAREDES, A. WIDERA, V. MURG, O. MANDEL, S. FOLLING, I. CIRAC, G. V. SHLYAPNIKOV, T. W. HANSCH, and I. BLOCH, *Nature (London)* **429**, 277 (2004).

- [20] Z. HADZIBABIC, P. KRUGER, M. CHENEAU, B. BATTELIER, and J. DALIBARD, *Nature (London)* **441**, 1118 (2006).
- [21] N. MERMIN and H. WAGNER, *Phys. Rev. Lett.* **17**, 1133 (1966).
- [22] P. HOHENBERG, *Phys. Rev.* **158**, 383 (1967).
- [23] L. CHOMAZ, L. CORMAN, T. BIENAIMÉ, R. DESBUQUOIS, C. WEITENBERG, S. NASCIMBÈNE, J. BEUGNON, and J. DALIBARD, *Nat. Commun.* **6**, 6162 (2015).
- [24] A. GÖRLITZ, J. M. VOGELS, A. E. LEANHARDT, C. RAMAN, T. L. GUSTAVSON, J. R. ABO-SHAEER, A. P. CHIKKATUR, S. GUPTA, S. INOUE, T. ROSEN BAND, and W. KETTERLE, *Phys. Rev. Lett.* **87**, 130402 (2001).
- [25] L. PITAEVSKII and S. STRINGARI, *Bose-Einstein condensation*, International Series of Monographs on Physics, Clarendon Press, 2nd edition, 2016.
- [26] M. UEDA, *Fundamentals and new frontiers of Bose-Einstein condensation*, World Scientific, Singapore, 2010.
- [27] C. PETHICK and H. SMITH, *Bose-Einstein condensation in dilute gases*, Cambridge University Press, 2nd edition, 2008.
- [28] R. FEYNMAN, *Int. J. Theor. Phys.* **21**, 467 (1982).
- [29] J. AKRAM, *Sculpting a quasi one-dimensional Bose-Einstein condensate to generate calibrated matter waves*, Ph.D. thesis, Freie Universität Berlin, <http://users.physik.fu-berlin.de/~pelster/Theses/akram.pdf>, 2016.
- [30] K. KOPITZKI, *Einführung in die Festkörperphysik*, Teubner Studienbücher Physik, Vieweg+Teubner Verlag, 2013.
- [31] S. HUBER, *Lecture Notes: Experimental and Theoretical Aspects of Quantum Gases*, <https://cmt-qq.phys.ethz.ch/teaching/qg>, 2013.
- [32] A. PELSTER, *Ginzburg-Landau theory for bosons in optical lattices (I)*, <http://www.mpipks-dresden.mpg.de/~bec10>, 2010.
- [33] A. HOFFMANN, *Bosonen im optischen Gitter*, Diploma thesis, Freie Universität Berlin, <http://users.physik.fu-berlin.de/~pelster/Theses/hoffmann.pdf>, 2007.
- [34] W. ZWERGER, *J. Opt. B* **5**, S9 (2003).
- [35] D. JAKSCH, C. BRUDER, J. CIRAC, C. GARDINER, and P. ZOLLER, *Phys. Rev. Lett.* **81**, 3108 (1998).
- [36] K. K. DAS, *Phys. Rev. A* **66**, 053612 (2002).
- [37] U. AL KHAWAJA, N. PROUKAKIS, J. ANDERSEN, M. ROMANS, and H. STOOFF, *Phys. Rev. A* **68**, 043603 (2003).
- [38] D. KADIO, M. GAJDA, and K. RZAŻEWSKI, *Phys. Rev. A* **72**, 013607 (2005).
- [39] S. DUTTA and E. MUELLER, *arXiv:1508.03352* (2015).
- [40] L. KHAYKOVICH, F. SCHRECK, G. FERRARI, T. BOURDEL, J. CUBIZOLLES, L. D. CARR, Y. CASTIN, and C. SALOMON, *Science* **296**, 1290 (2002).

- [41] A. WELLER, J. P. RONZHEIMER, C. GROSS, J. ESTEVE, M. K. OBERTHALER, D. J. FRANTZESKAKIS, G. THEOCHARIS, and P. G. KEVREKIDIS, *Phys. Rev. Lett.* **101**, 130401 (2008).
- [42] P. KRÜGER, S. HOFFERBERTH, I. E. MAZETS, I. LESANOVSKY, and J. SCHMIEDMAYER, *Phys. Rev. Lett.* **105**, 265302 (2010).
- [43] A. D. MARTIN and J. RUOSTEKOSKI, *Phys. Rev. Lett.* **104**, 194102 (2010).
- [44] P. DYKE, E. D. KUHNLE, S. WHITLOCK, H. HU, M. MARK, S. HOINKA, M. LINGHAM, P. HANNAFORD, and C. J. VALE, *Phys. Rev. Lett.* **106**, 105304 (2011).
- [45] T. YEFSAH, A. T. SOMMER, M. J. H. KU, L. W. CHEUK, W. JI, W. S. BAKR, and M. W. ZWIERLEIN, *Nature (London)* **499**, 426 (2013).
- [46] A. PELSTER, *Bose-Einstein-Kondensation, Vorlesung im Sommersemester 2004*, http://www.theo-phys.uni-essen.de/tp/ags/pelster_dir/SS04/skript.pdf, 2004.
- [47] M. ABRAMOWITZ and I. STEGUN, *Handbook of mathematical functions with formulas, graphs, and mathematical tables*, volume 55, Washington, D.C., 1964.
- [48] F. SCHWABL and W. BREWER, *Statistical mechanics*, Advanced Texts in Physics, Springer Berlin Heidelberg, 2006.
- [49] F. DALFOVO, S. GIORGINI, L. PITAEVSKII, and S. STRINGARI, *Rev. Mod. Phys.* **71**, 463 (1999).
- [50] W. KETTERLE and N. VAN DRUTEN, *Phys. Rev. A* **54**, 656 (1996).
- [51] J. ANDERSEN, *Rev. Mod. Phys.* **76**, 599 (2004).
- [52] A. GRIFFIN, T. NIKUNI, and E. ZAREMBA, *Bose-Condensed Gases at Finite Temperatures*, Cambridge University Press, 2009.
- [53] H. T. C. STOOF, D. B. M. DICKERSCHIED, and K. GUBBELS, *Ultracold Quantum Fields*, Springer, 2009.
- [54] N. M. HUGENHOLTZ and D. PINES, *Phys. Rev.* **116**, 489 (1959).
- [55] T. KHELLIL, *Weakly Interacting Bose Gas in Random Environment*, Ph.D. thesis, Freie Universität Berlin, <http://users.physik.fu-berlin.de/~pelster/Theses/khellil.pdf>, 2016.
- [56] V. A. KASHURNIKOV, N. V. PROKOF'EV, and B. V. SVISTUNOV, *Phys. Rev. Lett.* **87**, 120402 (2001).
- [57] H. KLEINERT, *Mod. Phys. Lett. B* **17**, 1011 (2003).
- [58] B. KASTENING, *Phys. Rev. A* **69**, 043613 (2004).
- [59] M. HAYN, *Über die dissipative Dynamik von ultrakalten Bosonen im optischen Gitter*, Diploma thesis, Freie Universität Berlin, <http://users.physik.fu-berlin.de/~pelster/Theses/hayn.pdf>, 2010.
- [60] T. GRASS, *Real-Time Ginzburg-Landau Theory for Bosonic Gases in Optical Lattices*, Diploma thesis, Freie Universität Berlin, <http://users.physik.fu-berlin.de/~pelster/Theses/tobiasgrass.pdf>, 2009.

Bibliography

- [61] K. V. KRUTITSKY, *Phys. Rep.* **607**, 1 (2016).
- [62] G. PARZEN, *Phys. Rev.* **89**, 237 (1953).
- [63] M. OLSHANII, *Phys. Rev. Lett.* **81**, 938 (1998).
- [64] A. HOFFMANN and A. PELSTER, *Phys. Rev. A* **79**, 053623 (2009).
- [65] M. A. CAZALILLA, *J. Phys. B* **37**, S1 (2004).
- [66] R. J. FLETCHER, M. ROBERT-DE SAINT-VINCENT, J. MAN, N. NAVON, R. P. SMITH, K. G. H. VIEBAHN, and Z. HADZIBABIC, *Phys. Rev. Lett.* **114**, 255302 (2015).
- [67] D. MORATH, D. STRASSEL, A. PELSTER, and S. EGGERT, (*to be published*) (2016).
- [68] F. E. A. DOS SANTOS and A. PELSTER, *Phys. Rev. A* **79**, 013614 (2009).
- [69] B. BRADLYN, F. E. A. DOS SANTOS, and A. PELSTER, *Phys. Rev. A* **79**, 013615 (2009).
- [70] P. FULDE and R. A. FERRELL, *Phys. Rev.* **135**, A550 (1964).
- [71] M. O. J. HEIKKINEN, D.-H. KIM, M. TROYER, and P. TÖRMÄ, *Phys. Rev. Lett.* **113**, 185301 (2014).
- [72] M. C. REVELLE, J. A. FRY, B. A. OLSEN, and R. G. HULET, *arXiv:1605.06986* (2016).

Selbständigkeitserklärung

Ich, Bernhard Irsigler, geboren am 29.1.1991, Matrikelnummer 4458035, erkläre gegenüber der Freien Universität Berlin, dass ich die vorliegende Masterarbeit selbstständig und ohne Benutzung anderer als der angegebenen Quellen und Hilfsmittel angefertigt habe.

Die vorliegende Arbeit ist frei von Plagiaten. Alle Ausführungen, die wörtlich oder inhaltlich aus anderen Schriften entnommen sind, habe ich als solche kenntlich gemacht.

Diese Arbeit wurde in gleicher oder ähnlicher Form noch bei keiner anderen Universität als Prüfungsleistung eingereicht und ist auch noch nicht veröffentlicht.

Berlin, den 1. September 2016

Bernhard Irsigler